Quantec Geoscience Ltd.
116 Spadina Ave., Suite 400
Toronto, ON, M5V 2K6
Phone (416) 306 1941
Fax (416) 306 1949

Geophysical Survey Interpretation Report

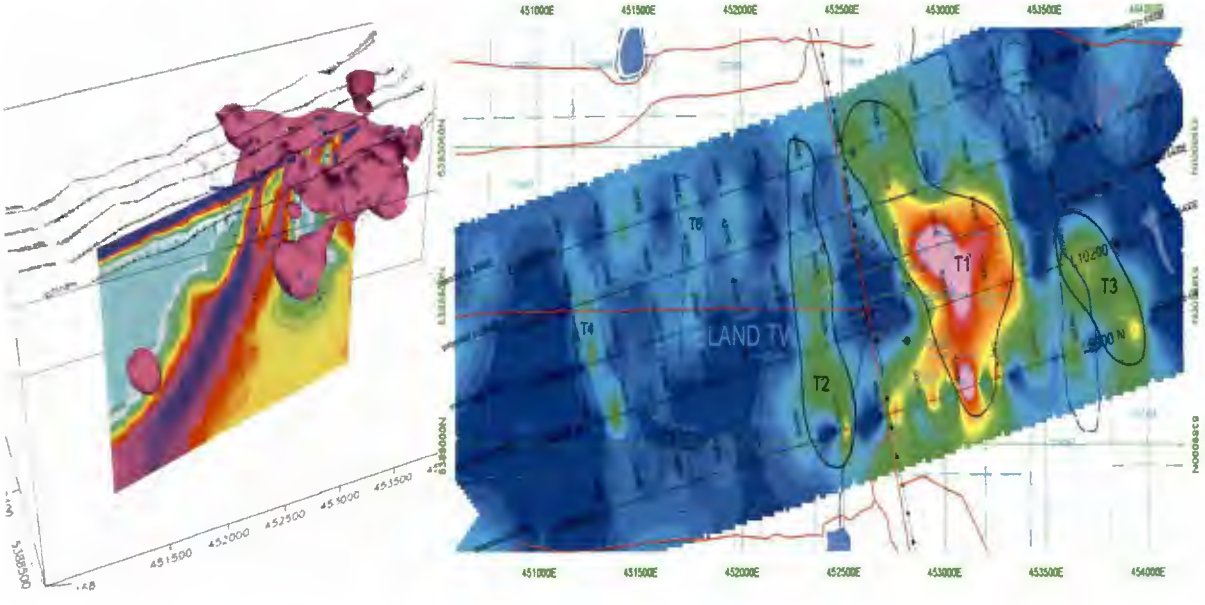

Regarding the TITAN-24 Tensor-Magnetotelluric, DC Resistivity and Induced Polarization Surveys over the LOVELAND PROJECT, near Timmins, ON, For: WESTERN KIDD RESOURCES LTD., Ontario, Canada.

2.43776

E. Martinez
R. Hearst

May, 2008
QGL Project CA00516T

EXECUTIVE SUMMARY

Quantec Geoscience Ltd. has undertaken Direct Current Resistivity, Induced Polarization (DCIP) and Magnetotelluric Resistivity (MT) surveys over the Loveland Project, owned by Western Kidd Resources Ltd. The survey was performed from December 3rd to December 15th, 2007.

The project is located approximately 30 km northwest of Timmins, and about 20 km west of the Kidd Creek mine in Northern Ontario, Canada. The main access routes are the regional Highway 101 and Highway 576, and local roads.

The property consists of 32 claims located in Loveland Township, covering an approximate area of 3817.9 square kilometers.

The primary objective of the Titan-24 survey at Loveland Project was to detect potential volcanogenic massive sulphide (VMS) mineralization from disseminated to stringer, to map geologic structures and alteration zones (chloritic or sericitic), and to develop targets for diamond drilling potential targets on the property.

The Titan 24 survey provides subsurface chargeability and resistivity at depth to assist geologic interpretations, delineating target mineralization and focus drilling. Mineralization is expected to be metal sulphides (pyrrhotite, chalcopyrite, pyrite, etc) and satellite minerals hosted in felsic to mafic volcanic rocks.

Results and Interpretation

The Titan-24 survey has successfully identified geophysical anomalies in the DCIP and MT raw data and inversion models which may represent zinc and copper VMS mineralization and/or alteration zones from near surface up to approximately 700 meters depth.

The MT inversion models show good resolution of the anomalies to approximately 1.5 kilometer depth. The DCIP & MT interpretation could possibly be affected by structures, which run parallel and/or sub-parallel to the survey lines.

The interpreted DCIP and MT anomalies and the target prioritization were mainly based on the anomaly amplitude, extent, the Titan multi-parameter association, and the available geological and sulphide mineralization on the property. However, the interpreted anomalies may not necessarily be related to zinc and copper mineralization. Other sources, such as iron-rich formations, graphite, clay and fault systems can produce similar DCIP and MT responses.

Conclusions and Recommendations

A total of seven (7) DCIP and MT anomalous zones have been identified for follow-up at Loveland. One (1) zone has been classified as high priority exploration target for zinc and copper sulphide mineralization at depth. Two (2) zones have been classified as moderate priority, and four (4) Titan anomalous zones represent low priority. In addition, the MT inversion models have resolved two (2) deep anomalous zones from approximately 600 meters to >1.5 kilometers depth that may represent deep mineralization, alteration zones, feeder channels and/or structures.

The following recommendations are derived from the interpretation at Loveland:

1. Drill testing the high priority targets ***T1***.
2. If favourable drill results are obtained when drilling the high priority zones, then the moderate priority targets T2 and T3 should be drilled.
3. Review and evaluate all available geological and geochemical data in the vicinity of the low priority areas *T4*, *T5*, *T6* and *T7* for further targeting these zones.
4. If mineralization is encountered when drilling the anomalies above the deep targets, consider extending the drilling to test the deep source of the MT responses.

5. When the deep MT targets (***MT1*** and ***MT2***) are drilled, follow up with downhole BHTEM, and consider physical property logging on all drilled Titan targets to understand and explain the source of the responses observed.
6. Integrate all available geo-scientific information into 3D Gocad earth model and perform physical property and 3D query evaluation to corroborate the interpreted Titan anomalies.
7. Examination and/or acquisition of additional surficial geophysical data (Gravity, Magnetics, TEM, etc) to further enhance the interpretation and drill targeting is recommended.

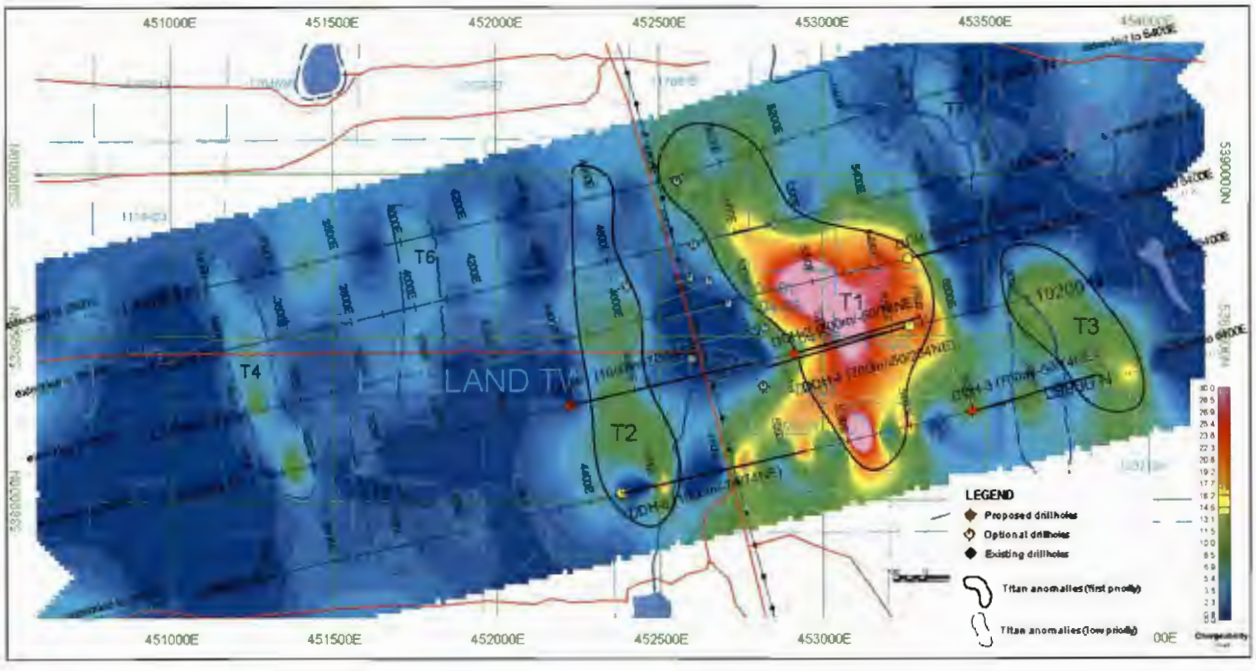

Titan Interpretation Plan Map over 2D Chargeability at 100m Depth

TABLE OF CONTENTS

APPENDICES

LIST OF FIGURES

LIST OF TABLES

1. INTRODUCTION

Quantec Geoscience Ltd. has undertaken Direct Current Resistivity, Induced Polarization (DCIP) and Magnetotelluric Resistivity (MT) surveys over the Loveland Project, owned by Western Kidd Resources Ltd. The survey was performed from December 3rd to December 15th, 2007.

The project is located approximately 30 km northwest of Timmins, and about 20 km west of the Kidd Creek mine in Northern Ontario, Canada. The main access routes are the regional Highway 101 and Highway 576, and local roads, see Figure 1.

The property consists of 32 claims located in Loveland Township, covering an approximate area of 3817.9 square kilometers.

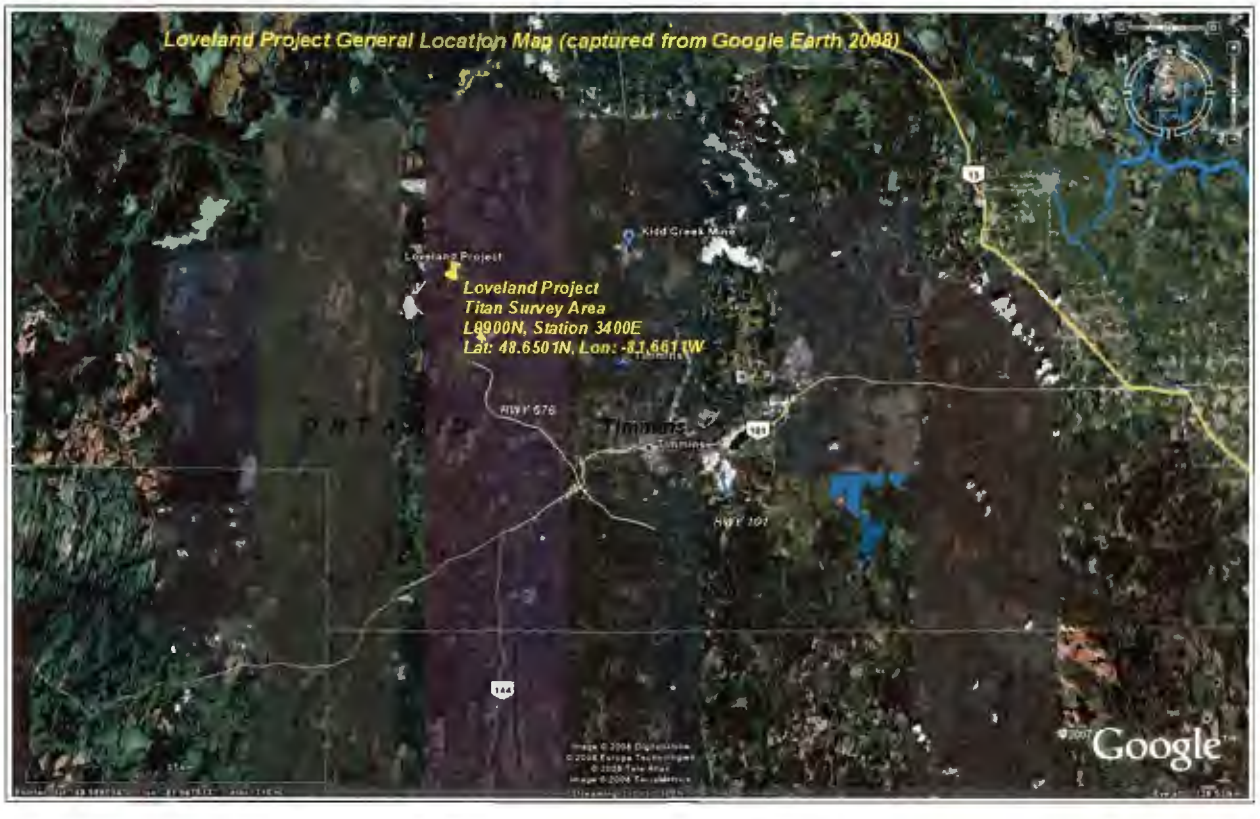

Figure 1: General Location Map[1]

1.1 SURVEY OBJECTIVES

The primary objective of the Titan-24 survey at Loveland Project was to detect potential volcanogenic massive sulphide (VMS) mineralization from disseminated to stringer, to map geologic structures and alteration zones (chloritic or sericitic), and to develop targets for diamond drilling potential targets on the property.

The Titan 24 survey provides subsurface chargeability and resistivity at depth to assist geologic interpretations, delineating target mineralization and focus drilling. Mineralization is expected to be metal sulphides (pyrrhotite, chalcopyrite, pyrite, etc) and satellite minerals hosted in felsic to mafic volcanic rocks.

[1] *General Location Map captured from Google Earth (v-4.2-Beta), 2008.*

1.2 TITAN-24 SURVEY OVERVIEW

The Titan-24 system combines Tensor Magnetotelluric (MT) Resistivity measurements capable of high resolution and deep penetration (>1.5 kilometers) with Galvanic DC Resistivity and Induced Polarization (DCIP) capable of high resolution and penetration (~750 meters). The system is designed to identify and discriminate between massive and disseminated metallic mineralization and mapping geological contacts and deep conductors that may potentially represent alteration or mineralization.

The Titan-24 is a multi-channel **D**istributed **A**cquisition **S**ystem (**DAS**), Sheard, N., (1998), which records full-waveform time series for each geophysical event (Direct Current Resistivity, Induced Polarization (DCIP) and Magnetotellurics (MT), enabling the application of sophisticated digital signal processing techniques to ensure the best possible data quality (Figure 2).

The DCIP survey utilised a pole-dipole configuration with 100 meters dipoles and current injection points located midway between the potential dipoles. To obtain continuous depth profiling over the length of the array current injection extensions of 600 meters off of each line end were used.

The MT data was acquired over the bandwidth of 0.1 Hertz to 10000 Hertz. The configuration used contiguous 100 meters dipoles measuring the in-line electric field (Ex) and 100 meters dipoles at every second site for measuring the orthogonal component (Ey). Two pairs of orthogonal magnetometers, one pair for the high frequency data and one pair for the low frequency data were used to record the Hx and Hy magnetic fields, respectively.

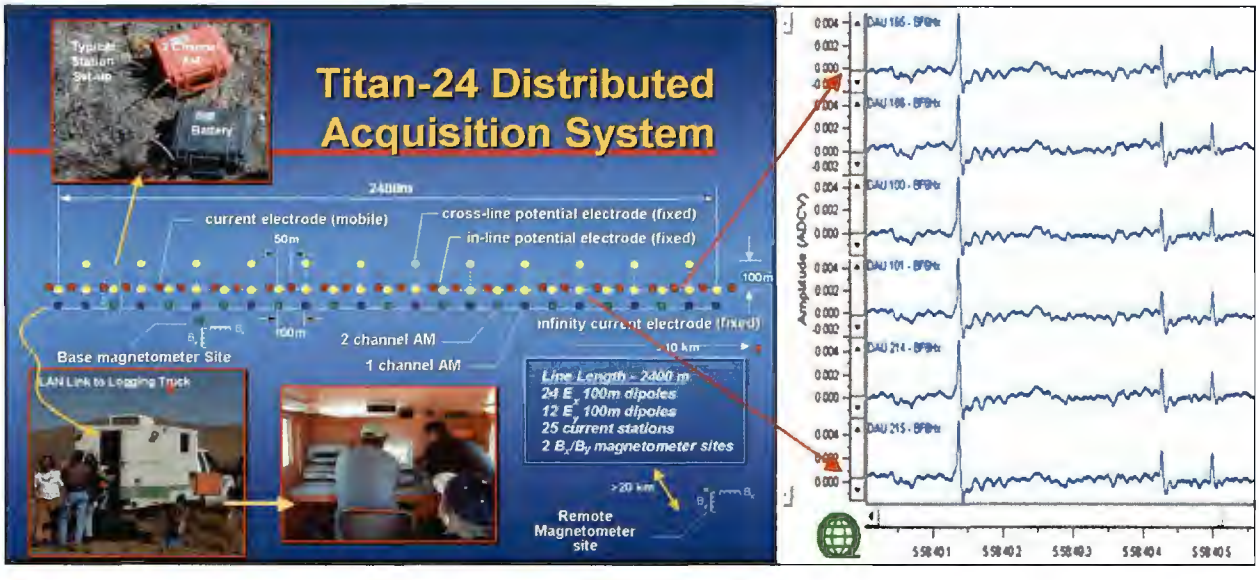

Figure 2: Titan-24 DCIP and MT Survey Layout

A remote reference site located approximately 20-30 kilometers away was used for noise reduction and monitoring. The remote reference station consisted of one pair of orthogonal dipoles for measuring the electric field (Ex and Ey) and two pairs of orthogonal magnetometers orientated in the same direction as the survey line spread. ***Appendices C***, ***D***, ***and I*** and the "*Geophysical Survey Logistics Report*" provide more information on the survey details.

For each line surveyed, three independent 2D earth models (IP Chargeability, DC and MT Resistivity) are calculated and presented for interpretation and targeting mineralization.

1.3 General Geology and Mineralization

The Loveland project is located in the southern part of the Archean greenstone belt of the Abitibi Subprovince in Northern Ontario.

The Titan survey area is underlain by sequences of mafic to felsic volcanic and sedimentary rocks of the Archean Kidd Volcanic Complex, which are in contact with intrusive ultramafic rocks. Sills and dikes of different origin and age may have intensively intruded into the volcanic complex as well.

Massive to stringer sulphide mineralization (sphalerite, chalcopyrite, galena and pyrrhotite) is expected to occur within the felsic volcanic and/or in the hanging wall, or the contact between felsic and mafic volcanic. Chlorite, sericite and carbonate alteration zones are observed within the complex, and are commonly associated with massive sulfide mineralization.

1.4 Previous Exploration

The full extent of previous exploration at Loveland is not known to the author. To date, relatively extensive drilling has been carried out on the property; the Western Kidd's historic drilling program includes more than 26 holes (Figure 3).

Mineralization of economic value has not been detected yet, although mineralization is believed to occur at depth and in unexplored areas on the property.

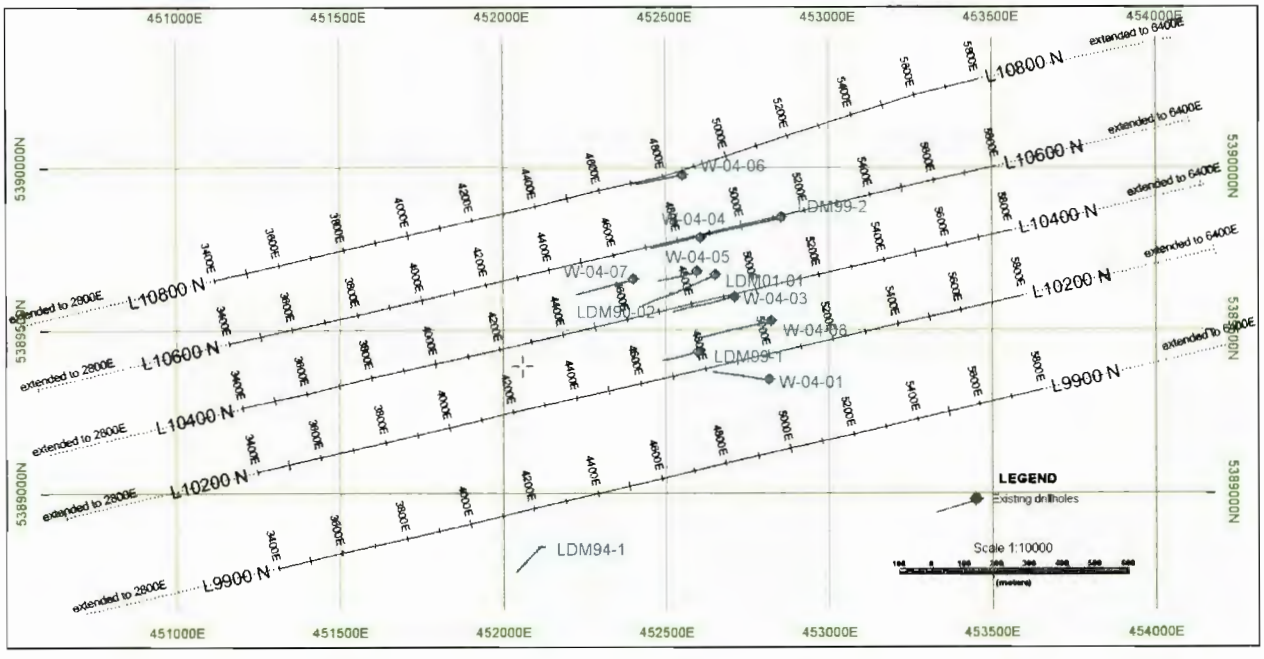

Figure 3: Historic Drilling Location Plan at Loveland

2. TITAN SURVEY DESCRIPTION

2.1 General Survey Details

- **Quantec Project N°:** CA00516T
- **Survey Period:** December 3rd to December 15th, 2007
- **General Location:** Ontario, Canada
- **District:** Timmins Mining District, Ontario
- **Nearest Settlements:** Timmins, Ontario
- **Coordinate System/Zone:** Universal Transverse Mercator Projection (UTM)
- **Datum/Zone:** NAD 83/Zone 17N
- **Lat/Lon:** approx: 48 39'23" N, 81 38'57" W
- **UTM position**[2]**:** approx: 452181mE, 5389487mN

2.2 Access

- **Base of Operations:** Howard Johnson Hotel
  1800 Riverside Drive
  Timmins , Ontario
  P4N 7J5
  705-267-6241
- **Mode of Access to Grid:** Highway 101, Highway 576, and local roads
- **Mode of Access to Lines:** Snowmobile and on foot

2.3 Survey Grid

- **Established by:** Western Kidd Resources Ltd.
- **Grid Azimuth:** approx. 74 degrees true North
- **Declination:** approx. 12 degrees West
- **Line Separation:** approx. 300-400 meters
- **Station Interval:** 100 meters
- **Coordinate Reference System:** Survey Grid referenced to UTM Coordinates, (Figure 4 and Table 1)
- **Method of Chaining:** Metric, slope distance, pickets, GPS surveyed

2.4 Survey Work Undertaken

- **Number of Lines Surveyed:** 5 lines/extended 600m east & west respectively (Table 1)
- **Survey Coverage:** DCIP survey: 12.00 kilometers
  MT survey: 12.00 kilometers

[2] *UTM coordinates (NAD 83, Zone17N) supplied by Western Kidd Resources Ltd., 2008.*

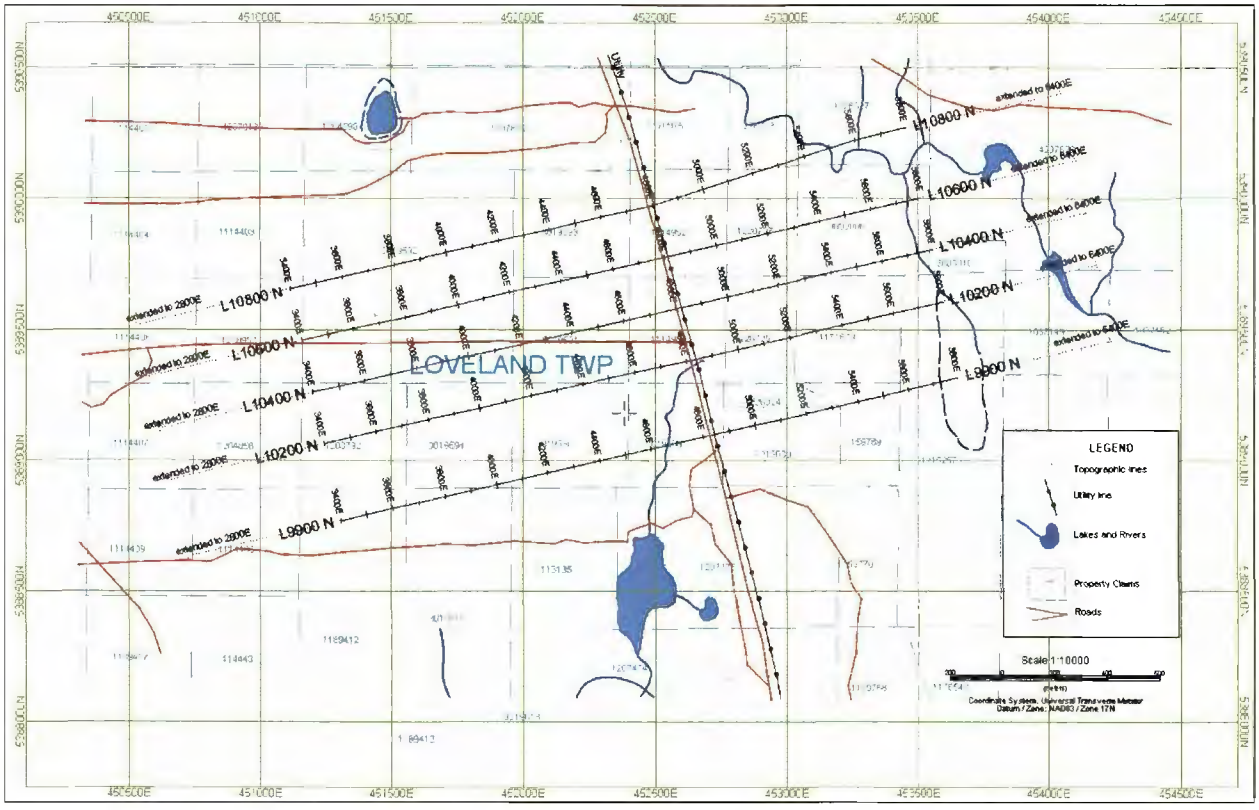

Figure 4: Titan Line Location Map and Surveyed Claims[3]

Line	Survey/Array Coord. Start	Survey/Array Coord. End	UTM Coord. Start		UTM Coord. End	
			Easting	Northing	Easting	Northing
10800N	3400E	5800E	451114	5389655	453454	5390272
10600N	3400E	5800E	451158	5389459	453512	5390005
10400N	3400E	5800E	451200	5389262	453554	5389807
10200N	3400E	5800E	451244	5389066	453594	5389608
9900N	3400E	5800E	451308	5388770	453652	5389318

Table 1: Titan Survey Lines (UTM Referenced NAD 83, Zone 17N)

[3] *Claim Map supplied by Western Kidd Resources Ltd, 2008.*

3. RESULTS AND INTERPRETATION

This section presents the interpretation of the Titan-24 data in context with the known geology, survey objectives and significance to future exploration for copper and zinc volcanogenic massive sulphide (VMS) mineralization at Loveland. ***Appendix E*** provides pseudo-section plots of the DCIP and MT data used in the 2D inversions along with a more complete description of data pre-processing.

In *Section 3.3* the 2D inversion models are presented graphically, along with an interpretation and comments on the most significant results. Scaled Geosoft format plans and cross-sectional plots of the DC resistivity, chargeability and MT models are also provided in ***Appendices F, G and H***.

3.1 DC Resistivity & Induced Polarization Inversions

In general, the DCIP raw data quality is good to excellent. Pre-processing of the DC Resistivity & Induced Polarization (DCIP) data involved adjustment of data errors and removal of poor quality data. For the DCIP inversions, the UBC DCInv2D^{TM} 2D platform was used (Oldenburg & Li, 1994).

The inversions were generally run with successive removal of poorly fitting data or error adjustment before arriving at the final 2D models. Some data acquired with large transmit-receiver separations were not of a high quality, and were removed prior to interpretation. A more detailed discussion of the UBC technique for inverting the DCIP data can be found in ***Appendix D***. Several DCIP inversion models were calculated. In some instances, using the DC inversion results as the resistivity distribution for the IP inversion produced models with abnormally large chargeability amplitudes coincident with the high resistivity zones that are not consistent with the raw data.

Additional IP models were derived by inverting the IP data assuming a constant resistivity distribution (half-space homogeneous conductivity). These models are thought to have provided a relatively better image of the apparent chargeability distribution. The 2D data was integrated and inverted in a 3D inversion platform. The UBC DCInv2D^{TM} 2D platform was used for the 3D inversions.

3.2 Tensor Magnetotelluric Inversions

The MT raw data quality is good to excellent, including the frequency range from 1000 Hertz to 3000 Hertz (dead band). The unconstrained Tensor Magnetotelluric (2D MT) inversion models were calculated using the Geotools^{TM} MT data processing and model-inversion platform. The initial data input into the Geotools database were line-station unrotated data, taken directly from the EDI archive[4].

One-dimensional (1D) inversions for each mode[5] (XY and YX) of the unrotated data were generated at each site. The apparent resistivity and phase from the 1D model were interpolated to obtain twelve (12) frequency responses per decade. Stitched 1D XY-YX and Determinant sections were also created.

2D RLM smooth models were constructed using the Mackie inversion method (Rodi & Mackie, 2001). Four (4) inversion models (rlme1 to 4) were calculated using the interpolated resistivity and phase curves for the TM (resistivity + phase) and TE (resistivity + phase) modes, in the 0.1 to $10x10^3$ Hertz bandwidth. 1D Stitched Determinant sections were also used as starting models for the 2D "rlm-4" smooth inversions.

Four (4) sets of 2D PW models (pwe1 to 4) were derived from inverting the unrotated data using the RLM as starting models. Different combinations of datasets (TM phase, TM resistivity, TE phase and TE resistivity) and starting models were tested before arriving at the final 2D models. The pw4 inversion models[6] were found to produce the most consistent models for interpretation. For further details on inversion parameters and alternate inversion models and MT interpretation refer to ***Appendix E*** and ***Appendix I***.

---

[4] *Electronic Data Interchange (EDI) data are available in the digital archive submitted along with the "Geophysical Survey Logistics Report", Martinez, E., (2008).*

[5] *MT Modes include: Transverse Electric field (TE or XY) parallel to geology (strike direction) and Transverse Magnetic field (TM or YX) perpendicular to geological strike (dip direction).*

[6] *(pw4) **P**lane **W**ave unrotated inversion models calculated from TM (phase & resistivity) & TE (phase & resistivity) using rlm4 and 1D Stitched Determinant sections as starting model.*

3.3 TITAN 2D MULTI-PARAMETER INTERPRETATION

This section[7] presents a description of the most significant geophysical anomalies and potential targets interpreted from the final Titan-24 DCIP and MT inversion models. A brief description of the results and targeting recommendations are also provided in this section.

The interpretation is presented as figures containing 2D sections and plan maps of the MT Resistivity (pw4 models), DC Resistivity (smDC models) and IP Chargeability (smIP models) with an overlay of the final Titan-24 target areas and anomaly trends. Additional 2D and 3D sections and plans are included in ***Appendix G*** and ***Appendix I***.

For the resistivity plots, cool colors (blue series) represent resistivity highs and warm colors (red series) resistivity lows. Alternatively, for the IP cool colors represent chargeability lows, warm colors represent chargeability highs. Unless specified otherwise, all resistivity plots are in the 100-100000 ohm-meters color range and the chargeability plots in the 0-30 milliradians range.

The interpreted target areas, which are not geologically unique, are derived from the 2D Chargeability and 2D DC Resistivity and MT inversion models. The 3D inversion results corroborate the interpretation derived from the 2D inversions, although less detailed results were obtained from the inversions. Details on 3D inversion models and parameters are available on ***Appendix I*** and ***J***.

The anomalies were classified and assigned a target priority according to amplitude, size and multi-parameter IP, DC and MT Resistivity association as follows:

- *High priority targets:*
  - Anomalies exhibiting a strong to moderate IP response (>15 milliradians), DC and MT resistivity low association (rho <10000 ohm-meters); interpreted to be massive to stringer copper and/or zinc sulphide mineralization.
  - Anomalies exhibiting a strong to moderate IP response (>15 milliradians), DC and MT resistivity moderate to high (or gradient) association (rho <100000 ohm-meters). Interpreted to be stringer to semi-massive zinc and/or copper sulphide mineralization.
- *Moderate priority targets:*
  - Anomalies exhibiting moderate IP response (>5-15 milliradians), DC and MT resistivity low association (rho <10000 ohm-meters); interpreted to be stringer to disseminated copper and/or zinc sulphide mineralization and alteration.
  - Anomalies exhibiting moderate IP response (>5-15 milliradians), DC and MT resistivity moderate to high (or gradient) association (rho <100000 ohm-meters). Interpreted to be stringer to disseminated sulphide mineralization and alteration.
- *Low priority targets:*
  - Weak IP response (<5 milliradians), DC and MT resistivity moderate to high association (rho 5000-100K ohm-meters); interpreted as consistent with weakly disseminated concentrations, alteration zones, or structures.
  - Deep MT resistivity lows (rho <1000 ohm-meters at >500 meters depth); consistent with deep mineralization, structures and/or feeder zones.

A total of seven (7) Titan multi-parameter IP Chargeability, DC & MT resistivity anomalous zones have been identified at Loveland. Of all the interpreted responses, one (T1) Titan anomaly has been classified as high priority target for follow up. Two (T2 and T3) anomalous zones are classified as moderate and four (T4 to T7) zones are classified as low priority. Additionally, two (MT1 and MT2) deep MT anomalies are classified as deep low priority targets for follow up, see Figure 5.

[7] *The final models of the inversion results only are shown in this section. It is useful to review the actual data input into the 2D inversion (Appendix E) and all the raw data, which is available in the Logistics Report previously submitted.*

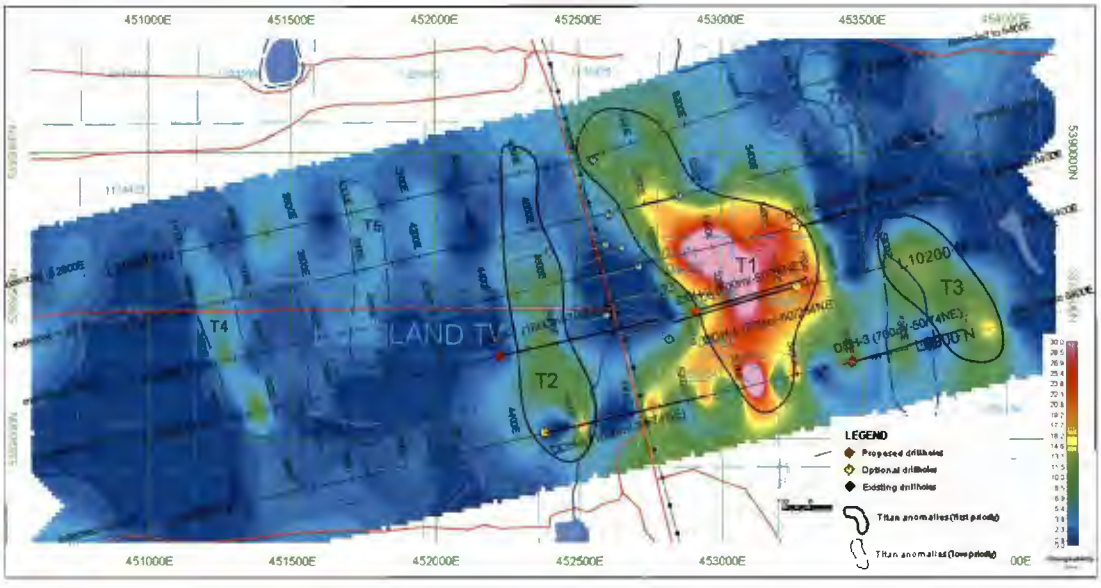

Figure 5: DCIP & MT Anomalous Zones and Priority Targets at Loveland

3.3.1 High Priority Titan Anomalous Zones

According to the IP chargeability models and the DC and MT resistivity association, one Titan anomaly "***T1***" has been interpreted as a high priority target for follow up at Loveland (see Figure 6).

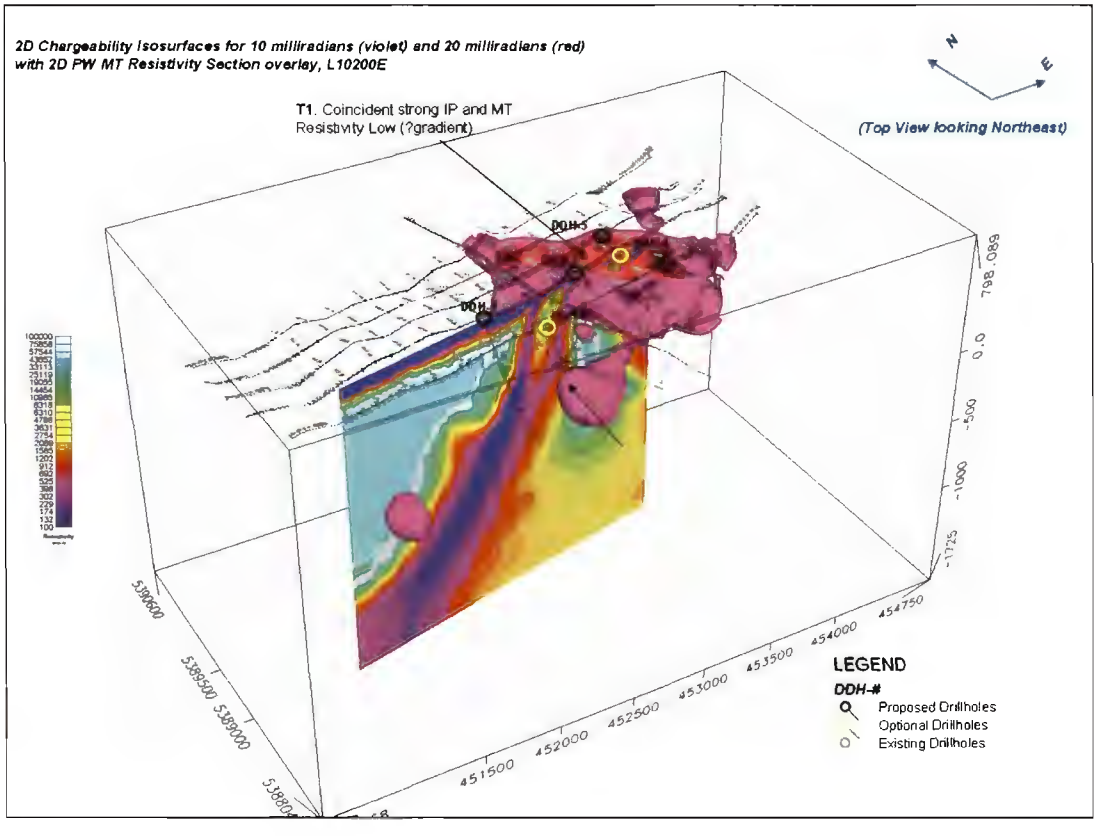

Figure 6: 3D View Depicting the High Priority DCIP & MT Zone T1 on L10200N

Anomalous zone T1 (high priority)

This zone is observed in the eastern part of the survey area and strikes north from line L9900N, station 5200E to line L10800E, stations 4800E to 5100E, see Figure 6 and Figure 7. Anomaly T1 consists of a large area, and depth limited IP response observed from surface to approximately 300 meters depth. Ii also exhibits a strong to moderate chargeability (>20 milliradians) with DC and MT moderate to high-gradient resistivity response (>5000 ohm-meters).

The most prospective portion for this zone is observed from lines L10200E to L10400E and from L4100E to L4400E. The inversion models indicate a sub-horizontal feature slightly west dipping. The north and south portion of the anomaly is associated with a more resistive environment and the IP response decreases indicating weak zinc and/or copper mineralization or a chloritised-sericitised alteration zone. The full extent of the anomaly is well resolved, particularly for lines from L10200N to L10600N.

The DC and MT resistivity models show at least two different conductive features suggesting discontinuity in the mineralization or structural break in the main zone. A fault may exist and crosscut the area from L9900E, station 4900E to L10600E, station 5500E. Copper and zinc sulphide mineralization has been documented in the area, explaining the source for this Titan anomaly.

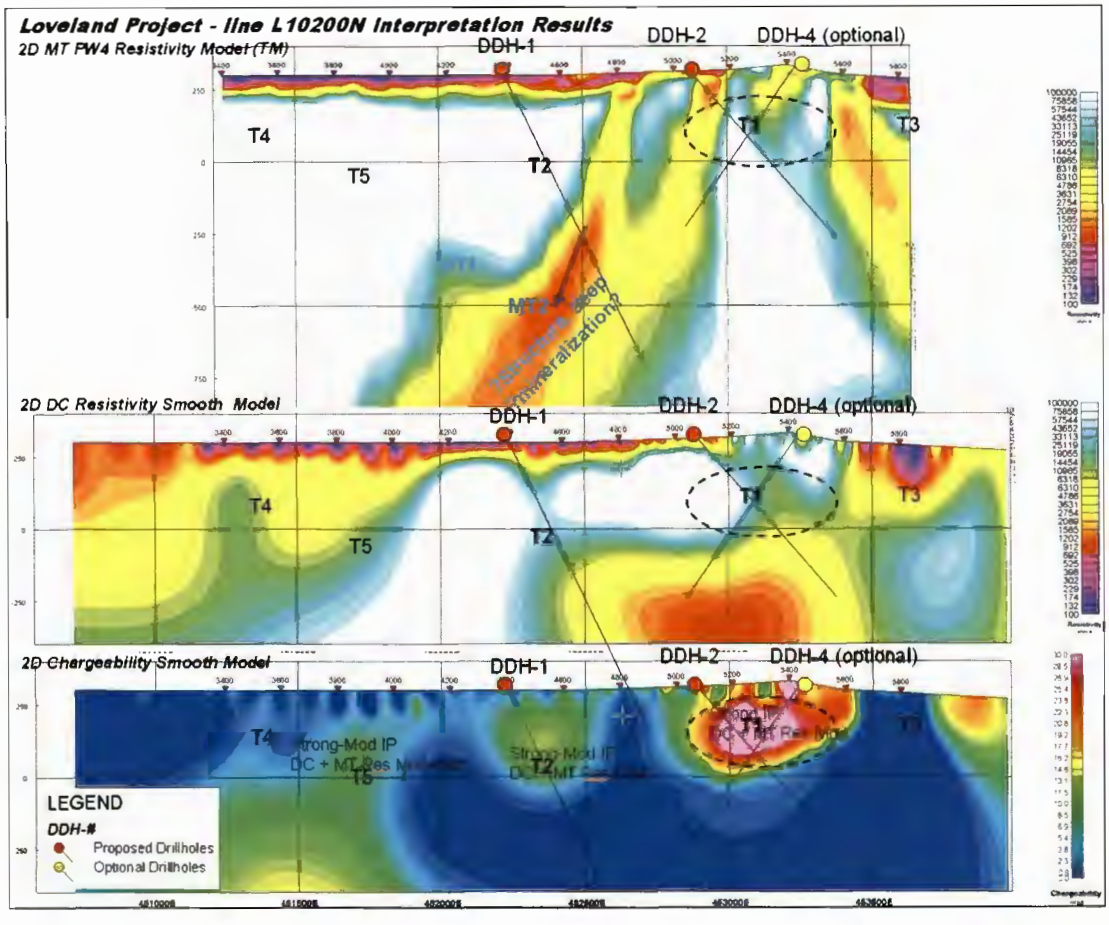

Figure 7: Anomalous zone T1 on line L10200N

The high resistivity association for this anomaly suggest semi-massive or more disseminated mineralization with significant zinc content.

The amplitude and extent of the IP response along with the DC and MT low resistivity association make this zone a high priority target for further exploration. Drillhole ***DDH-2*** has been recommended to target T1. A second optional hole ***DDH-4*** is recommended to test this signature in case no mineralization is documented in the first drillhole (see Table 2).

3.3.2 Moderate Priority Titan Anomalous Zones

Two (2) anomalous zones (T2 and T3) are classified as moderate priority for drill targeting at Loveland.

Anomalous zone T2 (moderate Priority)

This zone (T2) is located in the central part of the survey grid and extends from line L9900N at station 4400E, to L10800N at station 4600E, see Figure 8, Figure 9 and Figure 10.

This anomaly consists of a near surface moderate IP response (<15 milliradians) associated with moderate to low DC and MT resistivity response (<15000 ohm-meters). The southern part of the anomaly show stronger response with low resistivity association, and is probably associated with an increase in the sulphide mineralization. The MT model indicates a significant low resistivity anomaly beneath T2, indicating a deep source of mineralization.

No significant mineralization is documented for the south portion of T2. Although, zinc and copper sulphide mineralization have been documented on W-04-04 (on L10600N) at approximately 100m depth, explaining the source for this anomaly, see Figure 10.

The potential for T2 is located from line L9900N to L10200N. Drillholes ***DDH-1*** on L10200N at station 4400E, and ***DDH-6*** on L9900N at station 4500E are recommended for testing this Titan anomaly.

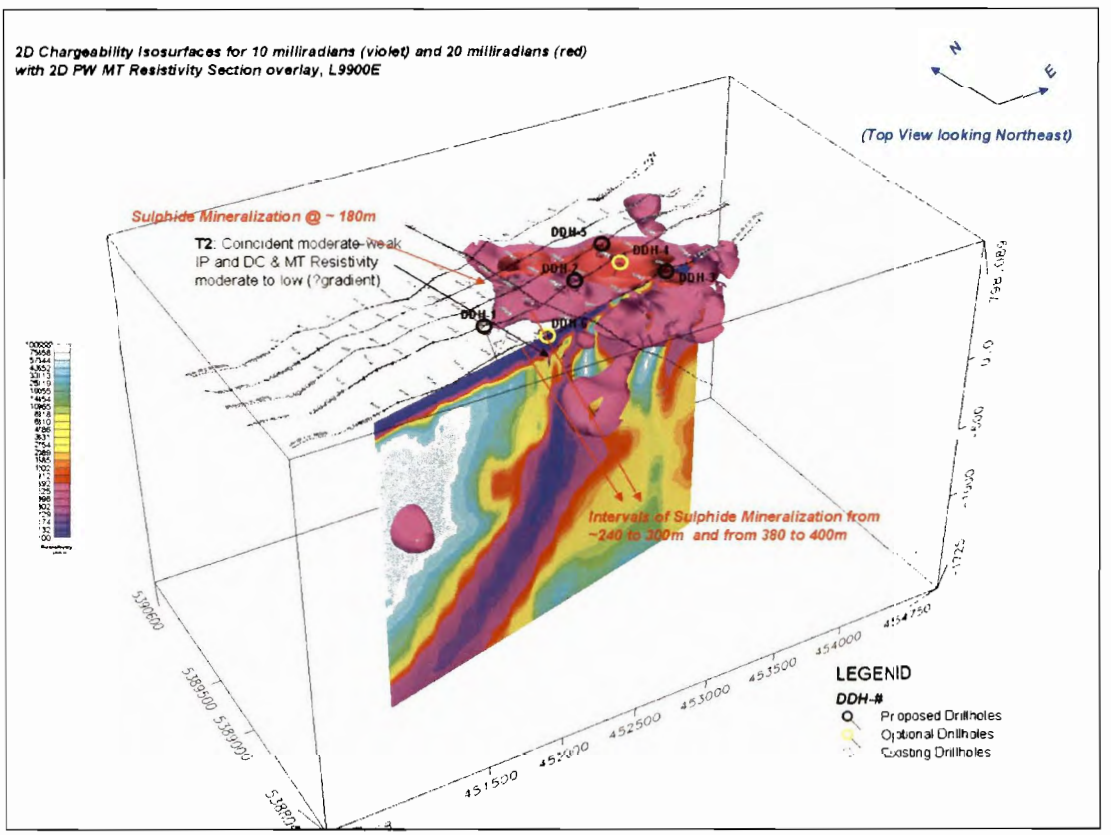

Figure 8: 3D View Depicting the Moderate Priority DCIP & MT Zone T2 on L9900N

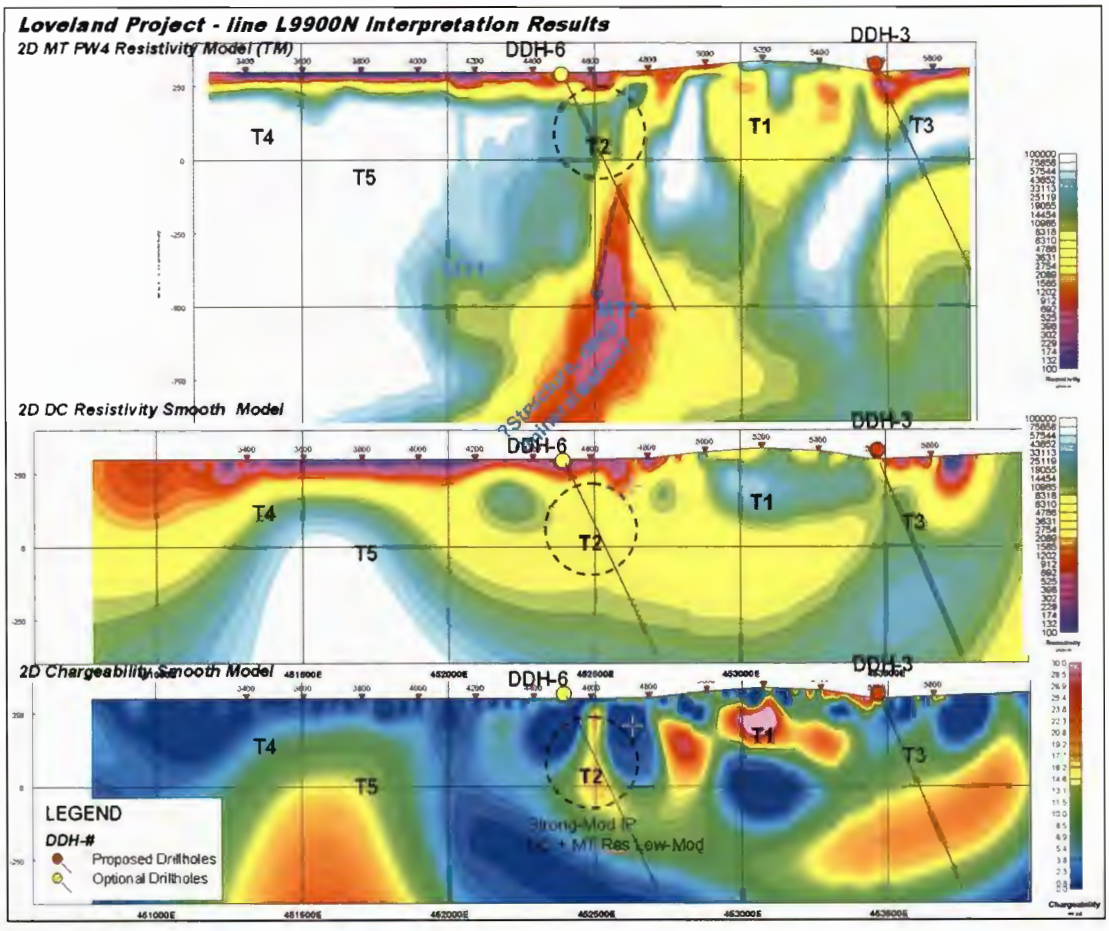

Figure 9: Anomalous zone T2 on line L9900N

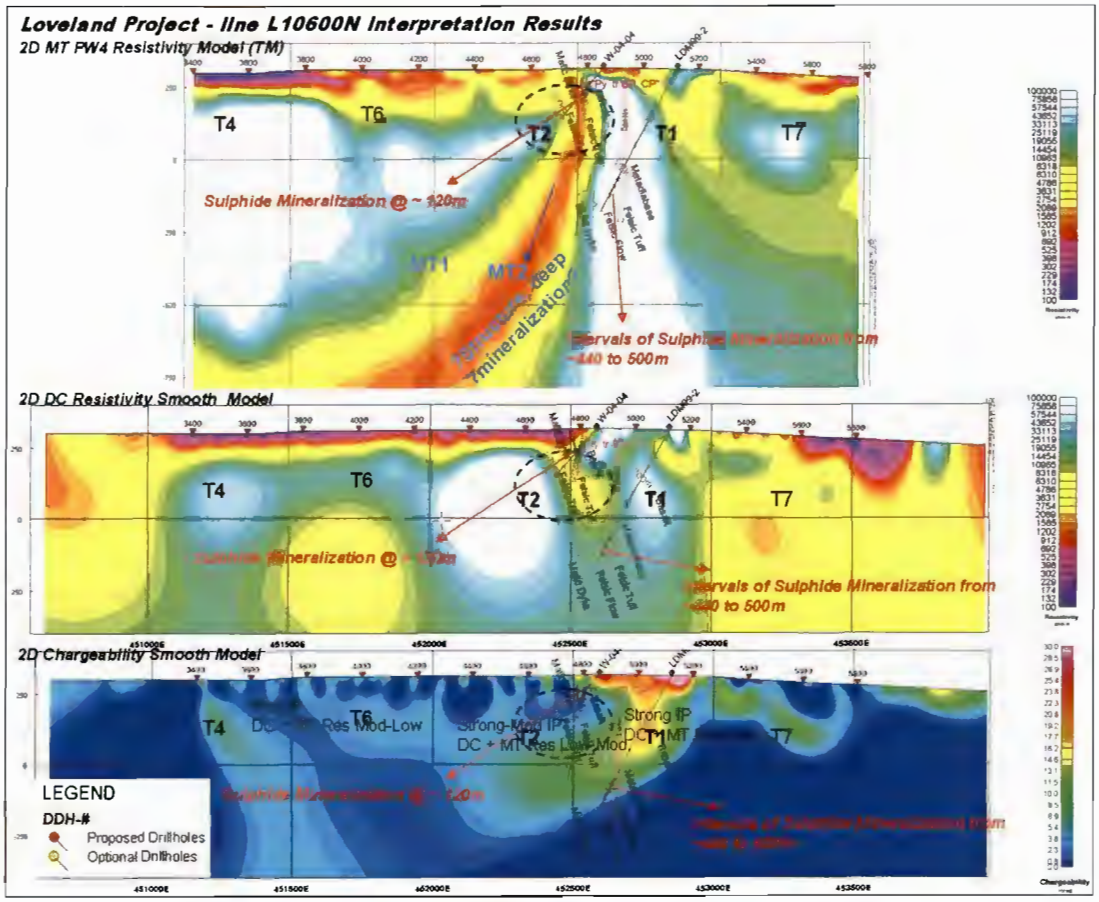

Figure 10: Anomalous zone T2 on line L10600N

Anomalous zone T3 (moderate Priority)

T3 is located in the eastern part of the survey grid and extends from line L9900N to L10200N at station 5800E, see Figure 12. This anomaly consists of a small area, and a moderate to weak IP response (<10 milliradians) associated with moderate DC and MT resistivity response (<5000 ohm-meters), which extends from near surface to approximately 300 meters depth. This anomaly is not well resolved to the east due to the limitations of the survey coverage.

The MT model exhibits a deep resistivity low located below the IP anomaly suggesting a deep source of mineralization, alteration or structure. No significant mineralization is documented over the east part of the anomaly. ***DDH-3*** is proposed to test T3 on L9900N at station 5600E.

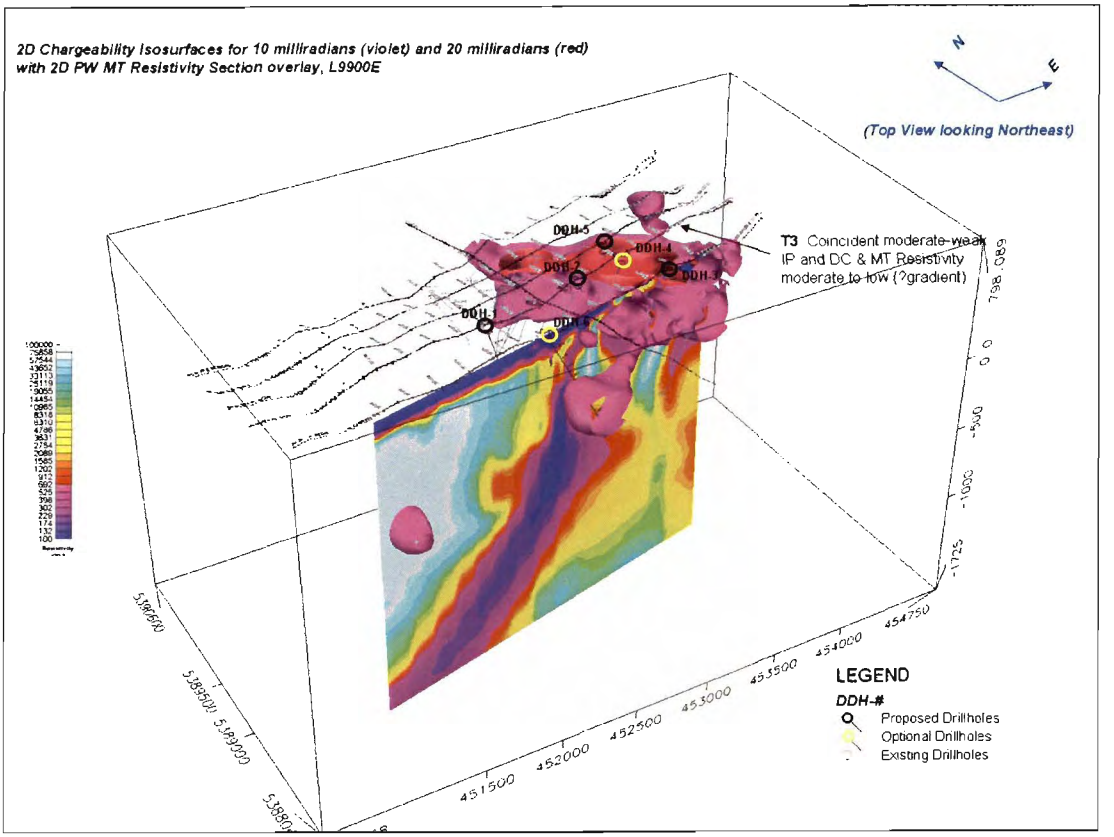

Figure 11: 3D View Depicting the Moderate Priority DCIP & MT Zone T3 on L9900N

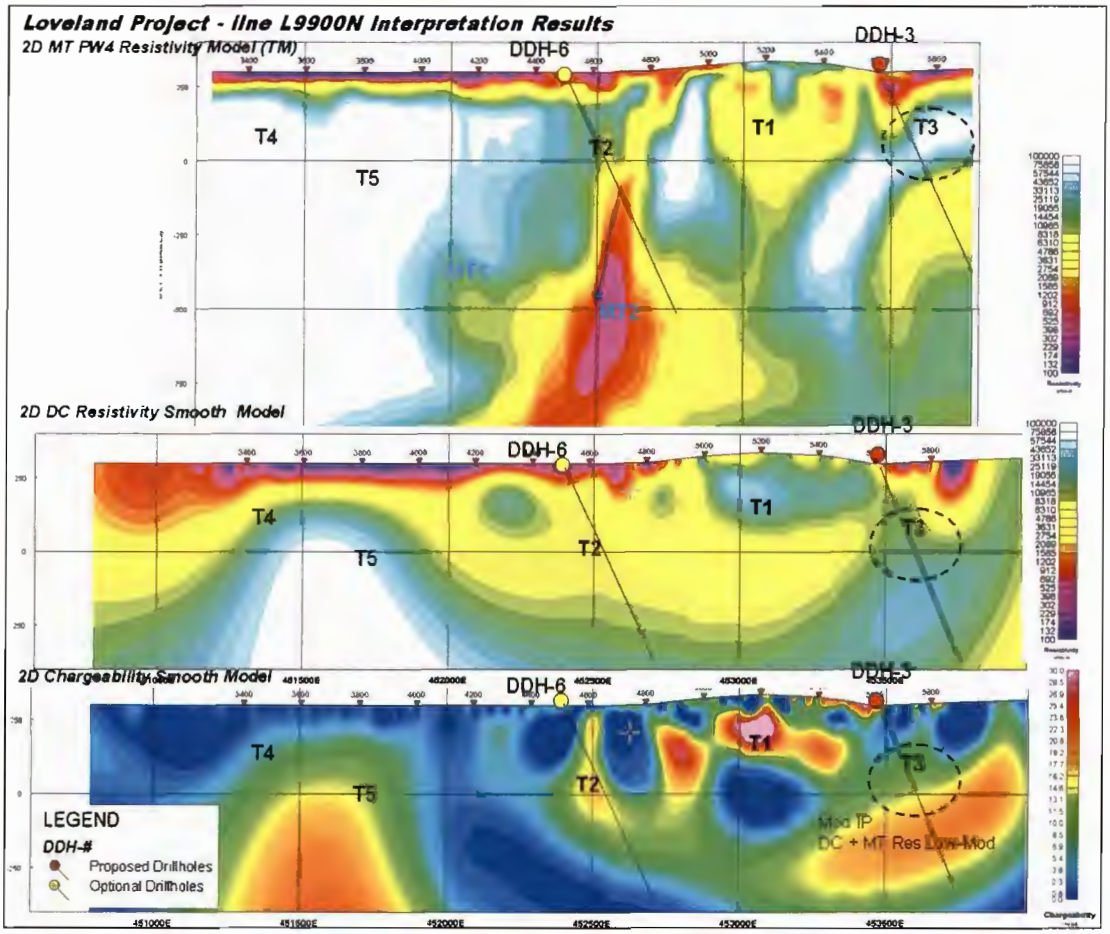

Figure 12: Anomalous zone T3 on line L9900N

3.3.3 Low Priority Titan Anomalous Zones

Four Titan anomalous zones (T4, T5, T6 and T7) are classified as low priority at Loveland. These anomalous zones consist of a small area, and a weak IP chargeability responses ranging in depth from near surface to only few hundred meters, see Figure 5.

Even though chlorite and sericite alteration is related to the low priority anomalous zones, they may represent significant exploration "pathfinders" for targeting deep potential zones at Loveland. Zinc and copper sulphide mineralization may also be encountered associated to near surface altered rhyolites and gabbro, and in the hanging walls of the fault systems and other geological contacts.

3.3.4 Deep MT Anomalous Zones

Two (2) deep Titan MT resistivity low anomalies (MT1 and MT2) are classified as low priority targets for follow up at Loveland (Figure 13).

Zinc and copper sulphide mineralization may be encountered in the footwall and fault systems or geological contacts (e.g. rhyolite and gabbro units) in excess of 500 meters depth. Chlorite and sericite alteration may be also related to the anomalous conductive MT zones and consequently they may represent significant exploration targets for deep mineralization at Loveland.

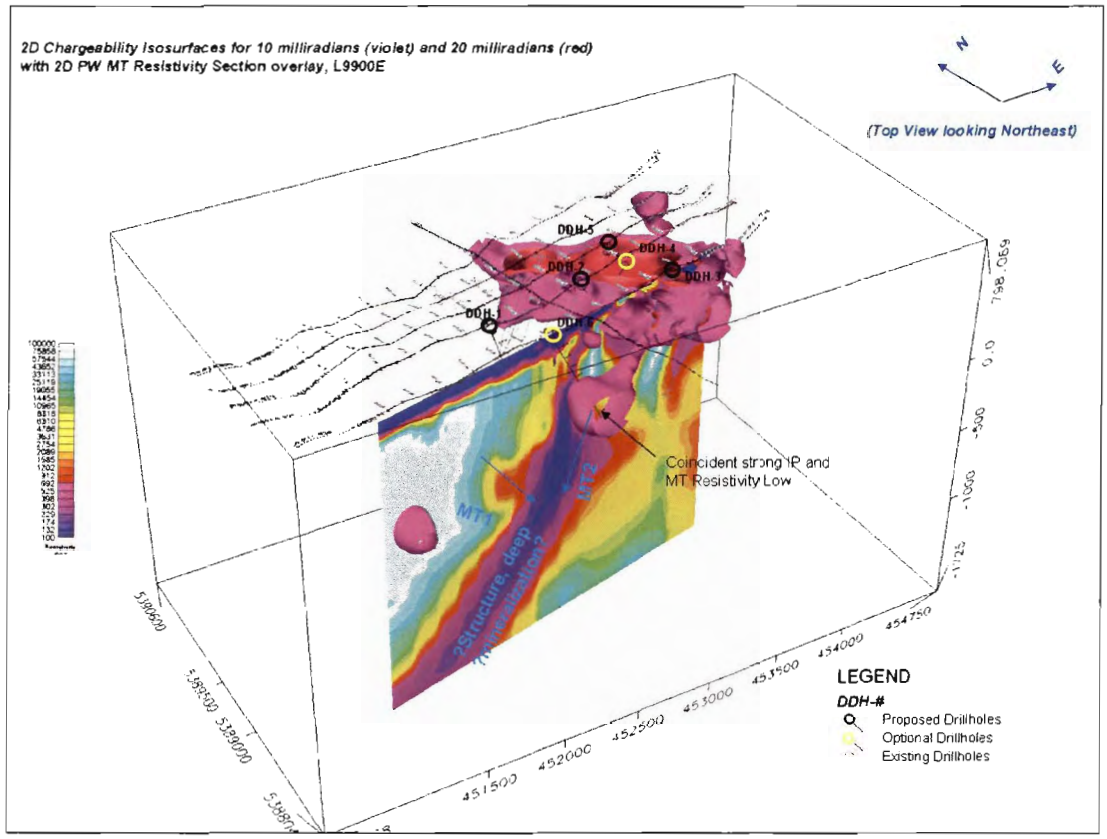

Figure 13: 3D View Depicting the Deep MT Zones MT1 & MT2 on L9900N

The interpreted MT anomalies may be caused not only by the presence of zinc and copper sulphide mineralization at depth. Iron sulphide, graphite and other rock forming minerals, alteration zones, geological structures (magnetic gabbro dykes), or a combination of the aforementioned factors can be the source of these Titan responses.

In cases where the deep MT anomalies are an extension of the shallower Titan DCIP chargeability and MT anomalies, a higher priority may be assigned to these responses if significant results are encountered when targeting the upper shallower anomalies.

Additional information on the inversion models and parameters are included in ***Appendix G*** and ***Appendix I***. Plan Maps and Sections in Geosoft format are also included in these appendices.

4. CONCLUSION AND RECOMMENDATIONS

4.1 CONCLUSIONS

The Titan-24 survey has successfully identified geophysical anomalies in the DCIP and MT raw data and inversion models which may represent zinc and copper VMS mineralization and/or alteration zones from near surface up to approximately 700 meters depth.

The MT inversion models show good resolution of the anomalies to approximately 1.5 kilometer depth. The DCIP & MT interpretation could possibly be affected by structures, which run parallel and/or sub-parallel to the survey lines.

The interpreted DCIP and MT anomalies and the target prioritization were mainly based on the anomaly amplitude, extent, the Titan multi-parameter association, and the available geological and sulphide mineralization on the property. However, the interpreted anomalies may not necessarily be related to zinc and copper mineralization. Other sources, such as iron-rich formations, graphite, clay and fault systems can produce similar DCIP and MT responses.

A total of seven (7) DCIP and MT anomalous zones have been identified for follow-up at Loveland. One (1) zone has been classified as high priority exploration target for zinc and copper sulphide mineralization at depth. Two (2) zones have been classified as moderate priority, and four (4) Titan anomalous zones represent low priority. In addition, the MT inversion models have resolved two (2) deep anomalous zones from approximately 600 meters to >1.5 kilometers depth that may represent deep mineralization, alteration zones, feeder channels and/or structures., see Table 2 and Figure 14.

4.2 RECOMMENDATIONS

The following recommendations are derived from the interpretation at Loveland:

1. Drill testing the high priority target ***T1***.
2. If favourable drill results are obtained when drilling the high priority zones, then the moderate priority targets T2 and T3 should be drilled.
3. Review and evaluate all available geological and geochemical data in the vicinity of the low priority areas *T4*, *T5*, *T6* and *T7* for further targeting these zones.
4. If mineralization is encountered when drilling the anomalies above the deep targets, consider extending the drilling to test the deep source of the MT responses.
5. When the deep MT targets (***MT1*** and ***MT2***) are drilled, follow up with downhole BHTEM, and consider physical property logging on all drilled Titan targets to understand and explain the source of the responses observed.
6. Integrate all available geo-scientific information into 3D Gocad earth model and perform physical property and 3D query evaluation to corroborate the interpreted Titan anomalies.
7. Examination and/or acquisition of additional surficial geophysical data (Gravity, Magnetics, TEM, etc) to further enhance the interpretation and drill targeting is recommended.

Titan Anomaly	Priority	Center Coordinates of the Target					TITAN Parameters		Proposed Drill Target					Comments
		Line	Station	UTM –E	UTM-N	Depth (m)	IP (mrads)	Resistivity (Ohm-m)	Hole ID	Ln/Stn	Depth (m)	Dip (°)	Azimuth (°N)	
T1	**High**	**L10200N**	**5300E**	**452911**	**5389449**	**~50**	**>20**	**<15000**	**DDH-2** **DDH-4**	**L10200N /5100E** **L10200N /5450E**	**700**	**~50**	**~74** **~254**	*Optional DDH-4*
T2	Moderate	L10200N	4500E	452223	5389292	~50	15-20	<15000	DDH-1 DDH-6	L10200N /4400E L9900N /4500E	700 1100	~70	~74	*Optional DDH-6*
T3	Moderate	L9900N	5700E	453459	5389273	~50	15-20	<15000	DDH-3 DDH-5	L9900N /5600E L10200N /5450E	700	~50	~74	*DDH-5 optional to test the DC resistivity anomaly*
T4	*Low*	*L10800N*	*3500E*	*451200*	*5389700*	*>150*	*<10*	*>15000*	*	*	*	*	*	
T5	*Low*	*L10200N*	*3900E*	*451600*	*5389148*	*>100*	*<10*	*>15000*	*	*	*	*	*	
T6	*Low*	*L10600N*	*4000E*	*451800*	*5389600*	*>100*	*<10*	*>15000*	*	*	*	*	*	
T7	*Low*	*L10600N*	*5600E*	*453500*	*5390000*	*>100*	*<10*	*>15000*	*	*	*	*	*	
MT1	Low	*L10800N*	*3900E*	*451400*	*5389700*	*>500*		*<15000*	*	*	*	*	*	
MT2	Low	*L9900N*	*4700E*	*452500*	*5389100*	*>500*		*<5000*	DDH-6	L9900N /4500E	1100	~70	~74	*Optional DDH-6*

Table 2: DCIP & MT Anomaly Table and Recommended Drill Targets

The proposed drillholes are designed to test the DCIP and MT anomalies and associated structures based on the criteria of sub-vertical features slightly dipping to the west, as indicated in the inversion models. West dipping drillholes may be adequate to test geology or structures plunging to the east.

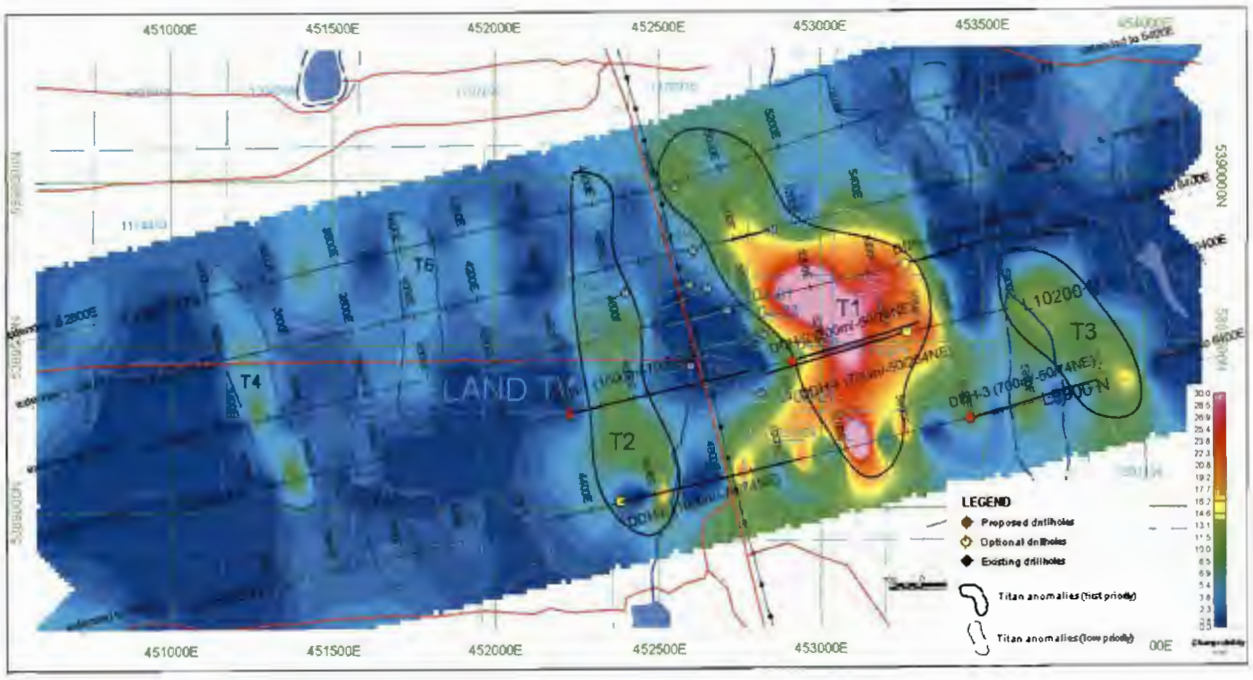

Figure 14: Titan Interpretation Plan Map over 2D Chargeability at 100m Depth

RESPECTFULLY SUBMITTED BY
QUANTEC GEOSCIENCE LTD.

Robert Hearst, M.Sc., P.Geo
Senior Geophysicist
Manager- Interpretation Group

Evelio Martinez, M.Sc., P.Geo.
Senior Geophysicist
Interpretation Group

Toronto ON
May, 2008

4.3 REFERENCES

- de Lugao, P.P., and Wannamaker, P.E. (1996). *Calculating the two-dimensional Magnetotelluric Jacobian in finite elements using reciprocity.* Geophysical Journal International, v. 127, pp. 806-810.
- Martinez, E., (2008). *Regarding the Quantec TITAN-24 Distributed Acquisition System TENSOR Magnetotelluric and DC Resistivity & Induced Polarization Surveys over the Loveland Project, near Timmins, ON, for WESTERN KIDD Resources Ltd.* Quantec Geoscience Ltd., Toronto, Canada.
- Galley, A., Hannington, M. and Jonasson, I. (2007). *Volcanogenic Massive Sulphide Deposits.* Vancouver, BC: Geological Survey of Canada.
- Oldenburg, D. and Li, Y. (1994). *Inversion of induced polarization data.* Geophysics, v. 59, pp. 1327-1341.
- Rodi, W., and Mackie, R.L. (2001). *Nonlinear conjugate gradients algorithm for 2-D magnetotelluric inversion.* Geophysics, 66, 174-187.
- Sheard, N. (1998). *MIMDAS: A new direction in geophysics.* Proceedings of the ASEG 13th International Conference, Hobart, Tasmania.

APPENDIX A - STATEMENT OF QUALIFICATIONS

I, Evelio Martinez del Pino, declare that:

1. I am a Geophysicist with residence in Hamilton, Ontario and am presently employed in this capacity with Quantec Geoscience Ltd., Toronto, Ontario.

2. I obtained a Bachelor's Degree in Engineering Geophysics at ISPJAE University in La Habana, CUBA, in 1993, and a Masters Degree in Applied Geophysics (M.Sc.) at the ITC in Delft, The Netherlands, in 2000.

3. I am a registered geoscientist, since 2004, with license to practice in the Province of Ontario, (APGO Lic. # 1058).

4. I am a member of the American Geophysical Union (AGU).

5. I have practiced my profession continuously since September 1993, in Cuba, The Netherlands, Portugal, and Canada.

6. I have no interest, nor do I expect to receive any interest in the properties or securities of **Western Kidd Resources Inc.**, its subsidiaries or its joint-venture partners.

7. I am the qualified Geophysicist and the supervisor for this project. I am responsible for the data acquisition, quality and compilation of the final processed results. I authored this interpretation report and I am responsible for the 2D DCIP and 2D MT inversions, compilation and geophysical data interpretation. I attest that the supplied information accurately and faithfully reflect the data acquired on site. The statements made in this report represent my professional opinion based on my consideration of the information available to me at the time of writing this report.

Toronto, Ontario
May, 2008

Evelio Martinez del Pino, M.Sc., P. Geo (ON).
Senior Geophysicist. Interpretation Group
Quantec Geoscience Ltd.

APPENDIX A

STATEMENT OF QUALIFICATIONS

I, Robert Hearst, declare that:

1. I am a Geophysicist with residence in Toronto, Ontario and am presently employed in this capacity with Quantec Geoscience Ltd., Toronto, Ontario.

2. I obtained a Bachelor of Science Degree with Honours (H.B.Sc.) in Geophysics and Geology, from the University of Western Ontario in London, Ontario in 1983, and a Master of Science Degree (M.Sc.), Geophysics and Geology, from McMaster University in Hamilton, Ontario in 1996.

3. I am a registered geophysicist, since 1992, with license to practice in the Northwest Territories and Nunavut (NAPEGG Licensee L935); a registered geophysicist, since 2006 with license to practice in the Province of Alberta (APEGGA member # M89621); a registered geoscientist, since 2006 with license to practice in the Province of Ontario (APGO member # 1415).

4. I am a member of the Society of Exploration Geophysicists (SEG); the Canadian Exploration Geophysical Society (KEGS); Prospectors and Developers Association of Canada (PDAC); Canadian Institute of Mining and Metallurgy (CIMM, National Branch); and the Environmental and Engineering Geophysicists Society (EEGS).

5. I have practiced my profession continuously since June 1983, in North America, South America, Africa, Asia, the Middle East, South East Asia, and Europe.

6. I have no interest, nor do I expect to receive any interest in the properties or securities of **Western Kidd Resources Inc.**, its subsidiaries or its joint-venture partners.

7. I am the Professional Geophysicist responsible for reviewing and preparation of this project. I co-authored this interpretation report and I can attest that these accurately and faithfully reflect the data acquired on site. The statements made in this report represent my professional opinion based on my consideration of the information available to me at the time of writing this report.

Toronto, Ontario
May, 2008

Robert Hearst, MSc. P. Geo.
Manager - Interpretation Group
Quantec Geoscience Ltd.

APPENDIX B - PRODUCTION SUMMARY

DATE	DESCRIPTION	LINE	START	END	READ (mi)		TOTAL (mi)	
					MT	IP	MT	IP
December 3, 2007	Mob to Timmins							
December 4, 2007	Unpack Gear - set up utility room Set up Infinite, Run Parallel Sensor Test							
December 5, 2007	Finish Parallel Sensor Test, set up Remote Site Unable to get line up and stable to run MT							
December 6, 2007	Transmitter problems - no IP read Read MT	L10800N L10800N	3400E	5800E			0.00	0.00
December 7, 2007	Read IP - noise due to improper grounding of Doghouse - need to repeat Repeat Low Frequency MT - Low signal	L10800N	3400E	5800E	2400		2.40	0.00
December 8, 2007	Repeat IP	L10800N	3400E	5800E		2400	2.40	2.40
December 9, 2007	Read IP Read MT	L10600N	3400E	5800E	2400	2400	4.80	4.80
December 10, 2007	Read IP Read MT	L10400N L10400N	3400E	5800E	2400		7.20	4.80
December 11, 2007	Finish IP Read MT	L10400N L10200N	3400E	5800E		2400	7.20	7.20
December 12, 2007	Read IP Repeat MT: Low Frequency 4800E - 5800E	L10200N L10200N	3400E	5800E	2400	2400	9.60	9.60
December 13, 2007	Read IP Read MT	L9900N L9900N	3400E	5800E	2400		12.00	9.60
December 14, 2007	Finish IP Pick up line	L9900N	3400E	5800E		2400	12.00	12.00
December 15, 2007	Finish Packing gear Demob							

TOTAL SURVEY DAYS	**13**
READ TIME	9
BREAK DOWN DAYS	0
SET UP DAYS	2
MOBILIZATION DAYS	2
WEATHER DAYS	0

TOTAL PRODUCTION: DC & IP: 12.00 Km
MT: 12.00 Km

APPENDIX C - MAGNETOTELLURIC (MT) THEORY

The magnetotelluric (MT) method measures time-variations in the Earth's natural electric (E) and magnetic (H) fields to image the subsurface resistivity structure. No source or transmitter is used. These natural fields penetrate much deeper than is practical with a transmitter. At the same time the natural signals are a plane-wave source. The plane-wave source is much simpler to model than complex transmitter geometries and signals.

The E and H fields are measured over a broad range of frequencies. Typically, the frequencies can range from above 10 kHz to below 0.001Hz. High frequency signals are attenuated more rapidly in the subsurface. High frequency data are indicative of shallow resistivity structure while low frequency data are indicative of deep resistivity structure.

At frequencies below 1Hz the signal source is due to oscillations of the Earth's ionosphere as it interacts with the solar wind. At frequencies above 1Hz the signal source is due to worldwide lightning activity. There is a lack of signal around 1Hz, often referred to as the "hole". Modern 24-bit recording hardware and signal processing techniques have largely eliminated the data quality problems that have been traditionally seen around the 1Hz signal hole.

Between about 8Hz and 300Hz the signal from worldwide lightning activity propagates in a "resonant" cavity (the resistive atmosphere) between the conductive ionosphere and the Earth's surface. Above 3 kHz the signal propagates as a ground wave. Between 300Hz and 3 kHz there is a "dead-band" where the signal does not propagate well. Despite hardware and signal processing improvements this dead-band remains problematic. When signal (atmospheric activity) is present within several hundreds of miles of the survey area the data is quite good. When no signal is being generated in the vicinity data quality is poor.

Both the electric and magnetic fields are measured. The measured fields depend on the ionosphere and lightning, and are essentially random. While the E and H fields are random the ratio of the fields depends on the subsurface resistivity structure. Note that it is primarily the orthogonal E and H fields that are related. The magnetic field must be measured perpendicular to the electric field. It is possible for complex subsurface resistivity structure to rotate the fields, and full tensor data are usually measured.

It is often useful to think of the magnetic field as the source signal and the electric field as the response. Time variations in the magnetic field induce currents to flow in the ground.

In the field the electric and magnetic fields are measured as a function of time. The electric field is measured using two orthogonal dipoles consisting of a wire connecting two grounded electrodes. In essence, the recording system consists of a voltmeter between the electrodes. The voltage measured depends on the electric field strength and the length of the dipole. The magnetic field is measured using an induction coil.

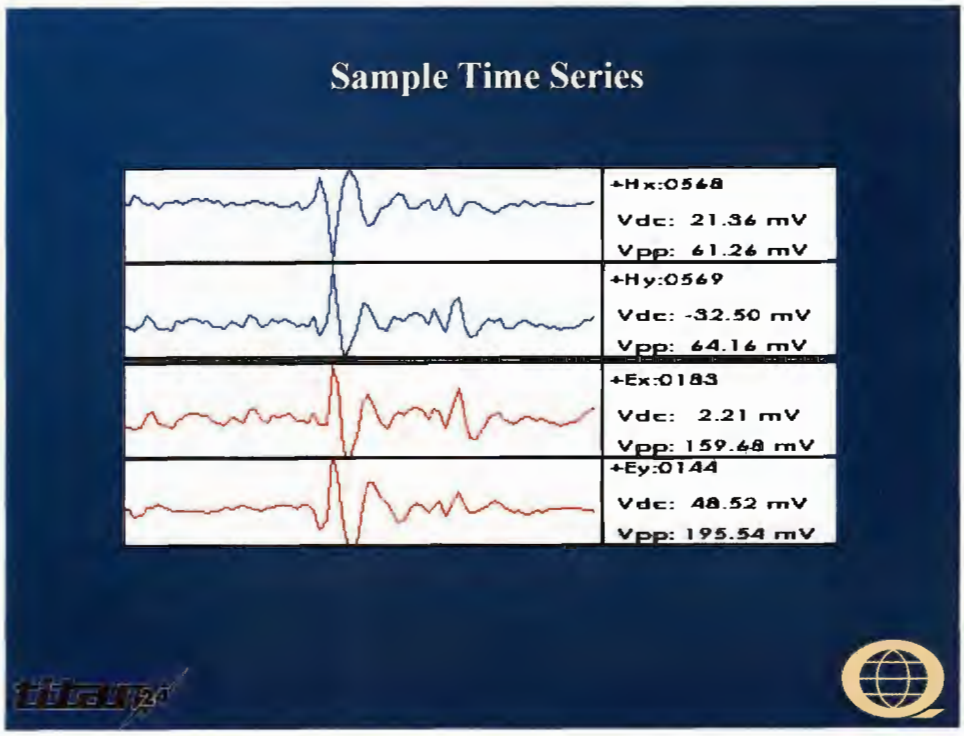

While the actual fields that are measured vary randomly (with solar and lightning activity), the relationship between the measured magnetic and electric fields is constant and depends on the subsurface resistivity structure. Extracting the subsurface resistivity structure from the measured magnetic and electric fields is a multi-step process. First time series processing techniques are used to derive geophysical parameters from the electric and magnetic fields. Then geophysical processing and inversion techniques are used to convert the geophysical parameters to a subsurface resistivity image. Finally, the resistivity image must be interpreted in terms of geologic units.

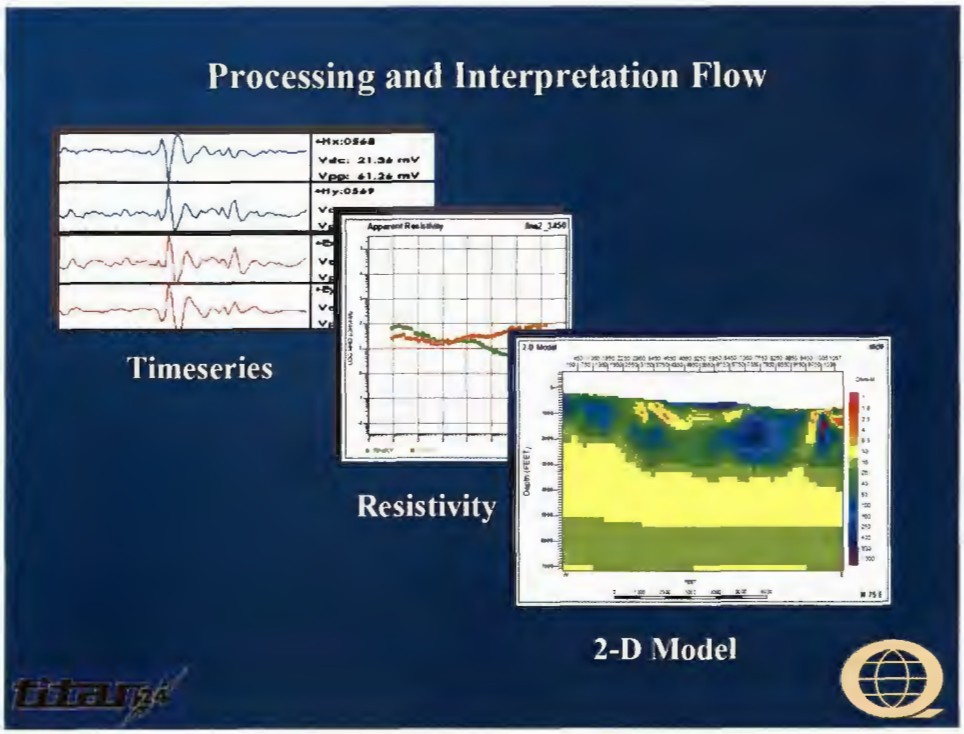

The measured magnetic and electric fields are Fourier transformed into the frequency domain. The system response is removed from the data (making the measurement independent of the hardware system). The Fourier coefficients represent the amplitude and phase of the electric and magnetic fields as a function of frequency.

A variety of signal processing techniques are used to minimize noise and bias in the estimation of geophysical parameters from the measured fields. The details are complex, but the approach is easily understood. Philosophically, the idea is to use multiple approaches to noise and bias reduction, not letting any one statistical approach have too much impact on the data, but relying on the combination of approaches to produce good estimates. The approaches include:

1. Spatial isolation of noise. A remote reference magnetic station is used to separate widely distributed signal from local noise.
2. Coherency sieves to find coherent signal. First the local and remote magnetic field measurements are compared and coherent signal kept. Then the local magnetic and electric fields are compared for coherency.
3. Frequency isolation of noise. Long Fourier transforms are used to provide extremely sharp isolation of noise in frequency.
4. Time isolation of noise. Short Fourier transforms are used to remove noise that is isolated in time (noise spikes, or noise that is randomly turning off and on).
5. Robust statistics that minimize biasing effects of a few isolated measurements.

Once the time series processing is complete geophysical parameters can be estimated. The primary geophysical parameters for MT are typically the apparent resistivity versus frequency and phase versus frequency.

The depth of penetration of the signal depends on its frequency and the resistivity of the rocks. The depth at which the signal amplitude has been attenuated to 37% (1/e) is called the skin depth and is defined:

$$\delta = \sqrt{\frac{2}{\mu\omega\sigma}} = 503\left(\sqrt{\frac{\rho}{f}}\right)(m)$$

where

δ = skin depth

μ = magnetic permeability

σ = conductivity=1/resistivity

ω = angular frequency=$2\pi f$

ρ=resistivity=1/conductivity

The ratio between the two measured components (E and H) is the electrical impedance. The impedance (denoted Z) is defined as $|Z| = |E/H|$. The impedance is a complex number because the E and H fields are out of phase. Note that Z, E, and H are all functions of frequency.

The complex impedance is used to calculate an apparent resistivity as follows:

$$\rho_a = \frac{1}{\mu\omega}|Z|^2 (ohm.m)$$

The apparent resistivity is also a function of frequency. At any frequency the fields must travel through the overlying geology. The apparent resistivity depends on the integrated (weighted) conductance of the rocks being sampled. It is a smoothly varying function of frequency because it represents the average resistivity of a progressively larger volume of the subsurface. On a log resistivity-log frequency plot the apparent resistivity generally can not exceed a slope of +/- 45 degrees.

The phrase "apparent resistivity" arises from the volume averaging. At a single frequency the electric and magnetic fields measurements can be used to calculate an impedance. This impedance depends on the resistivity of a large volume of the subsurface. The impedance can be thought of as the impedance of a half-space that would provide identical measurements to the actual subsurface.

The calculated phase or apparent phase is the difference between the measured E field phase and the measured H field phase. If the subsurface is one-dimensional (1D) or two-dimensional (2D) the phase is related to the resistivity. The Hilbert formula (minimum phase wavelet) relates the phase to the slope of the apparent resistivity curve. If the slope of the resistivity curve (on a log-log plot) is 0 the phase is 45 degrees. If the resistivity is increasing with decreasing frequency the phase is less than 45 degrees. If the resistivity is decreasing with decreasing frequency the phase is more than 45 degrees. As the apparent resistivities are constrained to a slope of no more than 45 degrees on a log-log plot, the phases are constrained to remain in a quadrant, between 0 and 90 degrees.

The phase measurement is largely independent of the apparent resistivity measurement. The Hilbert relationship provides an independent way to calculate the apparent resistivity curve from the phase data. There are effectively two independent measurements of the resistivity curve, providing a powerful check on data quality.

The apparent resistivity and phase curves are the primary parameters used in the interpretation of MT data. For a layered (1D) earth the apparent resistivity and phase data can be converted into intrinsic resistivity versus depth simply by accounting for the volume averaging nature of the method. There are a variety of algorithms for doing the conversion. The conversion is not unique. Some algorithms provide smoothly varying intrinsic resistivity versus depth functions (Occam inversion, Bostick transform). Others provide distinct layered solutions (Marquardt inversion).

1D modeling and inversion raises the following points:

- A single MT site provides information about resistivity versus depth. This is a major distinction from potential fields techniques that only provide information about relative variations along a profile.
- The conversion from apparent resistivity versus frequency to intrinsic resistivity versus depth is not unique. It is susceptible to equivalence. In particular any sharp resistivity contrast can be replaced by an equivalent transition zone.
- In a layered model the thickness of a resistive layer is well resolved. The resistivity of a resistive layer is poorly resolved.
- In a layered model the conductance (conductivity*thickness) of a layer is resolved. Neither the thickness nor the conductivity is uniquely resolved.
- Once the constraint that the subsurface is composed of distinct, resolvable, units is imposed the 1D inversion of MT data is essentially unique. Resolution is excellent (better than 5% of depth).

Apparent resistivity versus frequency is the most fundamental way of looking at the data in the interpretation phase. While the overall process is complex, with advanced processing techniques and inversions, it is important to keep in mind that the subsurface structures are apparent in the raw data – the apparent resistivity plots.

The following sequence of illustrations is intended to introduce the apparent resistivity versus frequency sounding curves. But it is also intended to highlight the relatively complex, but understandable, relationships between the observed data and subsurface structure.

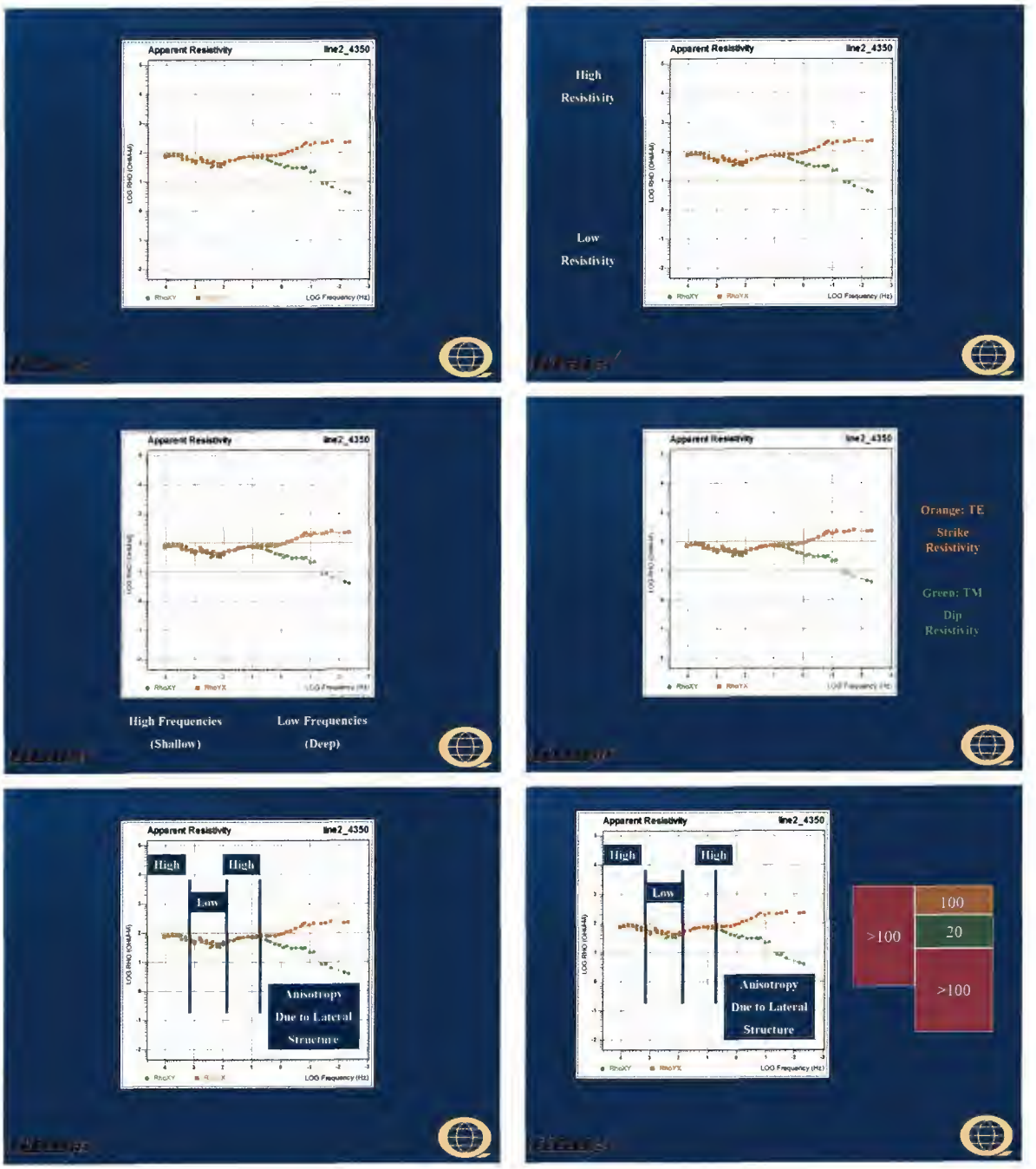

A simple layered subsurface structure is not generally the problem of immediate interest in exploration. In the case of more complex two-dimensional (2D) or three-dimensional (3D) structure the MT response will be affected by lateral resistivity variations.

The MT measurement relies on natural, plane-wave, source signals. The measured response depends on lateral resistivity variations as much as (or more than) resistivity variations below the immediate sounding site.

Full tensor measurements of the E and H fields are made at every site. For each site there are two apparent resistivity sounding curves (or modes) and phase curves. These two modes are arbitrarily

labeled Rho-XY and Rho-YX. The first, Rho-XY, refers to the apparent resistivity (Rho) calculated from Ex and Hy.

Once full tensor measurements are made in the field it is possible to mathematically rotate the fields to any arbitrary coordinate system. Traditionally, the data are rotated independently at each frequency to maximize the difference between the two apparent resistivity sounding curves. This puts the data into "geologic" or "principal" coordinates.

One sounding curve will have the electric field in the geologic strike direction and is referred to as "Transverse Electric" or TE. The other mode will have the electric field in the geologic dip direction and is referred to as "Transverse Magnetic" or TM. Note that TE and TM are interpretive designations, and refer to geologic strike. XY and YX were simply geometric designation.

For a layered (1D) earth the two measurements are identical. When the structure is 2D or 3D the lateral resistivity variations will distort (often severely) the simple 1D response. The distortion of the fields by complex structure is realized in the apparent resistivity data as "anisotropy". This is a divergence between the two apparent resistivity sounding curves.

The measurement of two orthogonal apparent resistivity sounding curves provides valuable information. Both curves reflect the resistivity structure underlying the site. Both curves will show increasing or decreasing resistivity at a frequency in response to resistivity structure under a site. The two apparent resistivity curves will diverge in response to lateral resistivity variations.

If the site is located on the resistive side of a lateral resistivity contrast the TE mode will be slightly suppressed due to the contact and the TM mode will be significantly biased up by the contact. If the site is located on the conductive side of a lateral resistivity contrast the TE mode will be slightly biased up while the TM mode will be significantly biased down by the contact.

For a 2D resistivity structure the TE mode is always providing an indication of the integrated conductance of the volume being sampled. It will always be a slowly varying function of position. The TM mode is responding dramatically to the presence of changes on the lateral resistivity boundaries, and will dramatically overshoot on the resistive side of a contact and undershoot on the conductive side. The anisotropy (divergence of the two sounding curves) is diagnostic of a lateral resistivity contrast.

The following simple model demonstrates most of the critical 2D behaviours. The model consists of a 100 Ohm-m host with a 10 Ohm-m basin on the right. There is a 1 Ohm-m layer buried within the host and below the basin. The response is shown at two sites, one immediately on the resistive side of the basin contact and the other immediately on the conductive side of the contact.

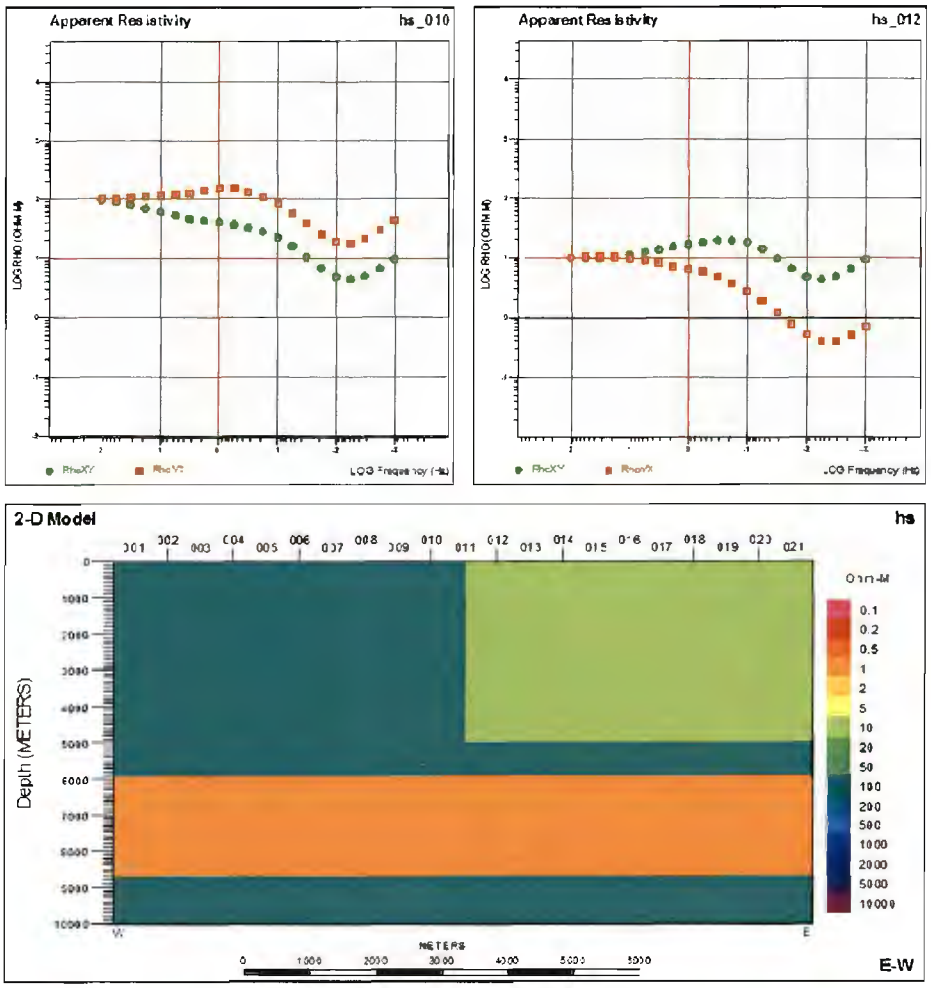

The following observations summarize the behaviour of 2D MT responses:

- The apparent resistivity at high frequencies reflects the true shallow resistivity.
- The apparent resistivities converge at high frequencies to the true shallow resistivity.
- The divergence in apparent resistivities occurs at a higher frequency for the site on the resistive side of the contact. Because the skin depth is larger in the resistive media the site on the resistive side of the contact is effectively "closer" to the contact than the site on the conductive side of the contact. The TE mode is constrained to the range of physical resistivities actually present in the model
- The TE mode "volume averages" the intrinsic resistivity. The TM mode exhibits apparent resistivities outside the range of physical resistivities in the model. Note that for the site on the right the TM mode indicates resistivities below 1 Ohm-m.
- Both the TE and TM modes respond in tandem, at the same frequency, to resistivity structure under the site. At both sites both the TE and TM modes indicate the top and bottom of the 1 Ohm-m layer. While 1D inversion of the TE and TM modes would place different apparent depths to the 1 Ohm-m layer the response is at the same frequency in both modes indicating it is the response of one layer.
- The intrinsic resistivity of the 1 Ohm-m layer is difficult or impossible to discern. Without physical property data only the conductance of the layer can be resolved.

These effects can also be clearly seen in pseudo-sections of the TE and TM apparent resistivity response of the model:

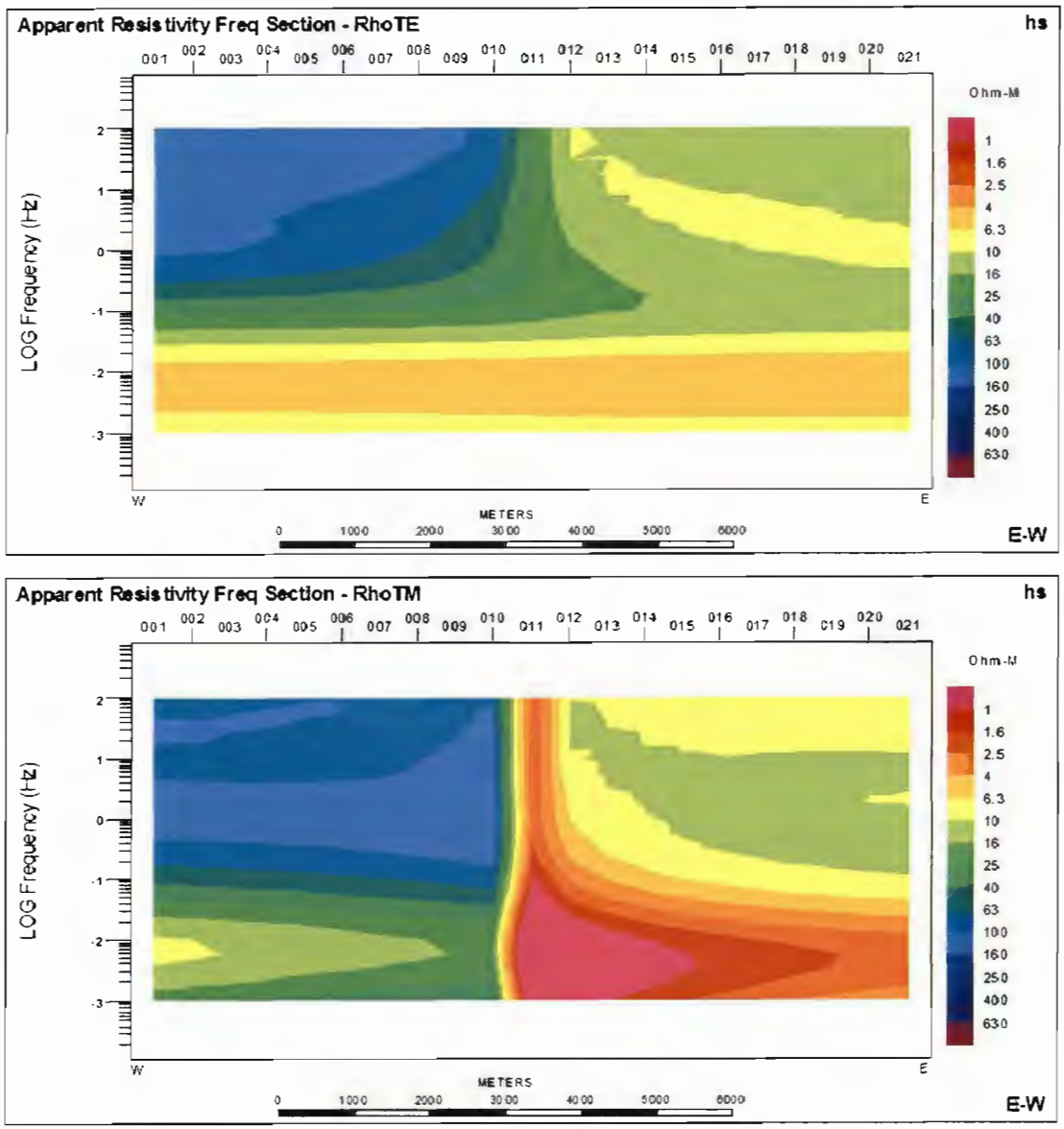

The apparent resistivity data at each site have been contoured, as a function of frequency. The inherent smoothness of the TE section can be clearly discerned. The distinctive "undershoot" of the TM response on the conductive side of the contact can be clearly seen.

One of the key factors in multidimensional MT data is "static shifts". The apparent resistivity sounding curves can be biased, up or down, by lateral resistivity contrasts too small to be resolved by the MT data. The curve is essentially DC shifted on the log-log apparent resistivity plot. This can be seen by examining the sounding curves from the previous 2D model. Assuming data had not been acquired above 1Hz the two sounding modes would be seen to be separated in the highest frequency data. Note that there are no static shift effects in the phase data.

Inversions and forward modeling are used to derive the subsurface resistivity structure from the data. The primary interpretation tools are 2D inversions. Problems emerge when the real world, complex, data are not consistent with the simplistic 2D assumptions. In a perfect world we would use modeling and inversion programs capable of reflecting the full complexity of the subsurface. However, in practice incorporating too much complexity in the modeling and inversion programs results in very coarse models which are incapable of resolving exploration targets. Instead, we must find ways to remove some of the complexity from the actual data. To this end, we have developed the Titan "EVA" data processing stream:

- Rotation to principal coordinates. The inversion algorithms presume that we have acquired a true geologic dip profile. In reality, geologic dip is often difficult to define, and seldom known prior to acquisition. However, because we have acquired full tensor data we can rotate our data to the geologic dip direction after acquisition.
- Eigenvector processing. 3D structures can introduce complex "rotations" of the electrical currents. These rotations produce effects, such as excessively steep resistivity curves and out-of-range phases, which would be impossible to fit with 2D modeling programs. By relaxing the assumption that the electric and magnetic fields are orthogonal, eigenvector analysis provides a unique and trivial methodology for simplifying complex 3D data.
- 1D inversion for curve fitting. Real data are often noisy, and inconsistent. Out-of-range phases are a typical example of features seen in real data that can not be fit using 2D inversion. It is often best to make use 1D inversion to make interpretative decisions about how to "best" fit the data, rather than letting the 2D inversion thrash trying to fit inconsistent data.

Once these data processing techniques have been completed the data are inverted. Generally, two inversions of the MT data are done. The first inversion uses an approach (a model norm) that explicitly looks for the "smoothest" model consistent with the data. This approach essentially finds the minimal subsurface structure consistent with the data. The second inversion uses an approach (a model norm) that looks for a model most consistent with the known geology.

For the geologically constrained inversion we use a proprietary approach developed by Dr. Phil Wannamaker. This approach uses the geologic constraints as a target, while not imposing any intrinsic smoothing on the inversion. The approach finds the maximum structural information, at the risk of sometimes including structure not required by the data. It represents an effort to extract the maximum exploration information from the data.

Both approaches are valid, and important. A smooth model approach to inversion can be viewed as finding the least possible useful exploration information. However, it does provide an independent assessment of what the data actually require. The geologically constrained inversion will provide a much sharper subsurface image. But it will also reproduce the known geology where the data does not require a change to the model. Without an independent smooth model inversion it can be hard to determine whether a geologically constrained inversion has confirmed the geologic interpretation, or simply doesn't have any information either way.

APPENDIX D – DIRECT CURRENT RESISTIVITY AND INDUCED POLRIZATION (DCIP) THEORY

INTRODUCTION

The resistivity is among the most variable of all geophysical parameters, with a range exceeding 10^6. Because most minerals are fundamentally insulators, with the exception of massive accumulations of metallic and submetallic ores (electronic conductors) which are rare occurrences, the resistivity of rocks depends primarily on their porosity, permeability and particularly the salinity of fluids contained (ionic conduction), according to Archie's Law. In contrast, the chargeability responds to the presence of polarizeable minerals (metals, submetallic sulphides and oxides, and graphite), in amounts as minute as parts per hundred. Both the quantity of individual chargeable grains present, and their distribution within subsurface current flow paths are significant in controlling the level of response. The relationship of chargeability to metallic content is straightforward, while the influence of mineral distribution can be understood in geologic terms by considering two similar, hypothetical volumes of rock in which fractures constitute the primary current flow paths. In one, sulphides occur predominantly along fracture surfaces. In the second, the same volume percent of sulphides are disseminated throughout the rock. The second example will, in general, have significantly lower intrinsic chargeability.

More detailed descriptions on the theory and application of the IP/Resistivity method can be found in Van Blaricom (1992) and Telford et al. (1976).

HALVERSON-WAIT CHARGEABILITY

The Titan-24 DCIP chargeability decays are described using the Halverson-Wait spectral model (Halverson et al., 1981), which is not well known, but is similar to the Cole-Cole model proposed by Pelton et al. (1978) which is a simple relaxation model that fits complex (frequency-dependant) resistivity results.

The time domain chargeability, originally proposed by Siegel (1959), is defined (Telford et al., 1976) as:

$$M = \frac{1}{V_C} \int_1^2 V(t)dt$$

Where $V(t)$ is the residual or secondary voltage at a time t, that is decaying after the current is cut off, between time t_1 and t_2, with the steady voltage V_C during the current flow interval. The ratio $V(t)/V_C$ is expressed in millivolts per volt.

In the frequency domain, the "frequency effect" is defined as:

$$fe = (\rho_{DC} - \rho_{AC}) / \rho_{AC}$$

Where ρ_{DC} and ρ_{AC} are apparent resistivities measured at d.c. and "very high" frequency, usually in the 0.1 to 10 Hz range. The Cole-Cole model for the chargeability m, as defined by Pelton et al. (1978) is given by the following:

$$Z(\omega) = R_0 \left[1 - m \left(1 - \frac{1}{1 + (i\omega\tau)^C} \right) \right]$$

Where $Z(\omega)$ is the complex impedance, R_0 is the DC resistivity, m is the chargeability in volts per volt, ω is the angular frequency in Hz, τ is the time constant in seconds, and c is the frequency dependence (unitless). The latter two physical properties describe the shape of the decay curve in time domain or the phase spectrum in frequency domain, and commonly range between 0.01s to +100s and 0.1 to +0.5, respectively (Johnson, 1984).

The Halverson-Wait model was proposed by Halverson et al. (1981) as an extension to the Wait (1959) model of the impedance of "volume loading" of spheres, given by:

$$Z(\omega) = \frac{\rho}{G}\left[1 - 3v\left(1 - \frac{3\delta}{1+2\delta}\right)\right]$$

Where G is a geometric factor, ρ is the resistivity of the media, v is the volume loading (the volume fraction of chargeable "spheres"), δ is the sphere surface impedance. The Wait model was designed to provide an explanation of the differences in the shape of decay curves from different polarizeable targets, but does not describe very well the physical attributes of the rocks.

The Halverson-Wait model expands the Wait coated sphere IP model to include a new formulation of the sulphide-rock interface impedance, based on field studies and laboratory tests on samples. It is closely correlated to the Pelton et al. (1978) Cole-Cole model and is given by:

$$Z(\omega) = \frac{\rho}{G}\left[1 - 3v\left(1 - \frac{3/2}{1+r[i\omega]^{K}}\right)\right]$$

Where r is the sphere radius and is equivalent to τ - the Cole-Cole time constant ($r = \tau^{K}$). The v volume loading compares well to m – the Cole-Cole chargeability (see equation below) – and the exponent k is equal to c - the Cole-Cole frequency dependence (Halverson et al., 1983). For sulphide systems, the *r*-factor reflects the size or interconnection of the sulphide grains and the *k*-factor reflects the electrical characteristics of the sulphide surfaces. An example of time domain Halverson-Wait model responses is shown in Figure J.1.

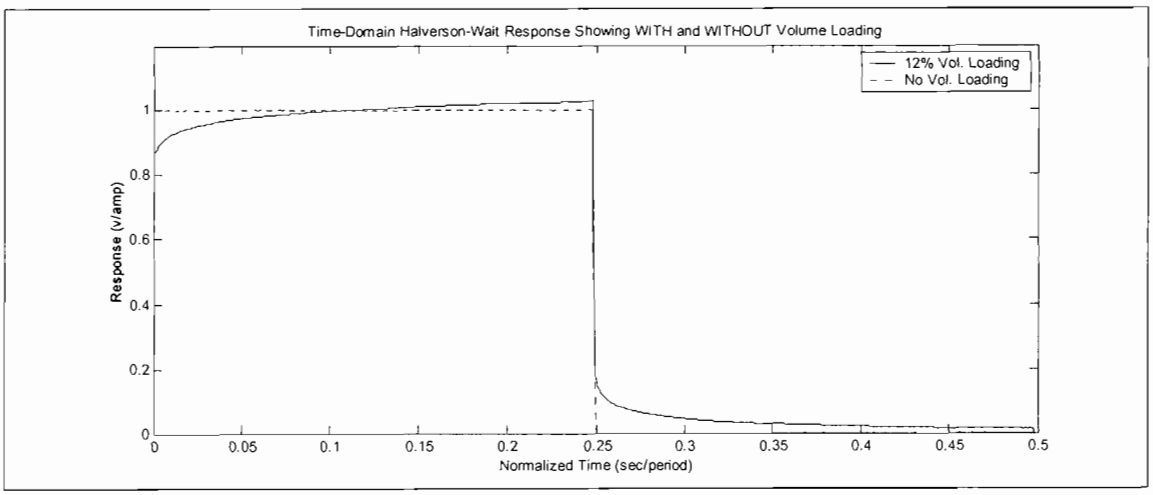

Figure J.1: Polarizeable versus Non-Polarizeable TDIP Response using Halverson-Wait Model

In practice the Titan chargeability decays are fit to a Halverson-Wait model. In order to solve for the volume loading v, the r-factor and k-factor are set to the standard (typical) Halverson-Wait values of 1.0 and 0.2, respectively. In the Halverson-Wait model the theoretical PFE (for infinite bandwidth), which equates to the theoretical chargeability in the Cole-Cole equation, is thereby defined by the volume loading:

$$PFE_0 = m_0 = \frac{9v}{(2+3v)}$$

and m is output in units of milliradians.

INVERSION THEORY

An excellent overview and introduction to both the philosophy and use of inversions in geophysics is available on the University of British Columbia (UBC) website (http://www.geop.ubc.ca/ubcgif/; Oldenburg et al., 1998).

Several points, detailed on the website, are crucial to understanding the Titan-24 approach to exploration:

- Inversion is a powerful 'tool', not a 'solution'.
- Inversion is not normally "unique". Given noisy and incomplete data of inherently limited resolution there are usually an 'infinite' range of models that 'fit' the data equally well. Recognition of this inherent non-uniqueness is why inversion must be viewed as a tool rather than a solution. Understanding and exploration of this non-uniqueness is an important part of the interpretive process.
- Inversion finds a model that 'fits' the data. The precise definition of 'fit' can be critical in the actual model that is found.
- The inversion depends on the data, and the data errors. The importance of the data errors is often overlooked.
- Inversion depends on a "model norm" – the mathematical definition of which model the inversion should try to find. This definition is almost as important as the actual data in determining the final inversion model.

Mathematically, inversion is the process of minimizing a function. The choice of which function to minimize ultimately defines the inversion model. Schematically, this function might be expressed:

$$\phi = \phi_d + \beta \phi_m = \text{(misfit)} + \beta\,\text{(model norm)}$$

$$0 < \beta < \infty \text{ is a constant}$$

This defines a function to be minimized that consists of some function that minimizes the data misfit, combined with some function that finds a "smooth" model. Beta represents a relative weighting between fitting the data and smoothing the model.

Clearly, the data misfit function must be defined in more detail. One approach might be:

$$\phi_d = \sum_{i=1}^{N} \left(\frac{F_i[m] - d_i^{obs}}{\varepsilon_i} \right)^2$$

This function defines the data misfit as the sum of the individual misfits squared, normalized by the errors associated with each data point. It is a very common, and stable, definition of the data misfit.

An important point not made on the UBC website is that the errors depend on many factors. The most common measure of data errors is simply the repeatability of the voltage and current measurements in the field. This may be misleading as there are also "errors" associated with electrode positioning, geologic complexity (2D vs 3D, but also coupling of shallow and deeper structure), and errors in the numerical calculation of model responses and inversion.

Another point not sufficiently detailed on the UBC site is the importance of not overestimating the data errors and fitting the data as closely as possible. Most geophysical techniques, but particularly electrical techniques, have large responses to shallow structure. This is expressed as "pant legs" in DC/IP, or "statics" in MT. The response to deep structure is generally a very subtle component of the data, compared to the sensitivity to shallow structure. Without excellent data, and an excellent match between the data and model response, the deep structure will not be imaged to the degree necessary for commercial exploration.

The model misfit function must also be defined in more detail. One of the most flexible definitions is the one used by UBC:

$$\phi_m(m,m_0)=\alpha_s\int_{vol}(m-m_0)^2dv+\alpha_x\int_{vol}\left(\frac{\partial(m-m_0)}{\partial x}\right)^2dv+\alpha_z\int_{vol}\left(\frac{\partial(m-m_0)}{\partial z}\right)^2dv$$

In this definition there are three components to the "model norm" (or "smoothness" constraint, or "regularization"), each of which contains an α constant (α_S, α_X, α_Z) that are commonly referred to as "alpha parameters". The first component is simply an overall difference between the model and a "target" model, the second component is a horizontal smoothness, and the third component is a vertical smoothness. The three "alpha" parameters (α_S, α_X, α_Z) represent a relative weighting of each component. A fourth variable, m_0, refers to the starting or reference model – either a half-space or geophysical constraint – that also has a profound influence on the model-misfit.

The UBC website provides an excellent example of the importance of selecting an appropriate "model norm", reproduced in Figure J.2

In this example the expected response of the top figure was computed. These 'data' were then inverted six times, using different "model norms" (α_S, α_X, α_Z, m_0). The lower six figures show the range of valid inversion models that can be produced. Note that six of these models are essentially mathematically equivalent, they all "fit" the data.

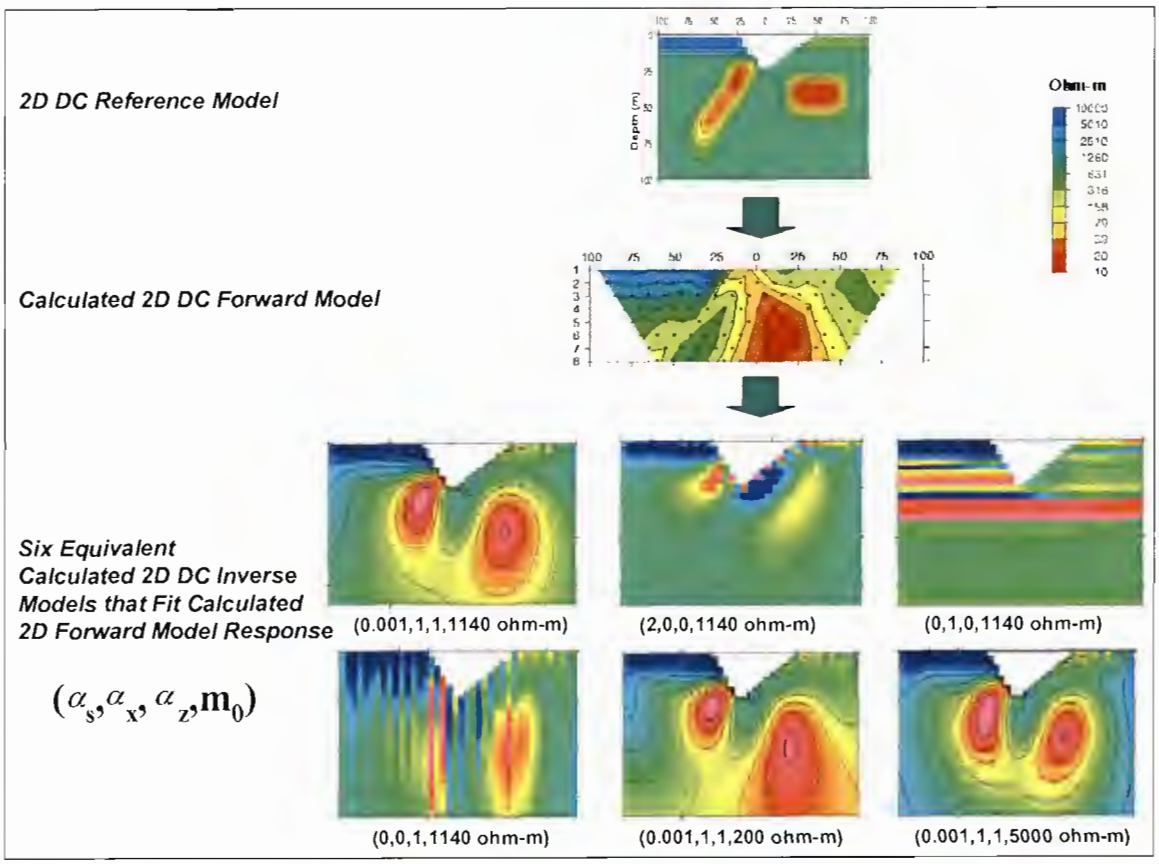

Figure J.2: Effects of Model Norm and Starting Model on Inversion Results (modified after Oldenburg, et al.,1998).

An important philosophy, driving much of the academic communities approach to inversion for the last two decades, is that the "best" model is the "smoothest" model consistent with the data. There are good reasons for taking this approach. However, from an exploration viewpoint this philosophy can be rephrased to "find the model with the least exploration value" – perhaps not reflecting the real goal of an exploration program.

Recently, several groups have taken major steps towards developing inversion approaches more tuned to exploration needs. Instead of using "smooth" model norms, they are being replaced with "focused (minimum transition zone) inversion, or smoothing to a geologic "target" model.

For exploration smoothing to a geologic target model makes sense. It requires good geologic control, and some understanding of the rock physical properties. There are three drawbacks to the geologic target approach:

- The geologic information is incomplete or inaccurate.
- Physical property data are incomplete.
- It is difficult to determine whether the geophysical data support the geologic model, or simply provide no information.

The most sensible approach is to combine smooth model inversion with geologic target inversion. For now, we are focusing on providing inversions using both approaches. It is up to the project geologist and geophysicist to review these inversions and develop a final interpretation.

APPENDIX E: TITAN INVERSION RESULTS

This appendix contains a description on the TITAN DCIP and MT data processing and inversion, as well as an outline on the inversion results for each individual model, including Quality Control and Assurance (QC/QA) comments.

DCIP Data Preprocessing:

For the inversions, the raw data was edited, including adjustment of data errors and removal of poor quality data, allowing the program to reach appropriate model misfits and consistent inversion models. The edition and preprocessing of the datasets included:

1. Filtering the raw data[1] using the ***DCIPSuper.exe*** program with the following "Quantec[2]" input parameters:
   - All the negative Vp values were excluded
   - All the high resistivity values were included
   - Small apparent resistivity values were excluded
   - All the high phase values where included
   - All low phase values were included
   - High Vp errors were included
   - High phase errors were included
   - Big apparent resistivity limit: 100 000 Ohm.meters
   - Small apparent resistivity limits: 0.001 Ohm.meters
   - Big phase limit: 100 mrads
   - Small phase limit: 0 mrads
2. Exclusion of the data points (for both the voltage and phase) with Vp errors higher than 5%.
3. Exclusion of negative phase data points (for the phase file only)
4. Exclusion of data points with phase errors >10% (for the phase file only).
5. Errors of 0.7 mrads added to the final phase data files for inversions.

[1] *Raw data contained in the digital files "Line#.csv".*
[2] *Quality Control Process passes all data thru except dipoles straddling current electrodes.*

2D DCIP Unconstrained Inversions:

The DC Resistivity and IP unconstrained inversion models were calculated using the ***UBC DCInv2D™ 2D***[3] algorithm (Oldenburg & Li, 1994) and ***IPView-IIC***[4] platform.

Multiple unconstrained inversion models were produced in order to arrive at the final 2D inversion models. Smooth inversions were executed for both, the DC resistivity and IP datasets.

The Smooth DC and IP Inversion Models[5] were derived from setting the ***chi***[6] factor to NULL. The ***αs***[7], ***αx*** and ***αy***[8] parameters were also set to default (NULL). The data was further edited as necessary to achieve convergence with a final resulting chi factor of 1 or less. No Sharp Inversion Models were produced or included in this interpretation report.

One set of Smooth IP inversion models was derived assuming a homogenous half-space (conductivity distribution set to NULL). This model (calculated apparent chargeability distribution) was useful for defining and/or improving the interpretation of the chargeability models when the resulting IP inversions were distorted by incorporating a DC model with high resistivity gradients.

Three DC and IP models were derived as follow:

1. **Line L# smDC**: Smooth DC "Resistivity" inversions from inverting the voltage data (contained in the raw *L#.csv* file). The Smooth DC inversions were topographically corrected according to the Quantec inversion mesh (*L#_meshPLDP.txt*), and the elevation file (*L#E.topo*) from the GPS survey files.
2. **Line L# smIP**: Smooth IP "Chargeability" inversions from inverting the phase data (contained in the raw *L#.csv file*). The Smooth IP inversions used the Titan 2D conductivity model (derived from the Smooth DC "Resistivity" inversions), and were topographically corrected according to the Quantec inversion mesh (*L#_meshPLDP.txt*), and the elevation file (*L#E.topo*) from the GPS survey files.
3. **Line L# smIP nullcond**: Smooth IP "nullcond or half-space conductivity" inversions from inverting the phase data (contained in the raw *L#.csv file*). The Smooth IP "nullcond" inversions used the half-space conductivity, and were topographically corrected according to the Quantec inversion mesh (*L#_meshPLDP.txt*), and the elevation file (*L#E.topo*) from the GPS survey files.

3D DCIP Unconstrained Inversions:

With the use of the 3D inversion codes written by de UBC-GIF group (university of British Columbia) DCIP3D both a conductivity and chargeability model were calculated using the same data (although with a different estimated error values to accommodate the difference in mesh and inversion approach), which was used as input for the 2D inversions. The input data were referenced according to NAD83 UTM zone 17 N, and a square grid was built, with 50 m x 50 m x 50 m cubes. The results from the 3D inversions are available in the digital archive in Geosoft Voxet format.

---

[3] *UBC-Geophysical Inversion Facility (GIF): Department of Earth and Ocean Sciences at the University of British Columbia.*
[4] *IPView: Version 2.1.5 beta (Industrial imaging Co., Inc.); Written by B. Petrick and Licensed to Quantec Geoscience Ltd.*
[5] *The inversion models presented in this report are the most consistent models according to the degree of association with the DC and MT results and the available geological information. Additional inversion models are available in the Digital Archive attached to this Interpretation Report.*
[6] *The **chi** parameter controls the inversion misfit.*
[7] *The **αs** parameter controls the degree of closeness between the constructed model and the initial model.*
[8] *The **αx** and **αy** parameters control the horizontal and vertical smoothness of the model respectively.*

MT Data Preprocessing:

The initial data input into the Geotools database were line-station data, taken directly from the EDI archive[9]. The raw impedance tensor data span the 0.1 Hertz to 10000 Hertz bandwidth, with a data density of approximately 6-8 points per decade. Data points with high noise levels were removed from the Apparent Resistivity and Phase curves prior to inversion. In some cases, low frequency data <1 Hertz was not included in the inversion due to low signal-to-noise levels. High frequency (>1000 Hertz) phase data, not consistent with the resistivity data, was excluded.

1D MT Inversions:

One-dimensional (1D) inversions for each mode (XY and YX) of the unrotated data (Eigenvector Latorraca Deconvolution) were generated for each site using the ***Occam 1D*** algorithm (Constable, S.C., R.L. Parker, and C.G. Constable, 1987). The 1D inversion is used to make interpretative decisions about how to "best" fit the data, and ensure that the apparent resistivity and phase are smooth and consistent. The calculated apparent resistivities and phases from the 1D models are then interpolated to obtain 12 frequency responses per decade. Stitched 1D Determinant sections were also created.

2D MT Unconstrained Inversions:

The MT inverse models were calculated using the Geotools™ MT processing and model-inversion platform. Several MT 2D PW inversions were run using different starting models ("RLM" smooth models and Stitched 1D Determinant sections), as well as different combinations of the data (TM phase, TM resistivity, TE phase and TE resistivity) before arriving at the final 2D models. Only two sets of RLM and PW models are presented for the final interpretation.

Four (4) "RLM" smooth ("Mackie") models were constructed using the conjugate gradient algorithm (Rodi & Mackie, 2001)[10]. The inversion parameters for the Smooth "RLM" models used a maximum of 100 iterations, Tau set to 3, and a noise floor of 5%. The inversion models were calculated using different combinations of the interpolated TM (resistivity & phase), and TM (resistivity & phase) curves, in the 0.1 to $10x10^3$ Hertz bandwidth. Stitched 1D Determinant sections were used as starting models for the smooth inversions as well. The RLM models were derived as follow:

1. **L# rlm1 it#**: Smooth inversions derived from inverting the 1D fitted and interpolated data, with no rotation of the principal components. "*rlm1*" uses the half-space equal to 2500 Ohm-meters as starting model, and was calculated using TM (phase + resistivity) data only.
2. **L# rlm2 it#:** Smooth inversions derived from inverting the 1D fitted and interpolated data, with no rotation of the principal components. "*rlm2*" uses the half-space equal to 2500 Ohm-meters as starting model, and was calculated using TM (phase + resistivity) and TE (phase) data only.
3. **L# rlm3 it#:** Smooth inversions derived from inverting the 1D fitted and interpolated data, with no rotation of the principal components. "*rlm2*" uses the half-space equal to 2500 Ohm-meters as starting model, and was calculated using TM (phase + resistivity) and TE (phase+ resistivity) data.
4. **L# rlm4 it#:** Smooth inversions derived from inverting the 1D fitted and interpolated data, with no rotation of the principal components. "*rlm42*" uses the Stitched 1D Determinant model as starting model, and was calculated using TM (phase + resistivity) and TE (phase+ resistivity) data.

[9] *Data contained in the "Geophysical Survey Logistics Report" Digital Archive.*
[10] *Rodi, W., and R.L. Mackie, 2001. Nonlinear conjugate gradients algorithm for 2-D magnetotelluric inversion: Geophysics, 66, 174-187.*

Four (4) sets of 2D PW models (pw1 to pw4) were derived from inverting the unrotated data, using different smooth "RLM" as starting models. Different combinations of datasets (TM phase, TM resistivity, TE phase and TE resistivity) were tested before arriving at the final 2D models. The TM (phs+rho) and TE (phs+rho) modes inversions (pw4 models[11]) were used for presenting the interpretation.

The PW inversion mesh parameters used 50 single rows, and a regularization width/depth ratio of 0.1. The finite element and regularization meshes were constructed using frequencies at 10k, 1k, 100, 10 and 0.1 Hertz, a column width of 40-50 meters (for smooth RLM and PW, inversions respectively), 100 rows maximum and a minimum row-thickness of 10 meters. The MT inversion models were calculated using the interpolated resistivity and phase curves, in the 10000 Hertz to 0.1 Hertz bandwidth, assuming a maximum of 5% error for the resistivity and 3 degrees for the phase, at a minimum of 4 to 6 equi-spaced frequencies per decade.

A total of four (4) PW models were derived as follow:

1. **L# pw1 it#:** Conjugate inversions derived from inverting the 1D fitted and interpolated data, with no rotation of the principal components. "*pw1*" models used the "*rlm1*" smooth inversions as starting models, and were constructed using TM (phase + resistivity) data.
2. **L# pw2 it#:** Conjugate inversions derived from inverting the 1D fitted and interpolated data, with no rotation of the principal components. "*pw2*" models used the "*rlm2*" smooth inversions as starting models, and were constructed using TM (phase + resistivity) and TE (phase) data.
3. **L# pw3 it#:** Conjugate inversions derived from inverting the 1D fitted and interpolated data, with no rotation of the principal components. "*pw3*" models used the "*rlm3*" smooth inversions as starting models, and were constructed using TM (phase + resistivity) and TE (phase+ resistivity) data.
4. **L# pw4 it#:** Conjugate inversions derived from inverting the 1D fitted and interpolated data, with no rotation of the principal components. "*pw4*" models used the "*rlm4*" smooth inversions as starting models, and were constructed using TM (phase + resistivity) and TE (phase+ resistivity) data.

It is useful to review the actual data input into the 2D inversions and all the raw data, which is available in the Project Logistical Report submitted previously. Only the final models of the inversion results are shown in this appendix. Note that the inversion models presented in this appendix are not always derived from the final iteration of the inversion program.

The following pages will present a set of five figures (***a*** to ***e***) per survey line containing the DCIP and MT raw data and the inversion results, in ascending order as:

a) 2D DC Resistivity (left) & 2D IP Unconstrained Inversion Results (right) with Observed Data and Calculated Models.

b) 2D IP Unconstrained Inversion Results (using half-space conductivity) with Observed Data and Calculated Models.

c) 2D MT unrotated Raw Data (left) and Stitched 1D Models (right).

d) MT Resistivity (left) and Phase (right) Frequency Profiles (resistivity range: 100 to 100,000 ohm-m, phase range: 180 to –180 degrees).

e) 2D PW MT Resistivity Inversion Models.

[11] *(pw4) **P**lane **W**ave Unrotated inversion models calculated from TM (phase & resistivity) and TE (phase & resistivity) data.*

Line L9900N

L9900N - UBC 2D DCIP Inversion Results

Smooth 2D DC Resistivity Inversion

Smooth 2D IP Chargeability Inversion (using Titan conductivity)

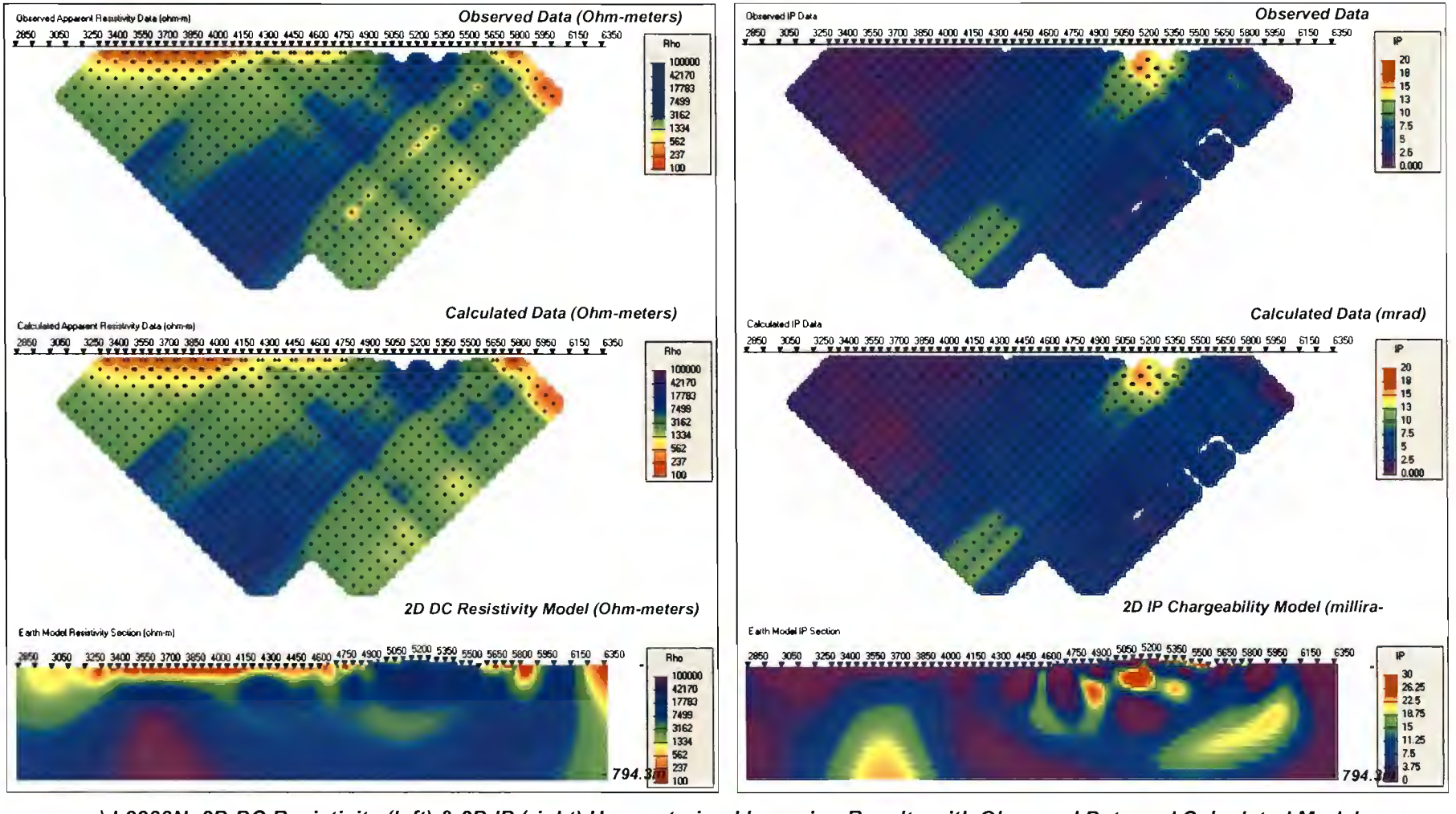

a) L9900N: 2D DC Resistivity (left) & 2D IP (right) Unconstrained Inversion Results with Observed Data and Calculated Models

L9900N - UBC 2D DCIP Inversion Results (cont...)

Smooth 2D IP Chargeability Inversion (using half-space conductivity)

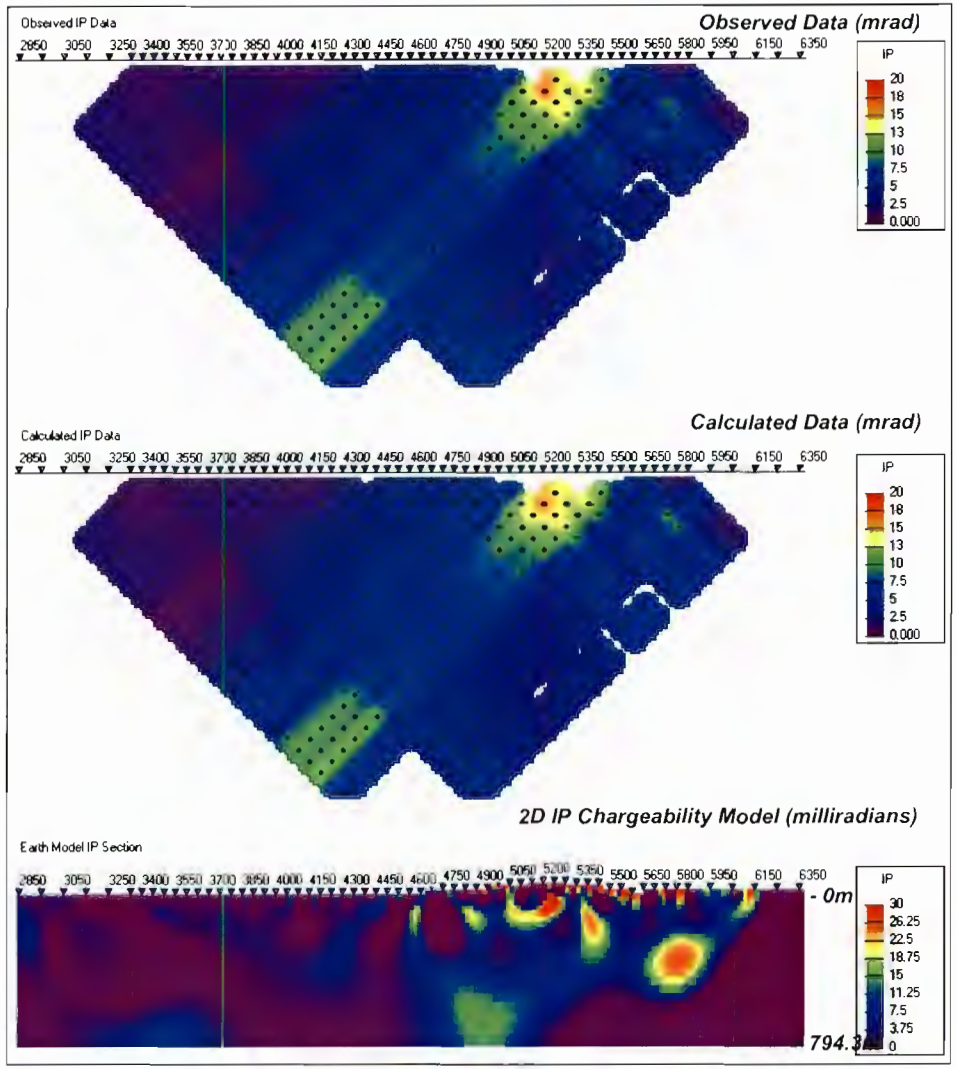

b) L9900N: 2D IP Unconstrained Inversion Results with Observed Data and Calculated Models (using half-space conductivity model)

L9900N - 2D MT Raw Data

Raw data input to inversions (edited & interpolated)

Stitched 1D model

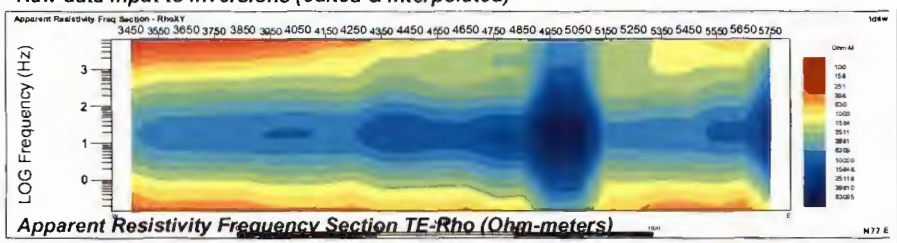

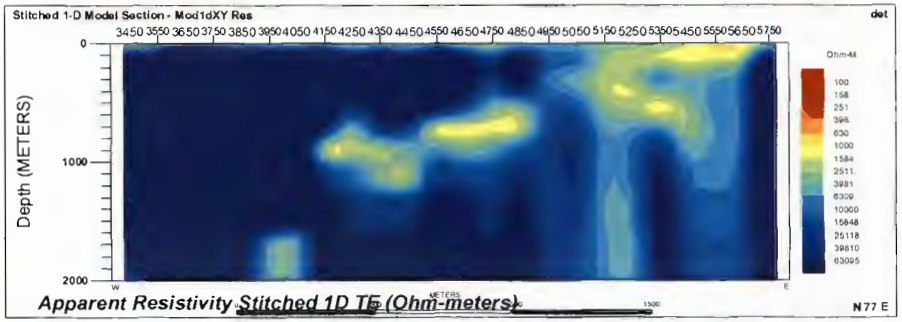

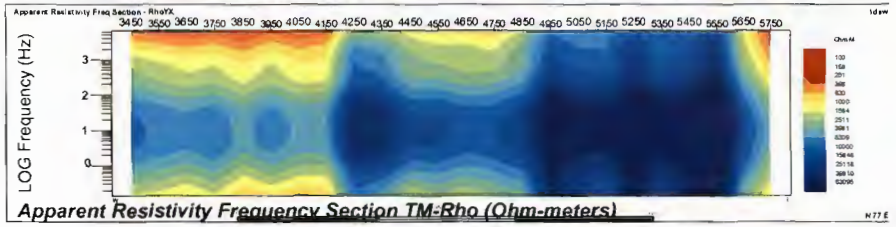

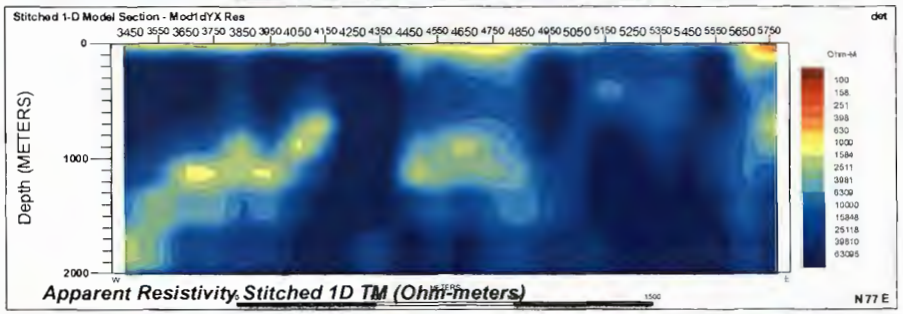

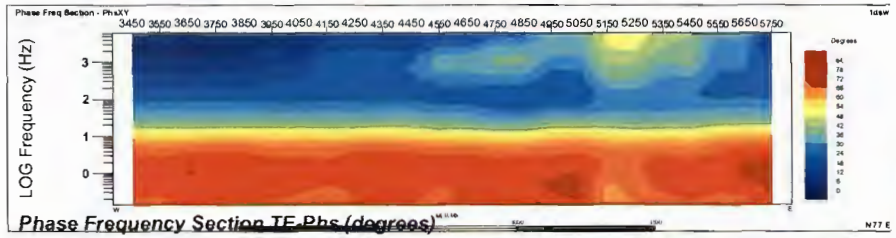

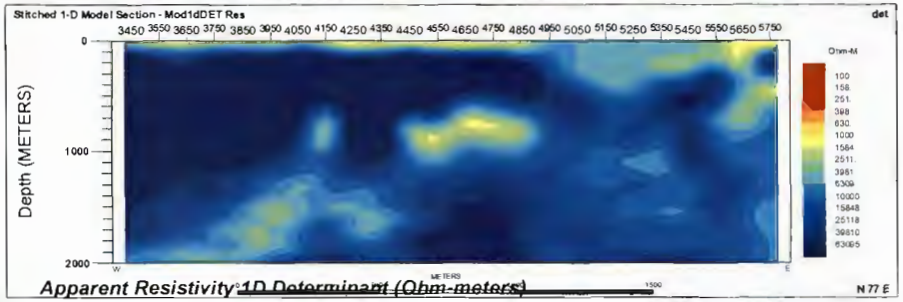

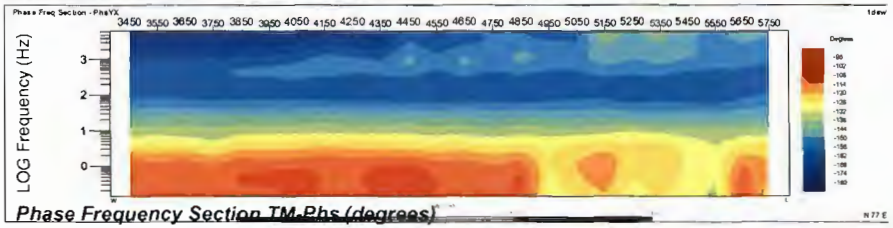

c) L9900N: 2D MT unrotated Raw Data (left) and Stitched 1D Models (right)

L9900N MT Frequency Profiles

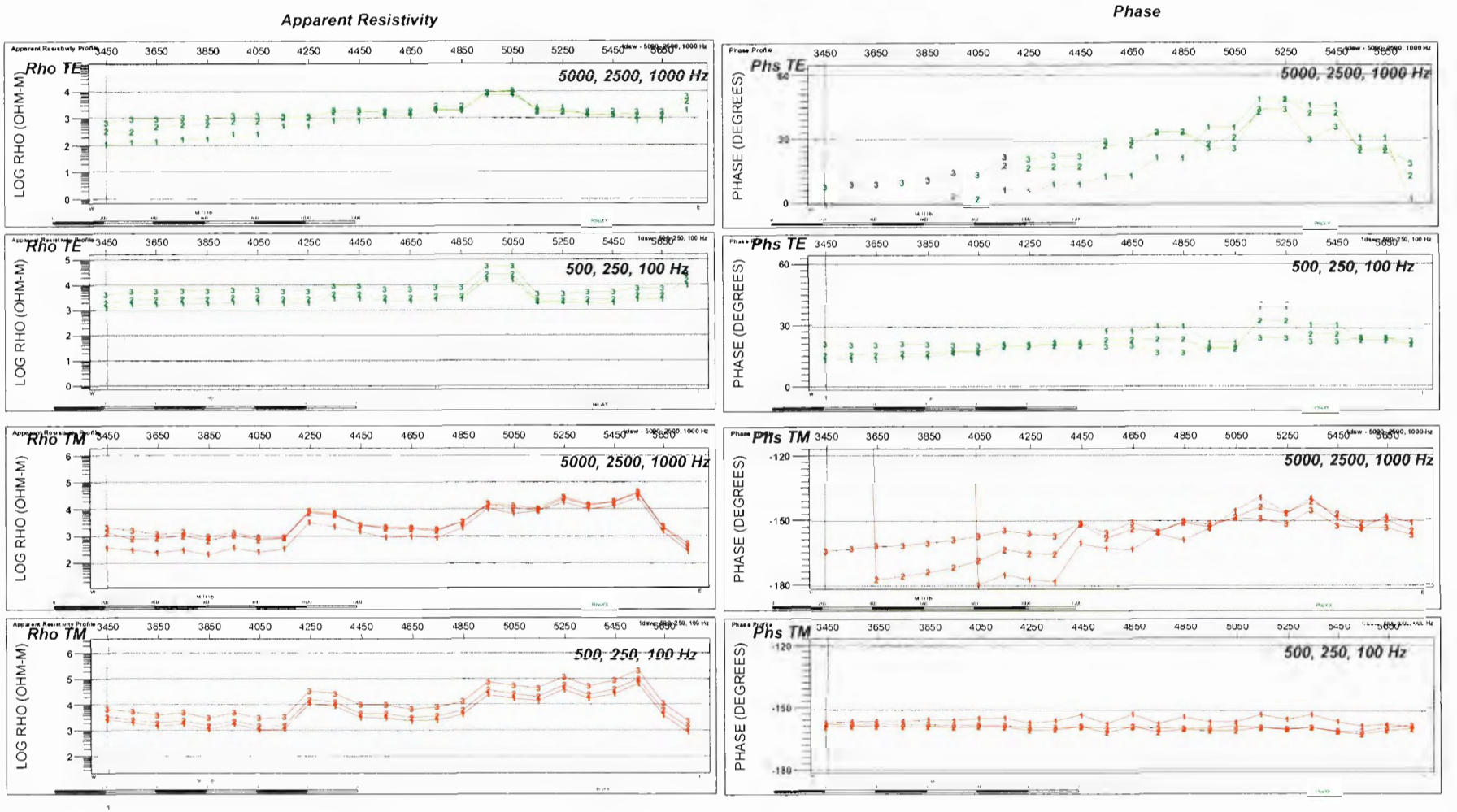

d) L9900N: MT Resistivity and Phase (right) Frequency Profiles

L9900N- 2D MT Inversion Models

2D MT PW1 Model (ohm-m), Starting model: rlm1, Input data: TM (Phs+Rho)

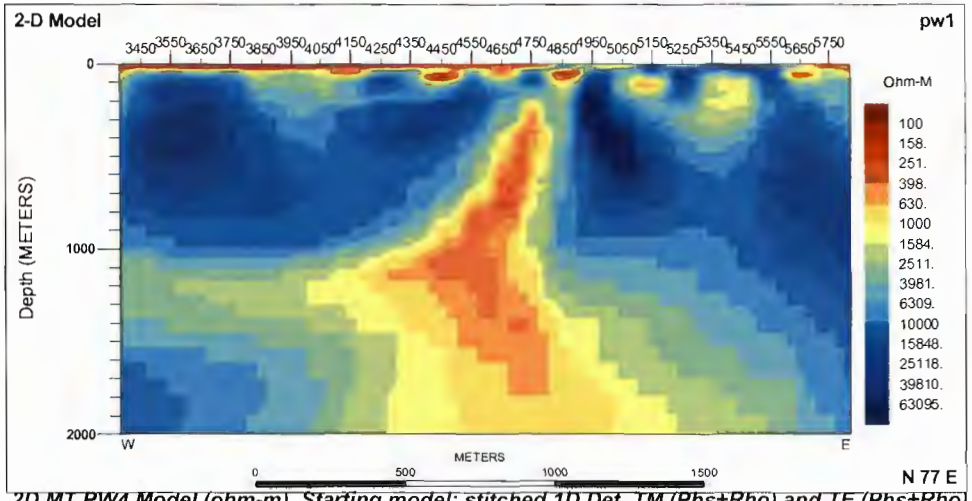

2D MT PW4 Model (ohm-m), Starting model: stitched 1D Det, TM (Phs+Rho) and TE (Phs+Rho)

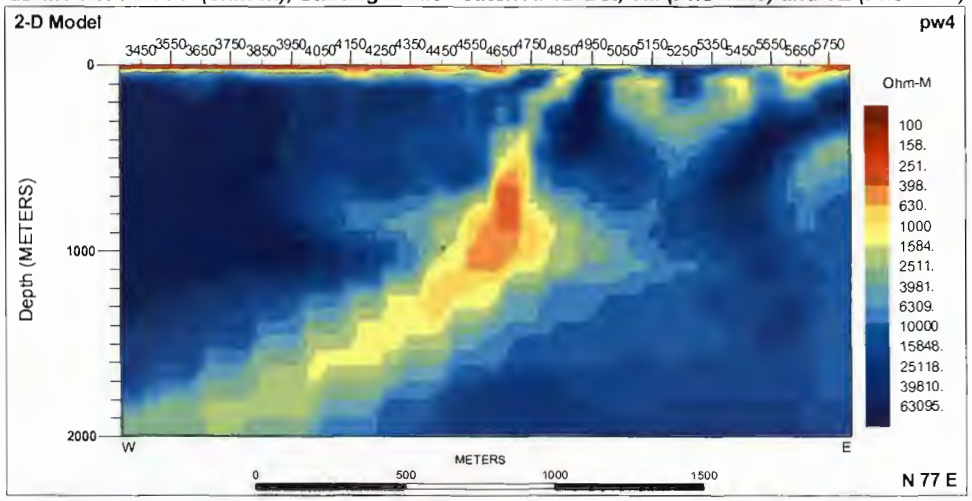

e) L9900N: 2D PW MT Resistivity Inversion Models

Line L10200N

L10200N - UBC 2D DCIP Inversion Results

Smooth 2D DC Resistivity Inversion

Smooth 2D IP Chargeability Inversion (using Titan conductivity)

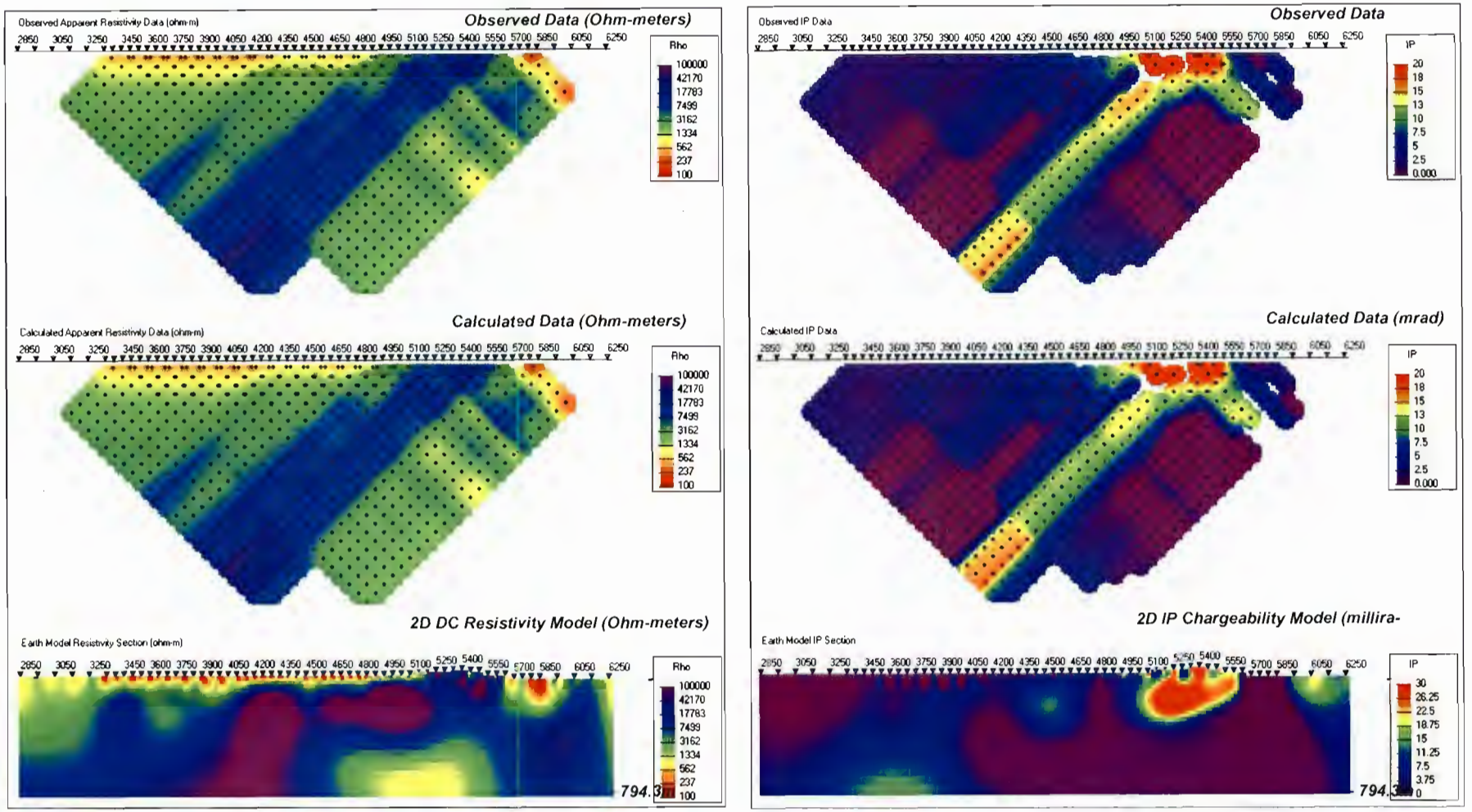

a) L10200N: 2D DC Resistivity (left) & 2D II² (right) Unconstrained Inversion Results with Observed Data and Calculated Models

L10200N - UBC 2D DCIP Inversion Results (cont...)

Smooth 2D IP Chargeability Inversion (using half-space conductivity)

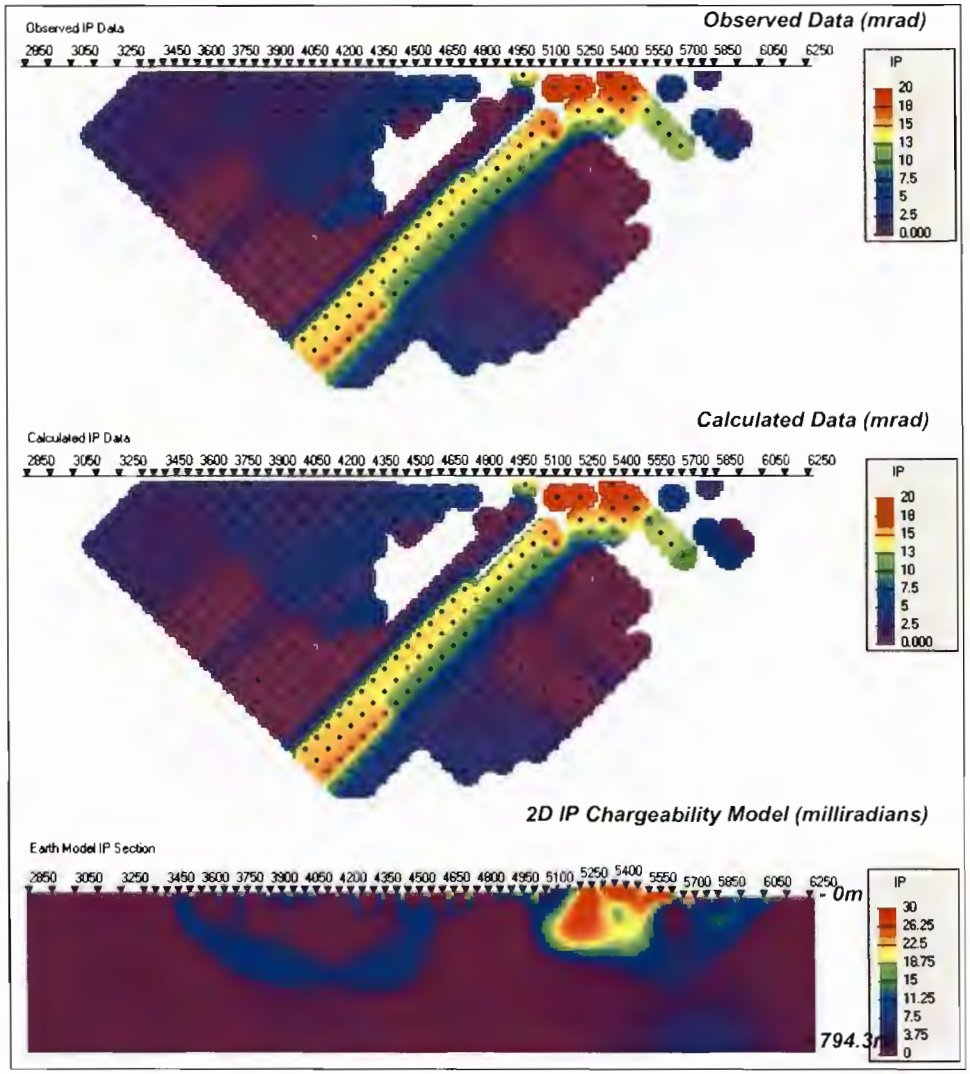

b) L10200N: 2D IP Unconstrained Inversion Results with Observed Data and Calculated Models (using half-space conductivity model)

L10200N - 2D MT Raw Data

Raw data input to inversions (edited & interpolated)

Stitched 1D models

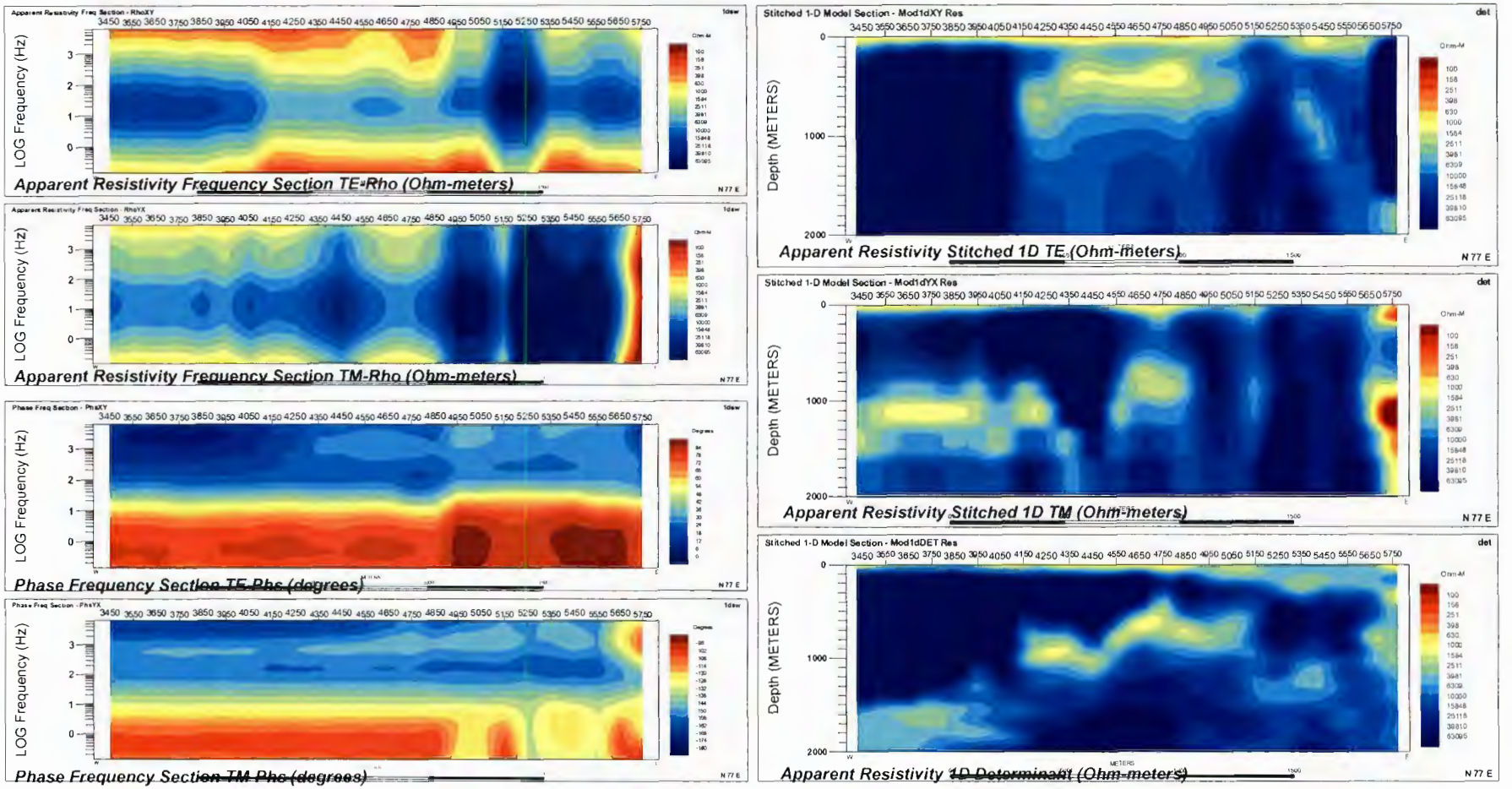

c) L10200N: 2D MT unrotated Raw Data (left) and Stitched 1D Models (right)

L10200N MT Frequency Profiles

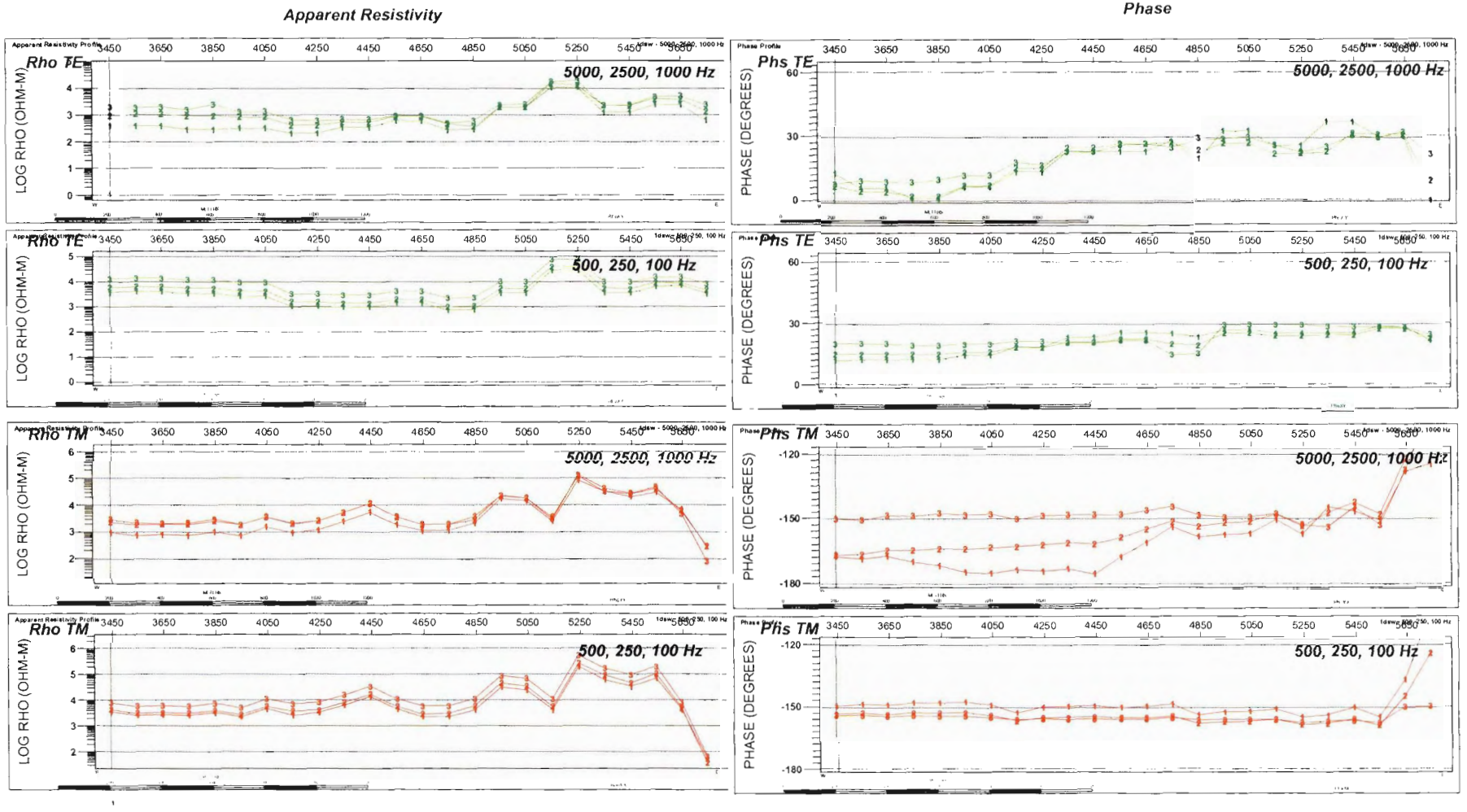

d) L10200N: MT Resistivity and Phase (right) Frequency Profiles

L10200N- 2D MT Inversion Models

2D MT PW1 Model (ohm-m), Starting model: rlm1, Input data: TM (Phs+Rho)

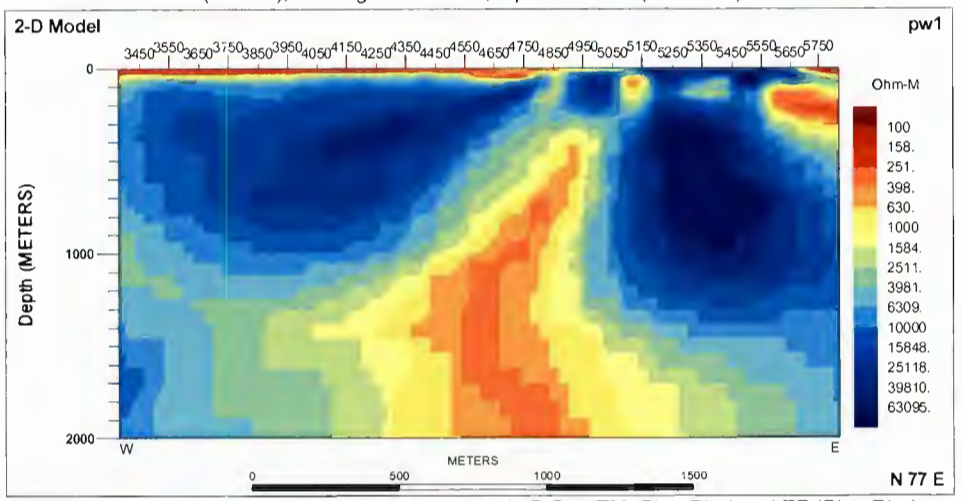

2D MT PW4 Model (ohm-m), Starting model: stitched 1D Det. TM (Phs+Rho) and TE (Phs+Rho)

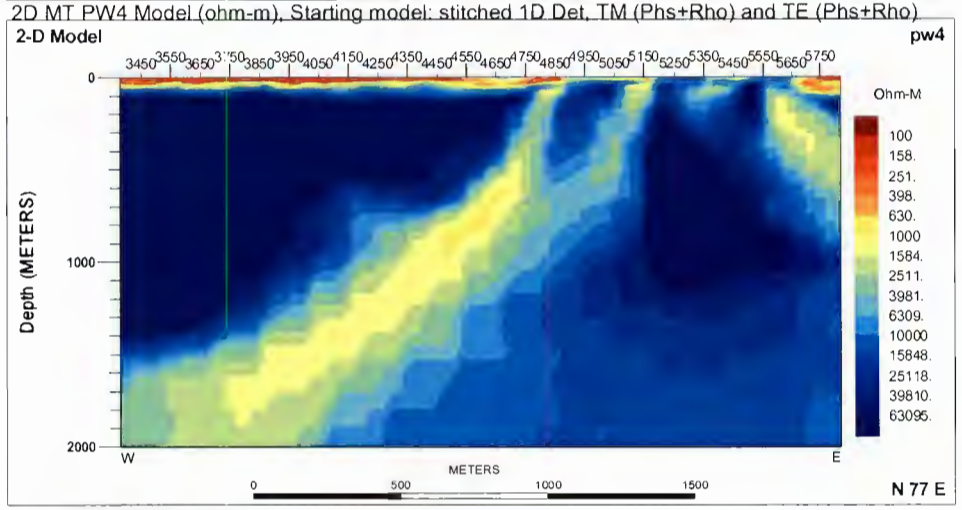

e) L10200N: 2D PW MT Resistivity Inversion Models

Line L10400N

L10400N - UBC 2D DCIP Inversion Results

Smooth 2D DC Resistivity Inversion

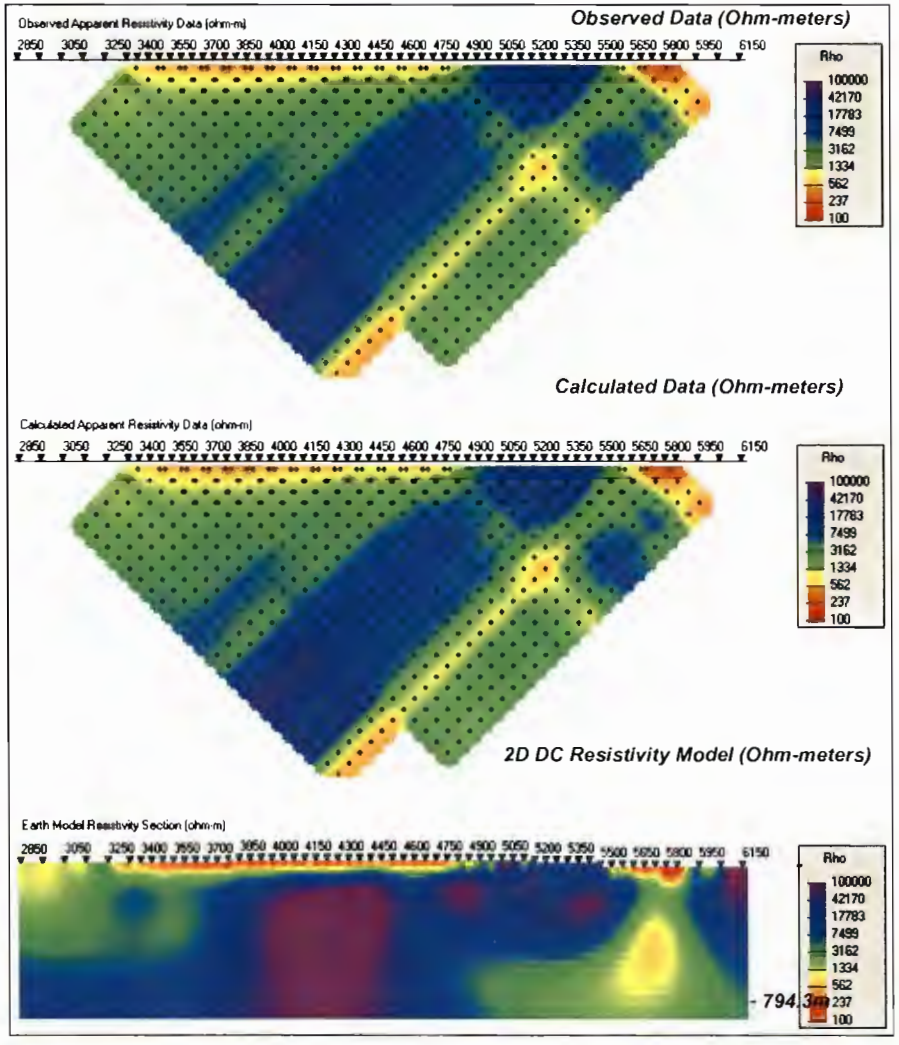

Smooth 2D IP Chargeability Inversion (using Titan conductivity)

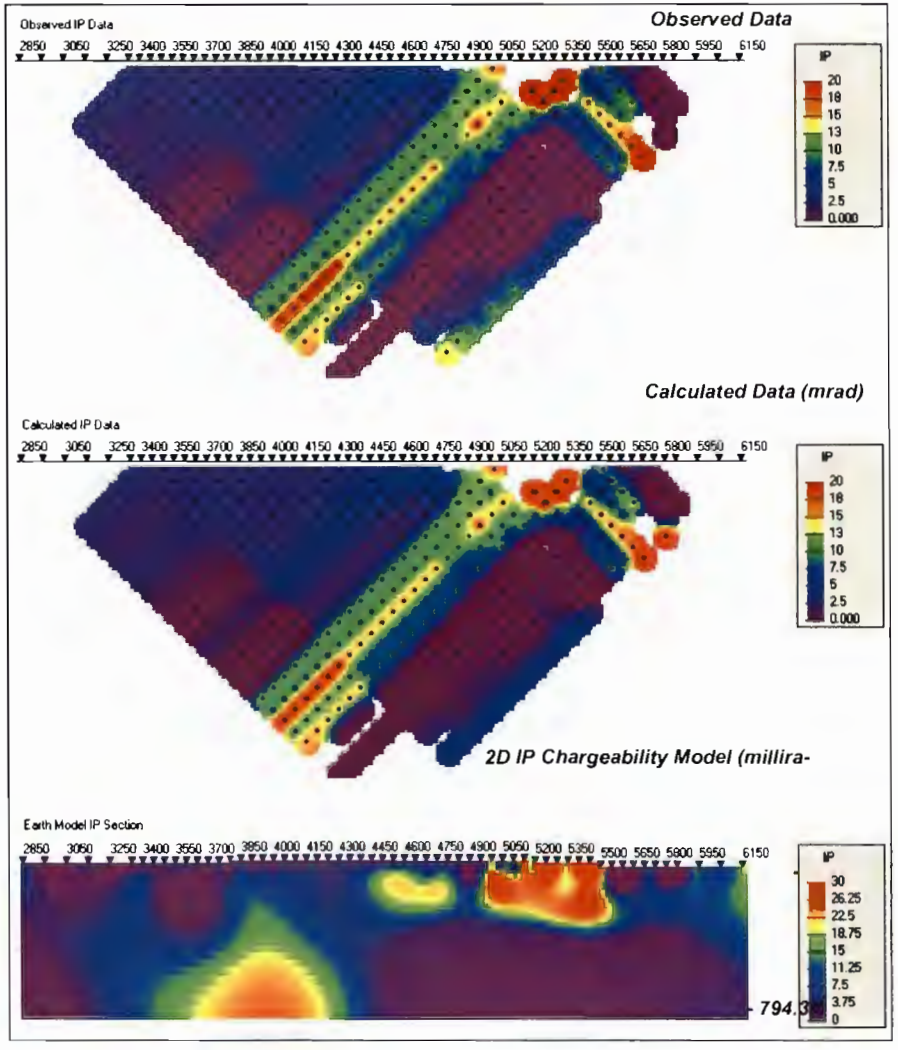

a) L10400N: 2D DC Resistivity (left) & 2D IP (right) Unconstrained Inversion Results with Observed Data and Calculated Models

L10400N - UBC 2D DCIP Inversion Results (cont...)

Smooth 2D IP Chargeability Inversion (using half-space conductivity)

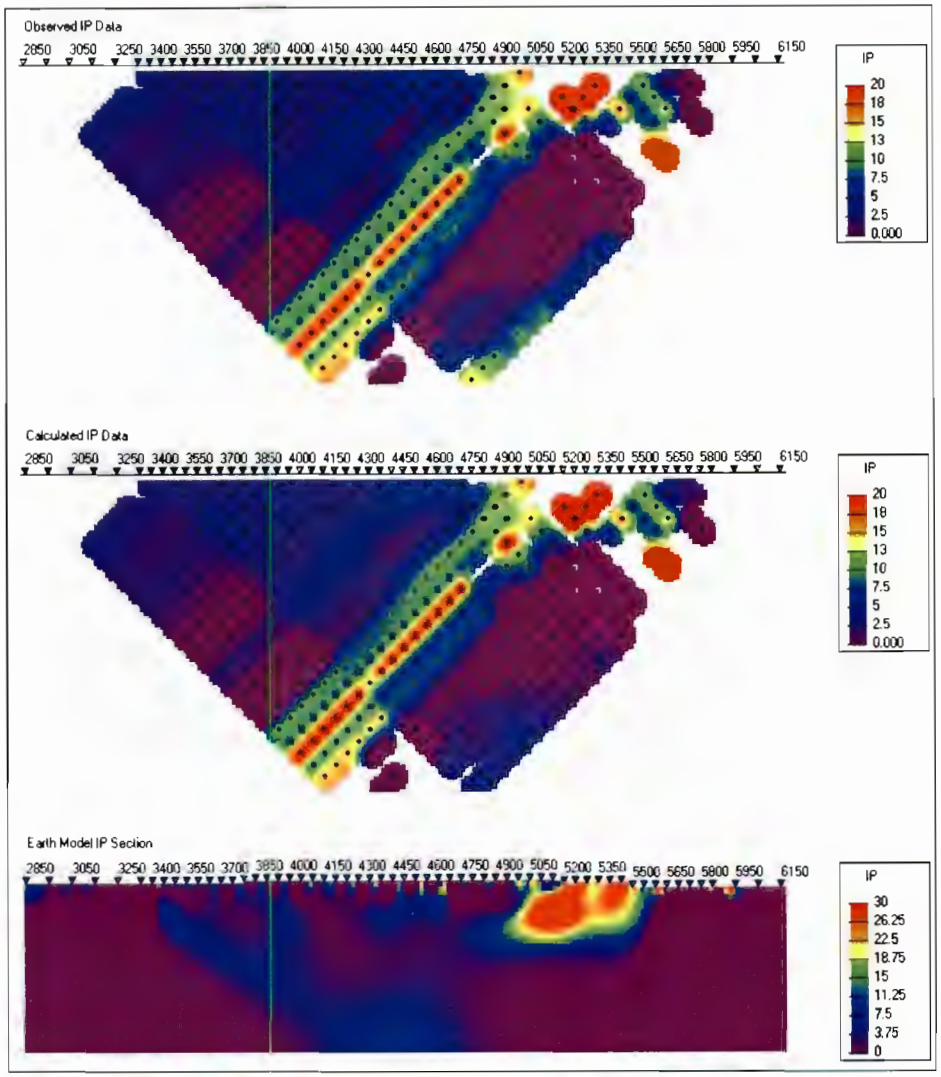

b) L10400N: 2D IP Unconstrained Inversion Results with Observed Data and Calculated Models (using half-space conductivity model)

L10400N - 2D MT Raw Data

Raw data input to inversions (edited & interpolated)

Stitched 1D models

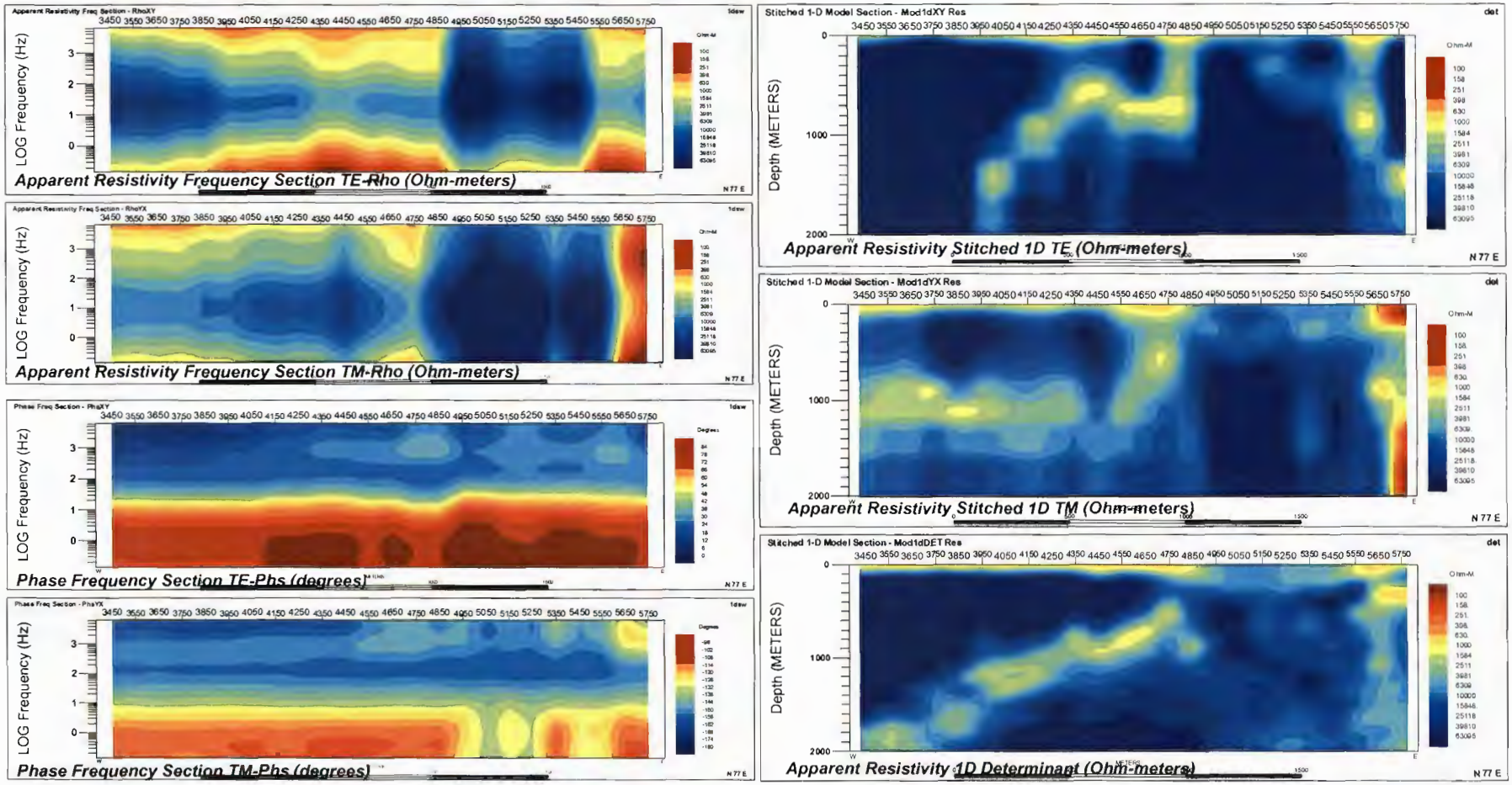

c) L10400N: 2D MT unrotated Raw Data (left) and Stitched 1D Models (right)

L10400N MT Frequency Profiles

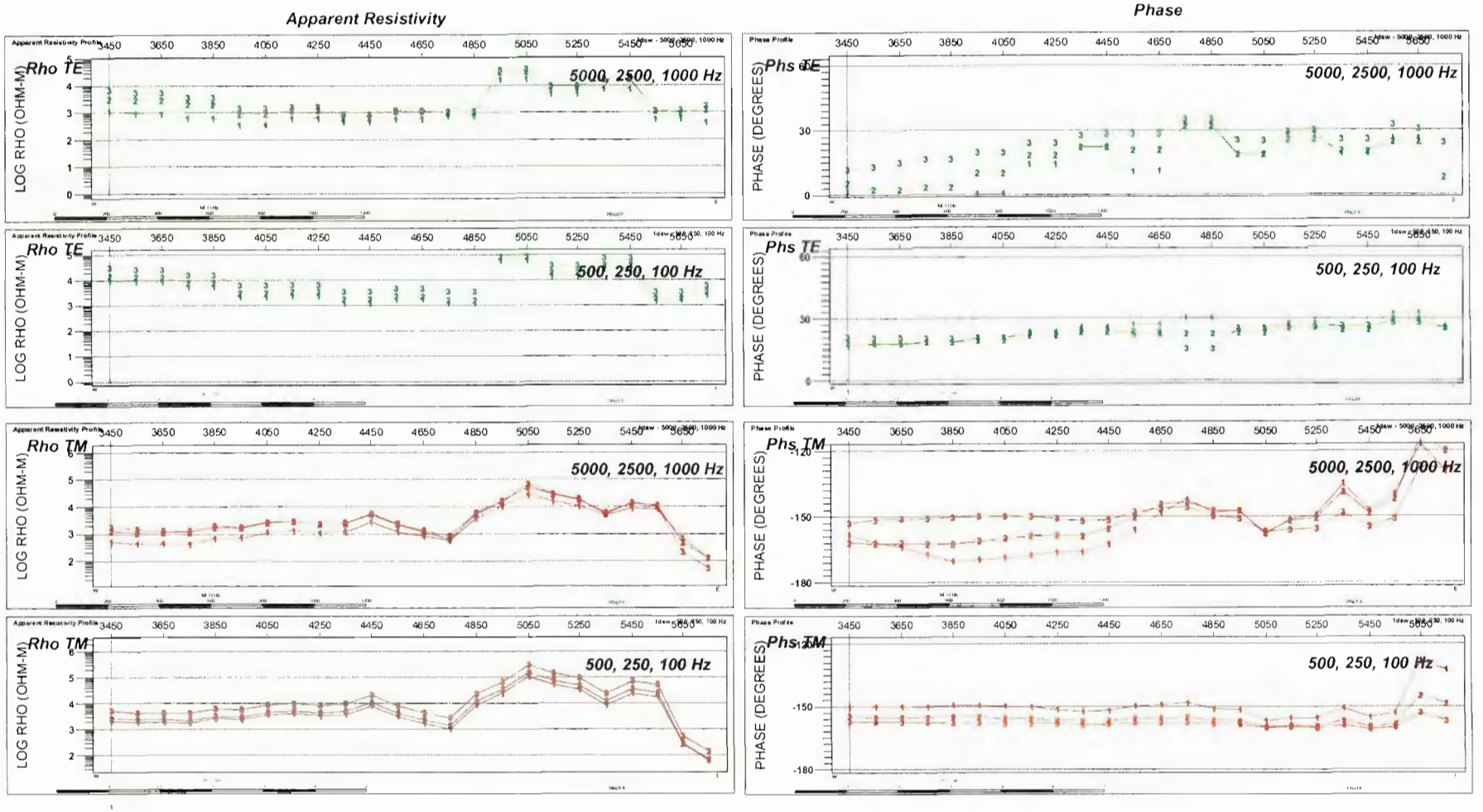

d) L10400N: MT Resistivity and Phase (right) Frequency Profiles

L10400N- 2D MT Inversion Models

2D MT PW1 Model (ohm-m), Starting model: rlm1, Input data: TM (Phs+Rho)

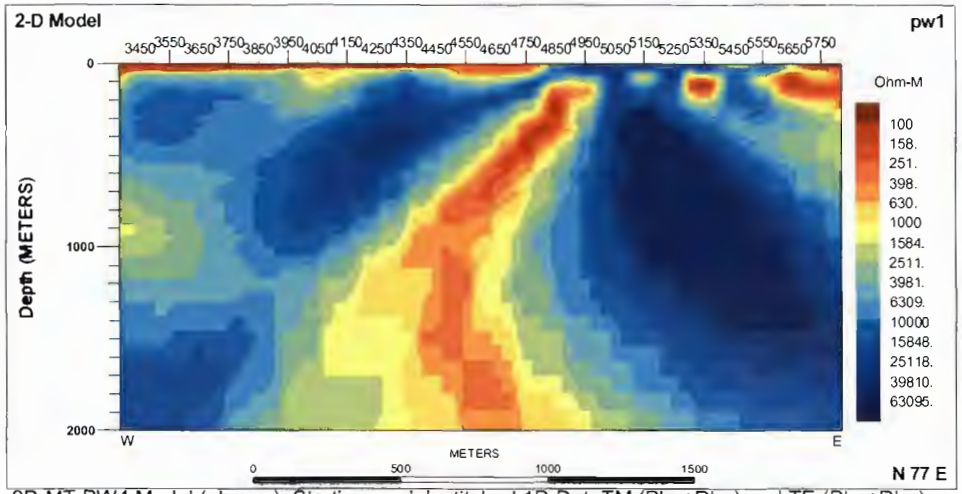

2D MT PW4 Model (ohm-m), Starting model: stitched 1D Det, TM (Phs+Rho) and TE (Phs+Rho)

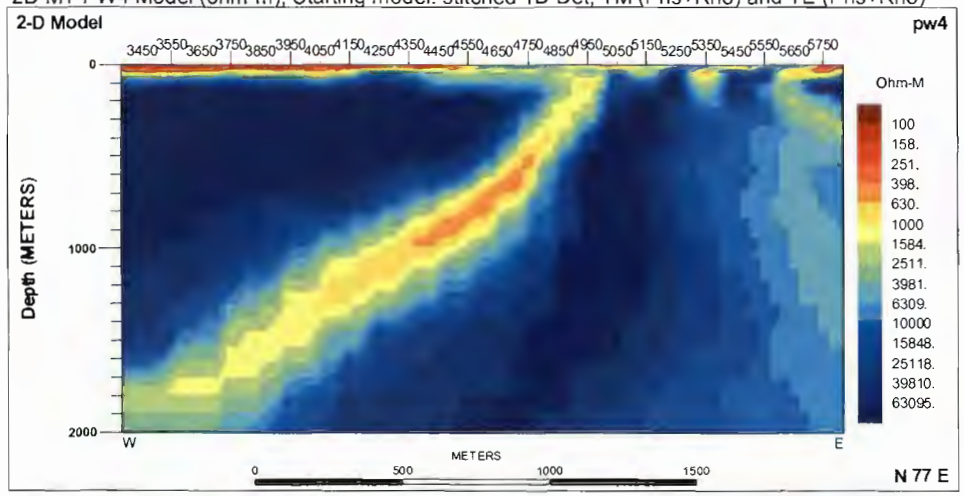

e) L10400N: 2D PW MT Resistivity Inversion Models

Line L10600N

L10600N - UBC 2D DCIP Inversion Results

Smooth 2D DC Resistivity Inversion

Smooth 2D IP Chargeability Inversion (using Titan conductivity)

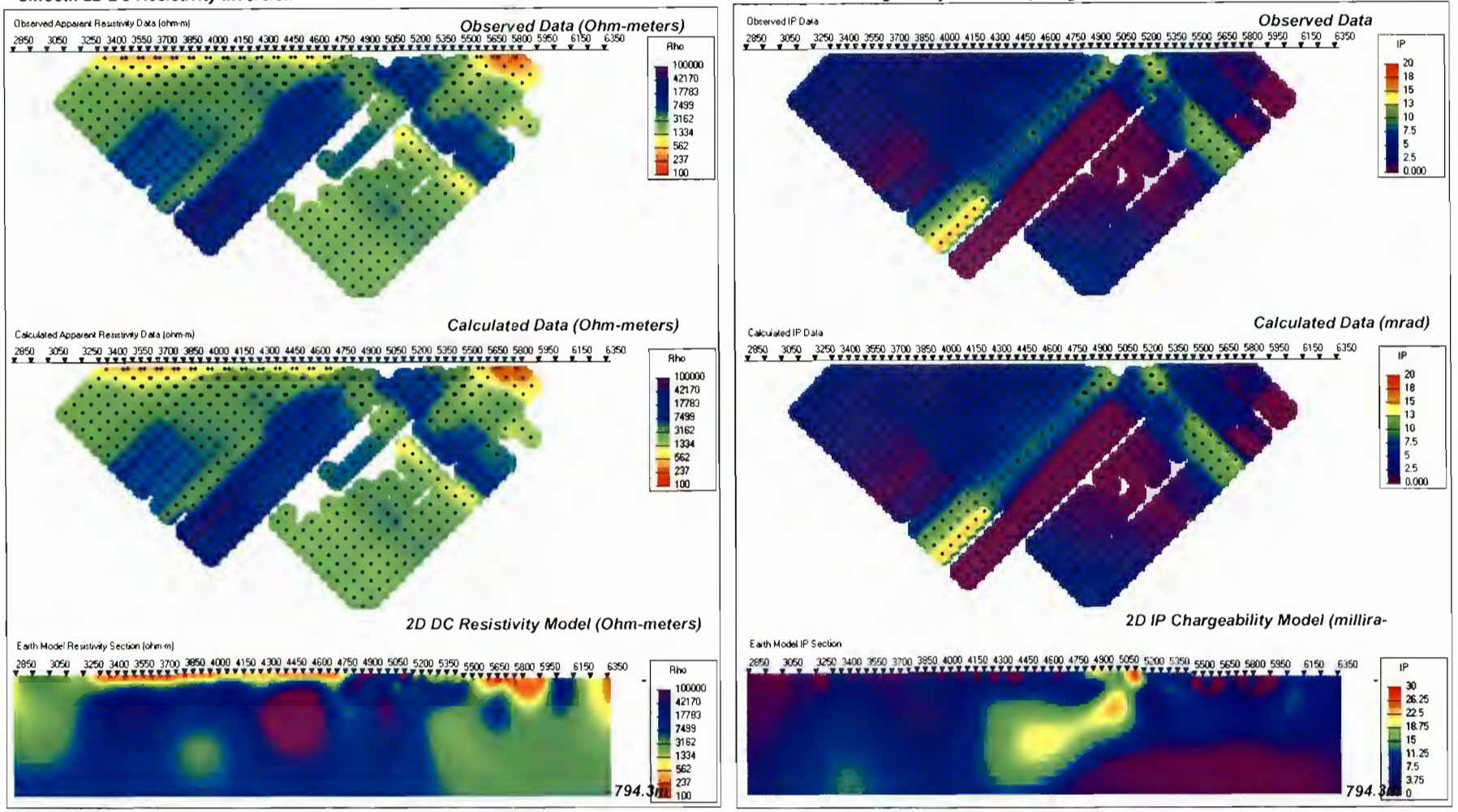

a) L10600N: 2D DC Resistivity (left) & 2D IP (right) Unconstrained Inversion Results with Observed Data and Calculated Models

L10600N - UBC 2D DCIP Inversion Results (cont...)

Smooth 2D IP Chargeability Inversion (using half-space conductivity)

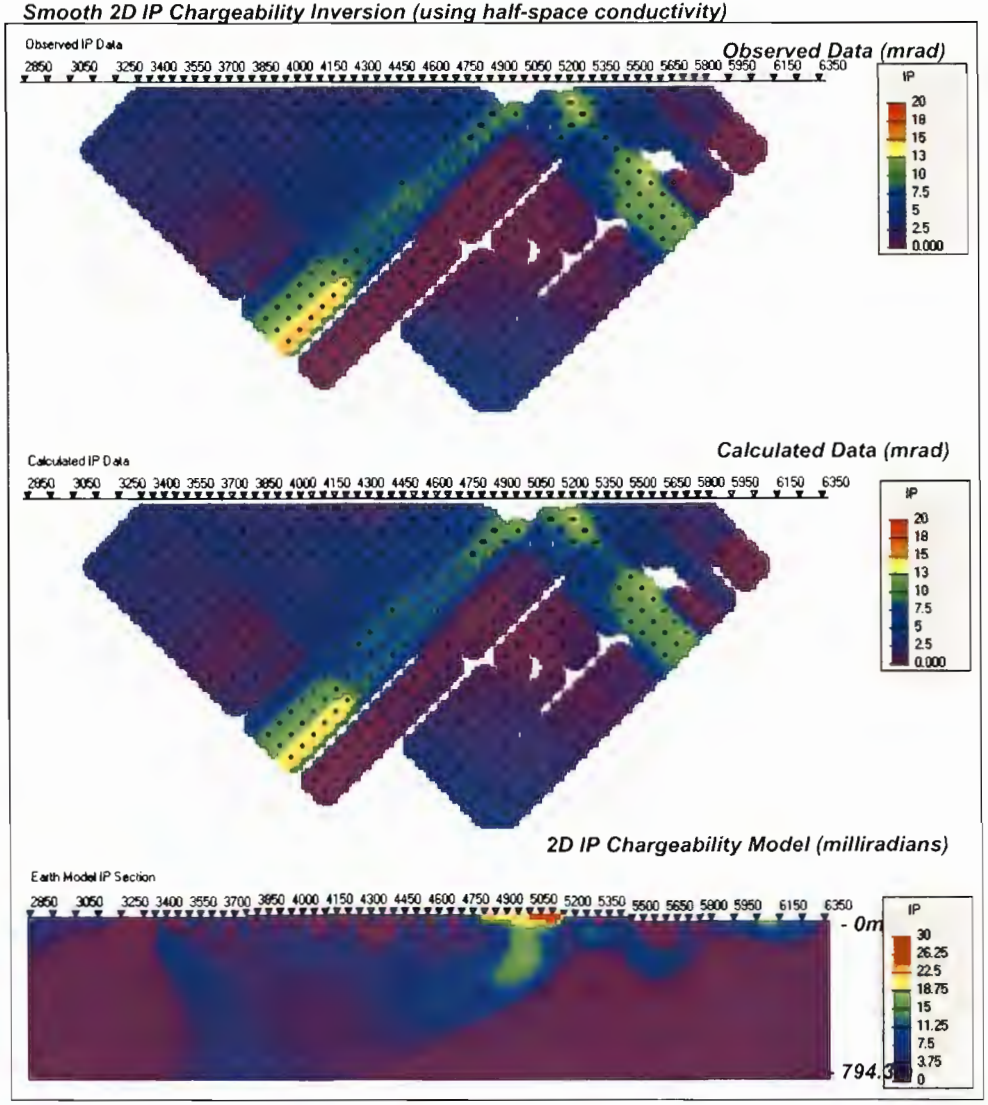

b) L10600N: 2D IP Unconstrained Inversion Results with Observed Data and Calculated Models (using half-space conductivity model)

L10600N - 2D MT Raw Data

Raw data input to inversions (edited & interpolated)

Stitched 1D models

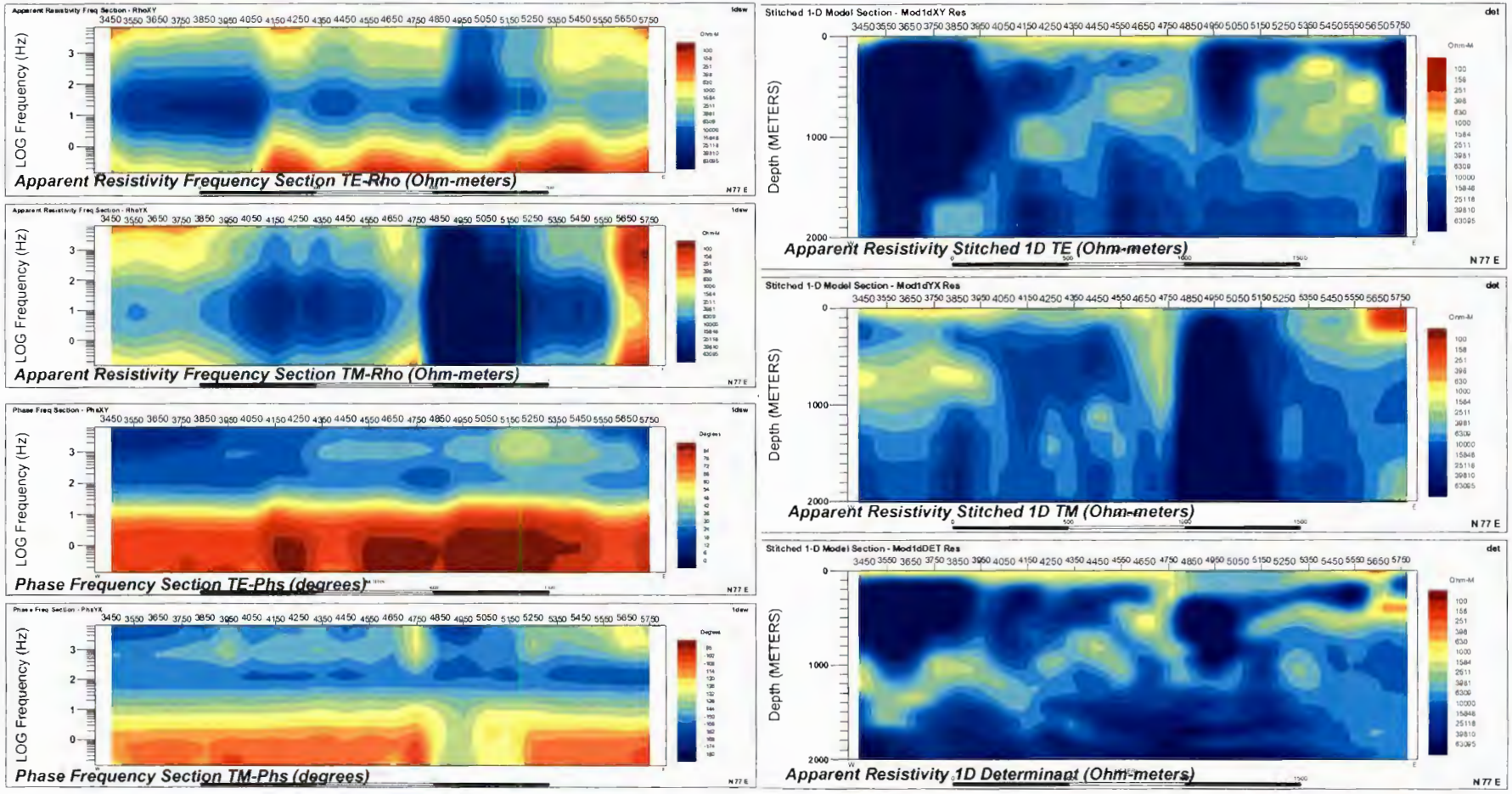

c) L10600N: 2D MT unrotated Raw Data (left) and Stitched 1D Models (right)

L10600N MT Frequency Profiles

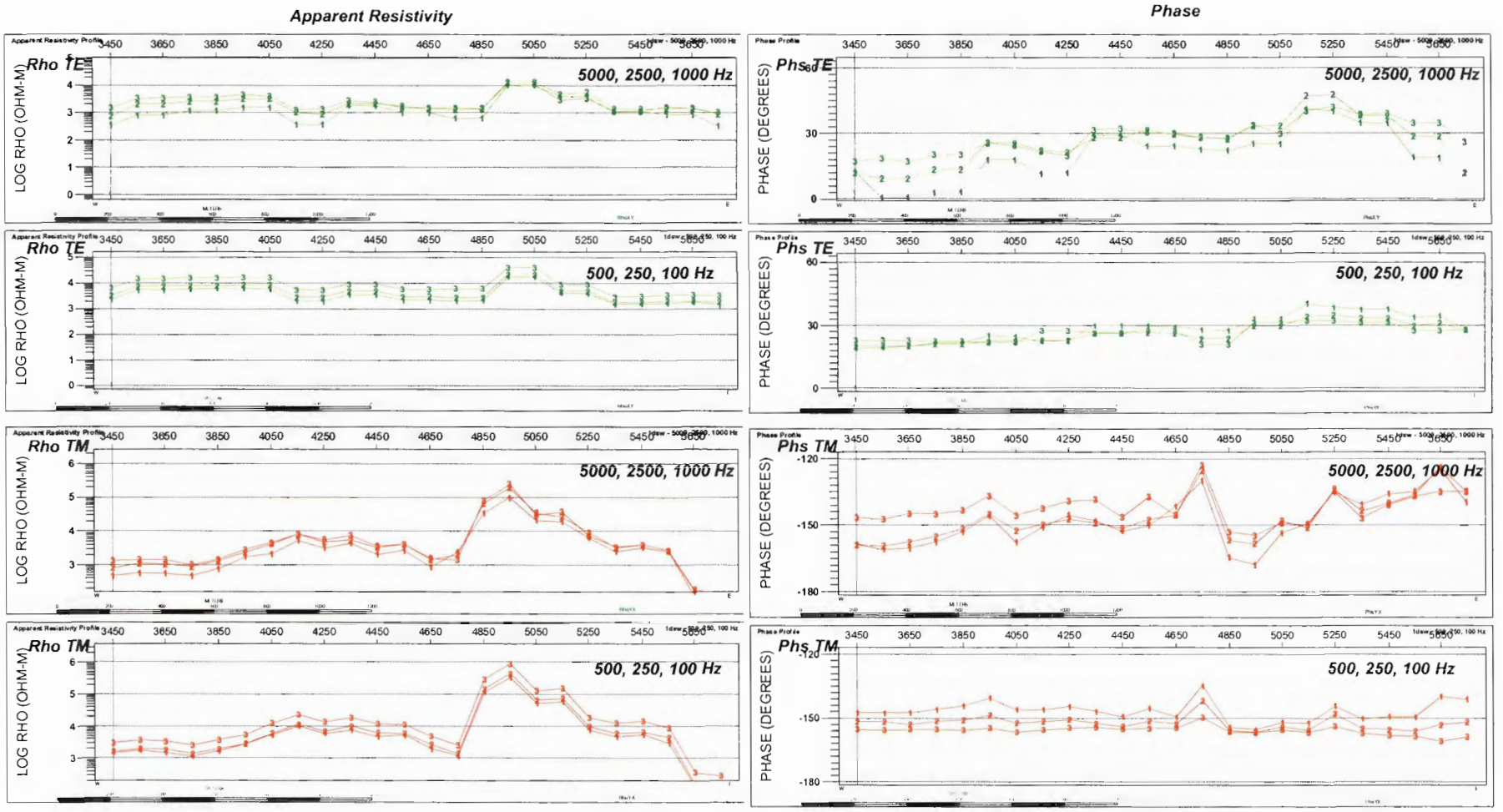

d) L10600N: MT Resistivity and Phase (right) Frequency Profiles

L10600N- 2D MT Inversion Models

2D MT PW1 Model (ohm-m), Starting model: rlm1, Input data: TM (Phs+Rho)

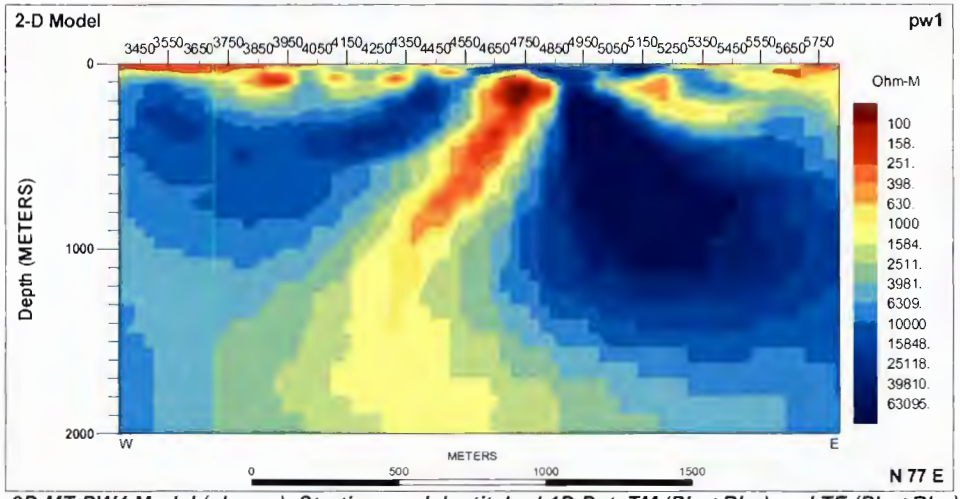

2D MT PW4 Model (ohm-m), Starting model: stitched 1D Det, TM (Phs+Rho) and TE (Phs+Rho)

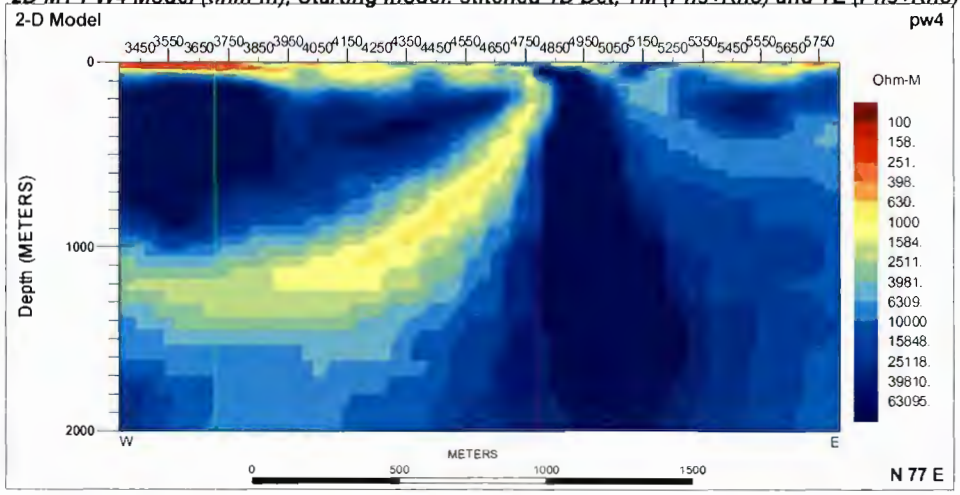

e) L10600N: 2D PW MT Resistivity Inversion Models

Line L10800N

L10800N - UBC 2D DCIP Inversion Results

Smooth 2D DC Resistivity Inversion

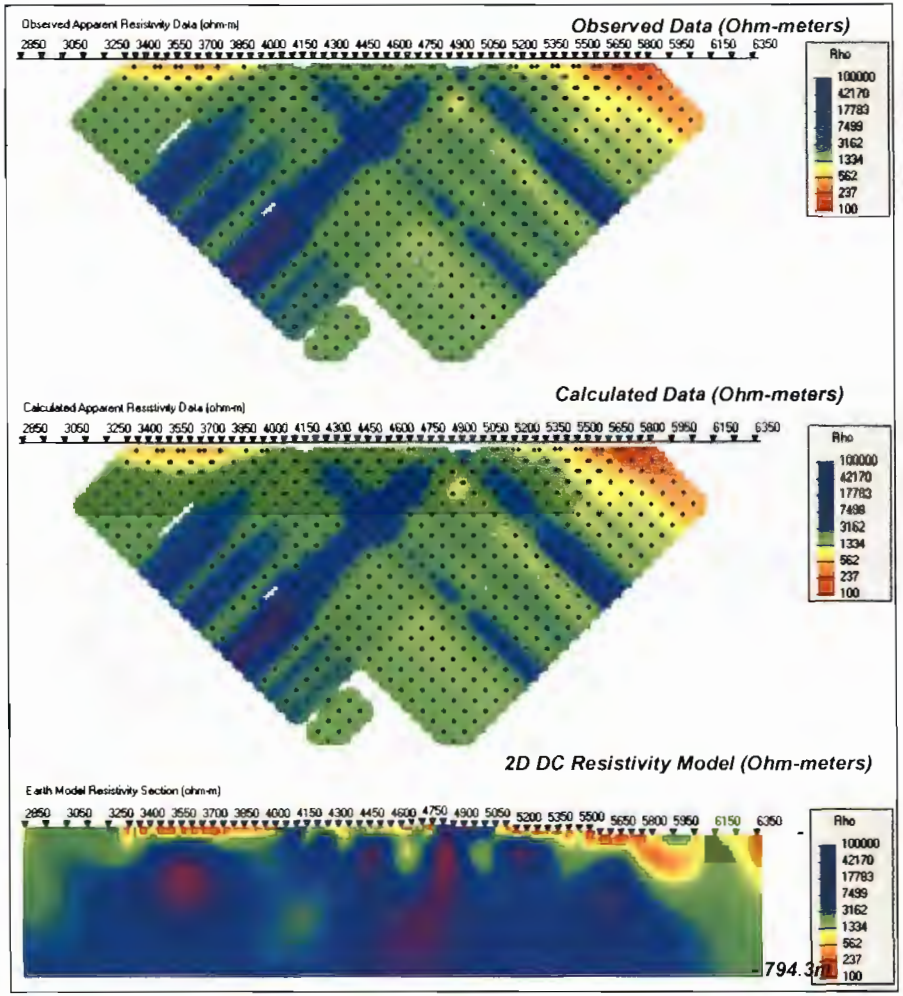

Smooth 2D IP Chargeability Inversion (using Titan conductivity)

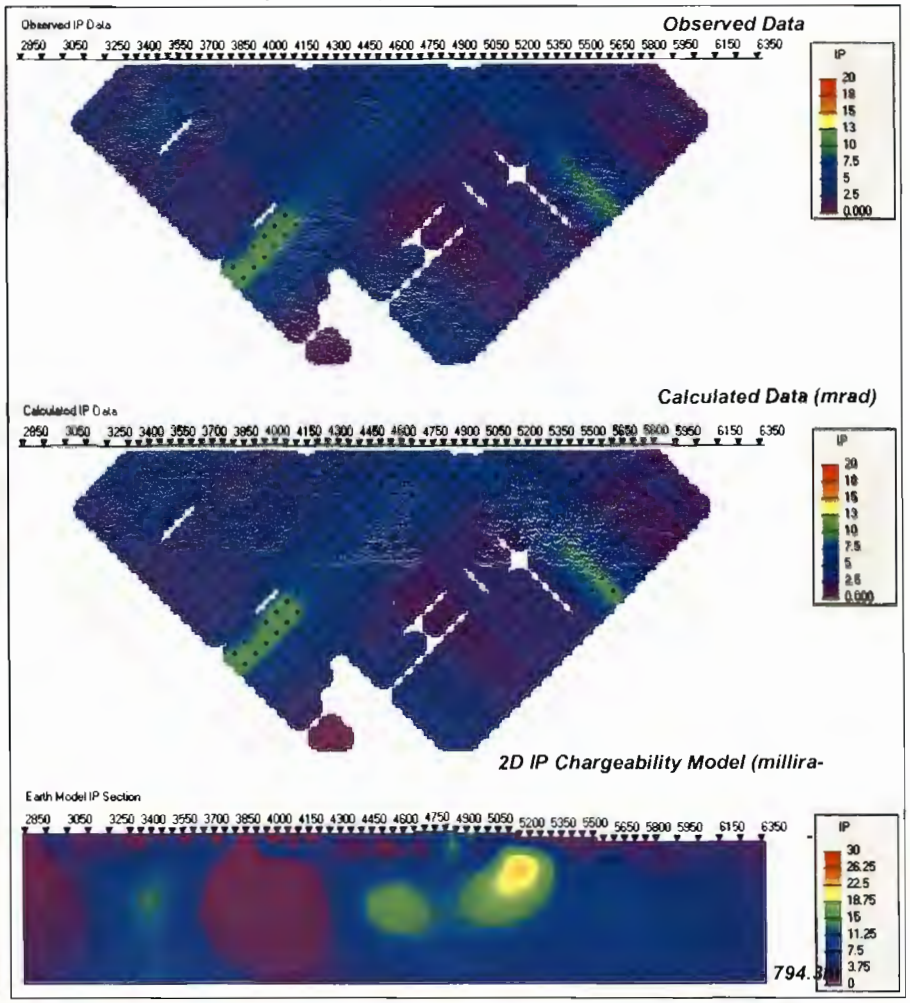

a) L10800N: 2D DC Resistivity (left) & 2D IP (right) Unconstrained Inversion Results with Observed Data and Calculated Models

L10800N - UBC 2D DCIP Inversion Results (cont...)

Smooth 2D IP Chargeability Inversion (using half-space conductivity)

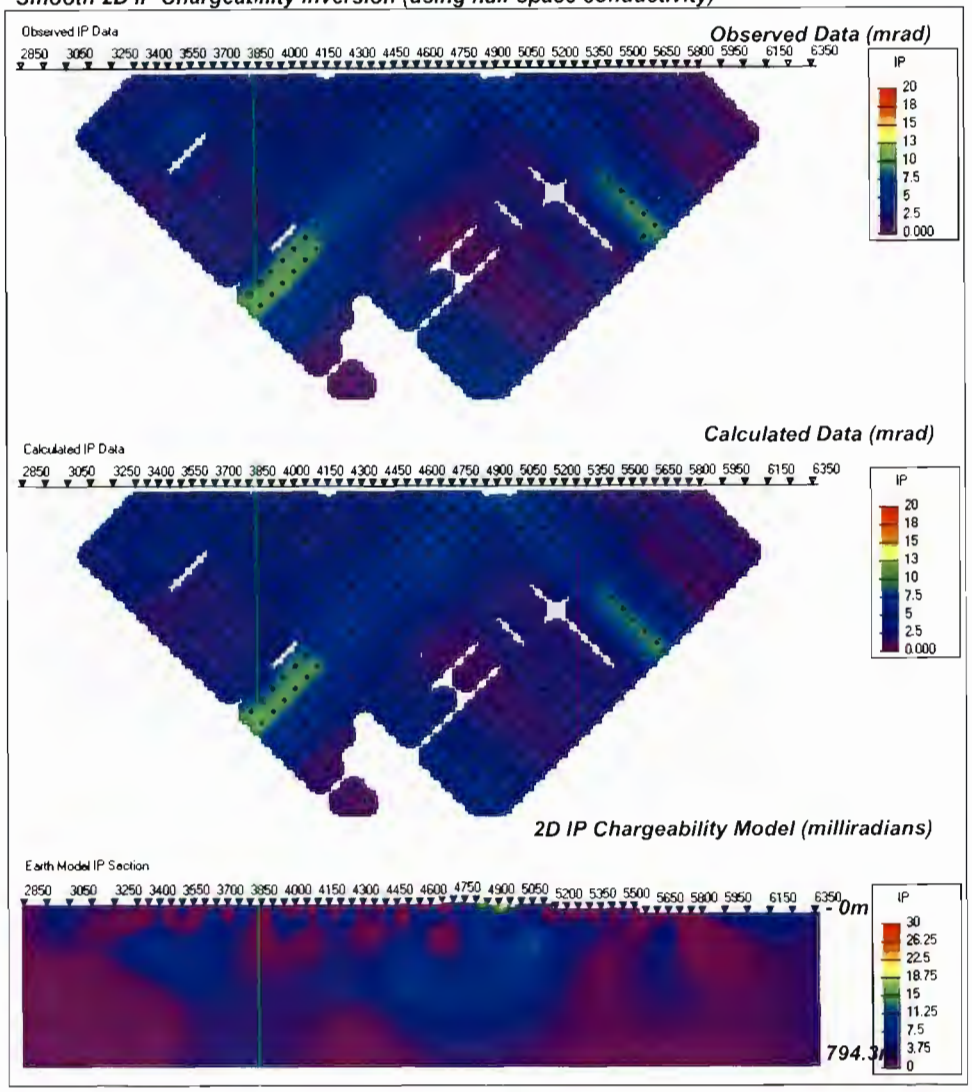

b) L10800N: 2D IP Unconstrained Inversion Results with Observed Data and Calculated Models (using half-space conductivity model)

L10800N - 2D MT Raw Data

Raw data input to inversions (edited & interpolated)

Stitched 1D models

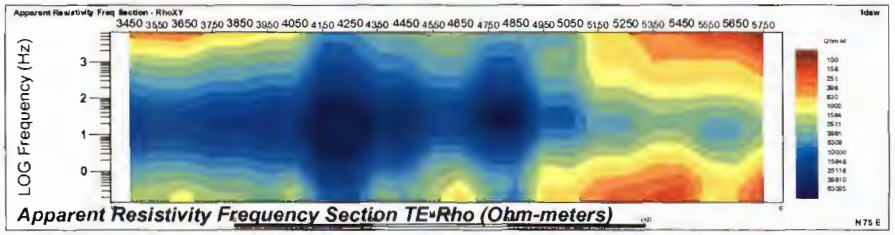

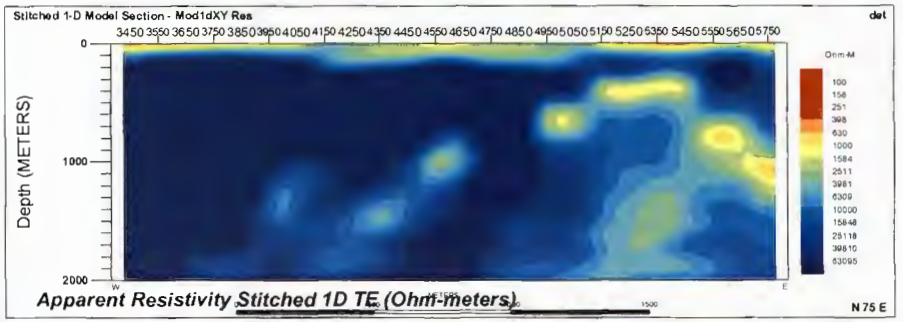

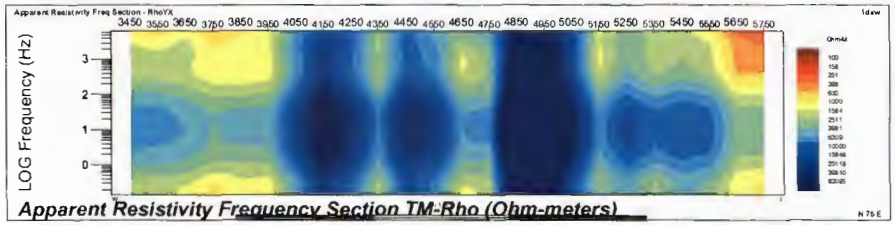

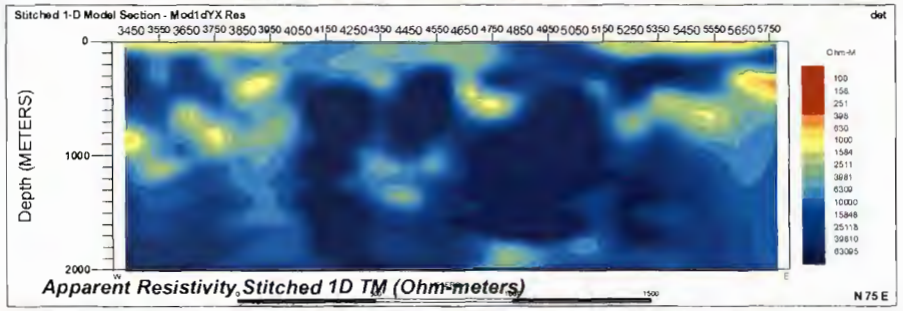

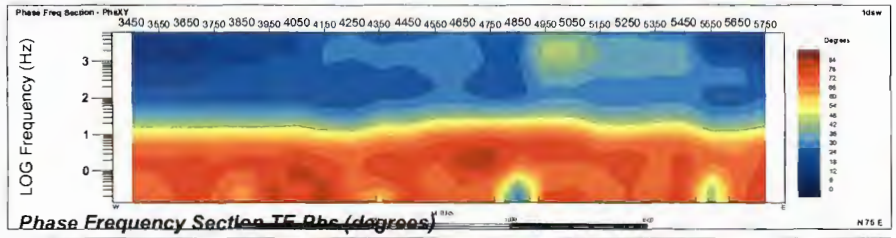

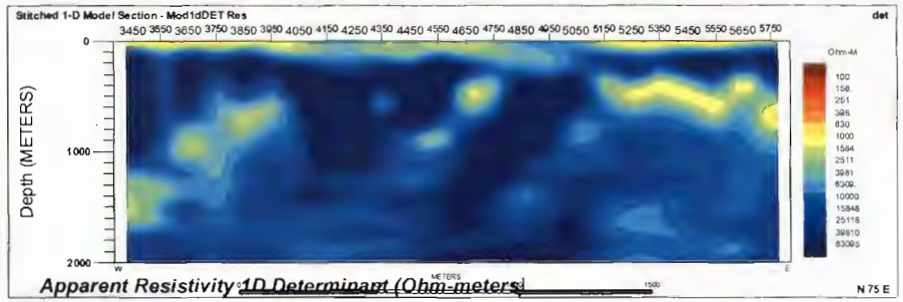

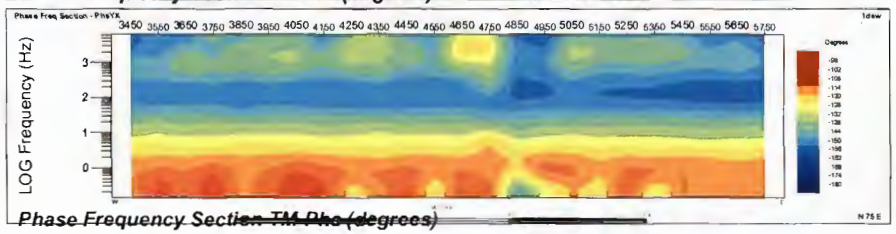

c) L10800N: 2D MT unrotated Raw Data (left) and Stitched 1D Models (right)

L10800N MT Frequency Profiles

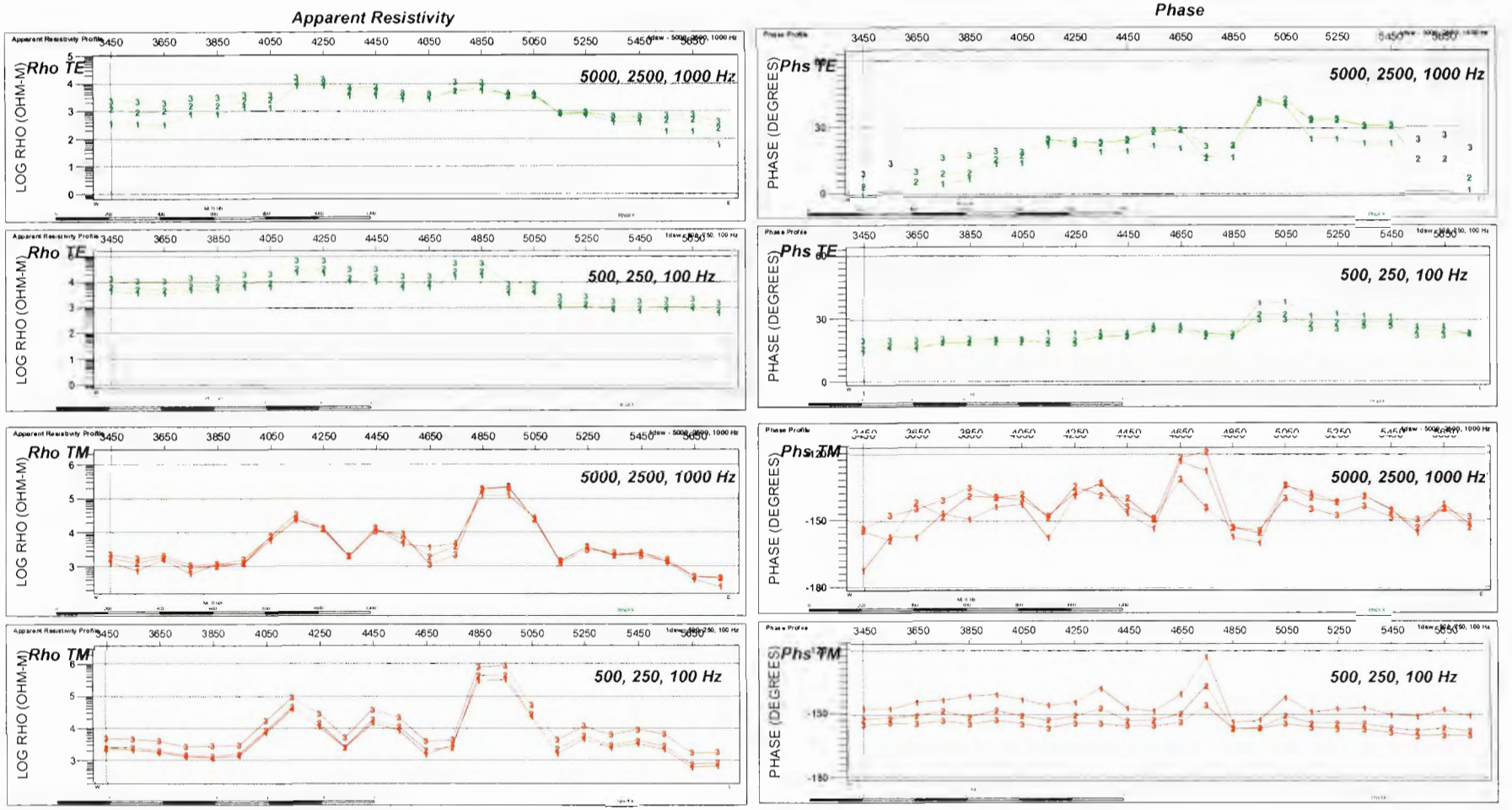

d) L10800N: MT Resistivity and Phase (right) Frequency Profiles

L10800N- 2D MT Inversion Models

2D MT PW1 Model (ohm-m), Starting model: rlm1, Input data: TM (Phs+Rho)

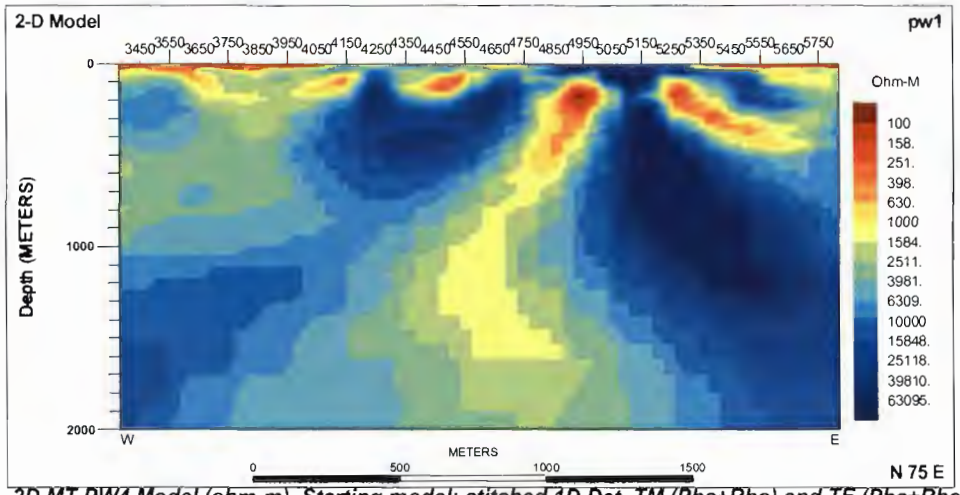

2D MT PW4 Model (ohm-m), Starting model: stitched 1D Det, TM (Phs+Rho) and TE (Phs+Rho)

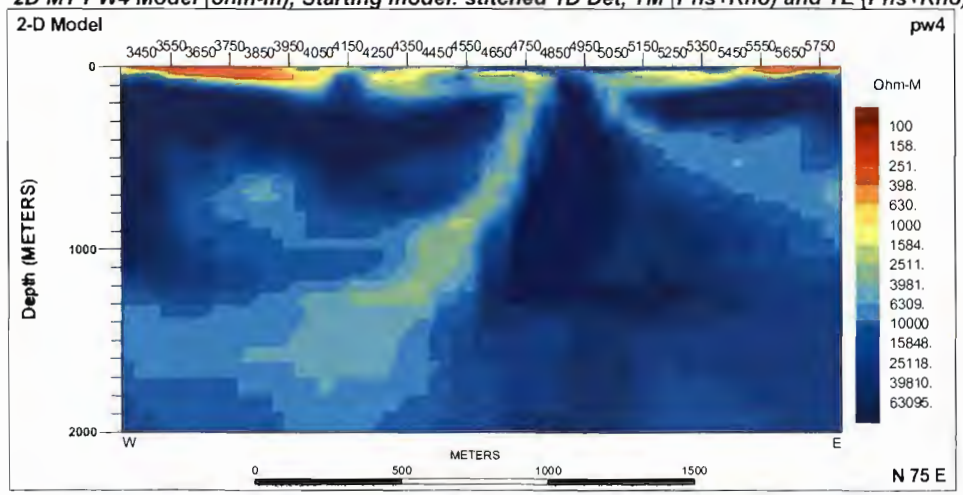

e) L10800N: 2D PW MT Resistivity Inversion Models

APPENDIX F. LIST OF MAPS[1]

GLOSSARY OF TERMS

SMDC – SMOOTH DIRECT CURRENT RESISTIVITY

SMIP – SMOOTH INDUCED POLARIZATION

NULLCOND – UBC INVERSION MODEL USING THE HALF SPACE CONDUCTIVITY AS REFERENCE

PW – PLANE WAVE MT INVERSION MODEL

TITAN 2D CROSS-SECTIONS (MAPS IN OASISMONTAJ FORMAT)

PAGE	MAP TYPE	Drawing Name (Line#maptype.map)
G1	Unconstrained UBC Smooth 2D DC Resistivity	L9900N smDC.map
G2	Unconstrained UBC Smooth 2D IP Chargeability (nullcon)	L9900N smIP nullcon.map
G3	Unconstrained UBC Smooth 2D IP Chargeability	L9900N smIP.map
G4	Unconstrained PW (TM + TE model) 2D MT Resistivity (determinant)	L9900N PW4_it30.map
G5	Unconstrained UBC Smooth 2D DC Resistivity	L10200N smDC.map
G6	Unconstrained UBC Smooth 2D IP Chargeability (nullcon)	L10200N smIP nullcon.map
G7	Unconstrained UBC Smooth 2D IP Chargeability	L10200N smIP.map
G8	Unconstrained PW (TM + TE model) 2D MT Resistivity (determinant)	L10200N PW4_it28.map
G9	Unconstrained UBC Smooth 2D DC Resistivity	L10400N smDC.map
G10	Unconstrained UBC Smooth 2D IP Chargeability (nullcon)	L10400N smIP nullcon.map
G11	Unconstrained UBC Smooth 2D IP Chargeability	L10400N smIP.map
G12	Unconstrained PW (TM + TE model) 2D MT Resistivity (determinant)	L10400N PW4_it30.map
G13	Unconstrained UBC Smooth 2D DC Resistivity	L10600N smDC.map
G14	Unconstrained UBC Smooth 2D IP Chargeability (nullcon)	L10600N smIP nullcon.map
G15	Unconstrained UBC Smooth 2D IP Chargeability	L10600N smIP.map
G16	Unconstrained PW (TM + TE model) 2D MT Resistivity (determinant)	L10600N PW4_it23.map
G17	Unconstrained UBC Smooth 2D DC Resistivity	L10800N smDC.map
G18	Unconstrained UBC Smooth 2D IP Chargeability (nullcon)	L10800N smIP nullcon.map
G19	Unconstrained UBC Smooth 2D IP Chargeability	L10800N smIP.map
G20	Unconstrained PW (TM + TE model) 2D MT Resistivity (determinant)	L10800N PW4_it28.map

[1] For details on other inversion models and Maps refer to *Appendix E "TITAN-24 Inversion Results", and "Digital Archive HDD"*. All section maps are grouped and archived in separated folders according to their line numbers.

DEPTH LEVEL PLAN MAPS (MAPS IN OASISMONTAJ FORMAT)

PAGE	MAP TYPE	Drawing Name (Line#maptype.map)
G26	2D Resistivity (Z=50m) - Unconstrained UBC Smooth 2D Resistivity	smDC at 50m depth.map
G27	2D Chargeability (Z=50m) - Unconstrained UBC Smooth 2D IP Chargeability (nullcon)	smIP nullcon at 50m depth.map
G28	2D Resistivity (Z=50m/TM +TE) - Unconstrained 2D PW4 MT Resistivity	mtRes PW4 at 50m depth.map
G29	2D Resistivity (Z=100m) - Unconstrained UBC Smooth 2D Resistivity	smDC at 100m depth.map
G30	2D Chargeability (Z=100m) - Unconstrained UBC Smooth 2D IP Chargeability (nullcon)	smIP nullcon at 100m depth.map
G31	2D Resistivity (Z=100m/TM +TE) - Unconstrained 2D PW4 MT Resistivity	mtRes PW4 at 100m depth.map
G32	2D Resistivity (Z=250m) - Unconstrained UBC Smooth 2D Resistivity	smDC at 250m depth.map
G33	2D Chargeability (Z=250m) - Unconstrained UBC Smooth 2D IP Chargeability (nullcon)	smIP nullcon at 250m depth.map
G34	2D Resistivity (Z=250m/TM +TE) - Unconstrained 2D PW4 MT Resistivity	mtRes PW4 at 250m depth.map
G35	2D Resistivity (Z=400m) - Unconstrained UBC Smooth 2D Resistivity	smDC at 400m depth.map
G36	2D Chargeability (Z=400m) - Unconstrained UBC Smooth 2D IP Chargeability (nullcon)	smIP nullcon at 400m depth.map
G37	2D Resistivity (Z=400m/TM +TE) - Unconstrained 2D PW4 MT Resistivity	mtRes PW4 at 400m depth.map
G38	2D Resistivity (Z=600m) - Unconstrained UBC Smooth 2D Resistivity	smDC at 600m depth.map
G38	2D Chargeability (Z=600m) - Unconstrained UBC Smooth 2D IP Chargeability (nullcon)	smIP nullcon at 600m depth.map
G40	2D Resistivity (Z=600m/TM +TE) - Unconstrained 2D PW4 MT Resistivity	mtRes PW4 at 600m depth.map
G41	2D Resistivity (Z=1000m/TM +TE) - Unconstrained 2D PW4 MT Resistivity	mtRes PW4 at 1000m depth.map
G42	2D Resistivity (Z=1500m/TM +TE) - Unconstrained 2D PW4 MT Resistivity	mtRes PW4 at 1500m depth.map

INTERPRETATION PLAN MAPS (MAPS IN OASISMONTAJ FORMAT)

PAGE	MAP TYPE	Drawing Name (Line#maptype.map)
G43	Titan-24 Geophysical Interpretation Plan Map over 2D Chargeability at 100m depth	Interpretation Plan over 2D Chargeability at 100m depth.map

APPENDIX G: OASIS SECTIONS AND PLAN MAPS[1]

DVD:\CA00516T- Loveland Project\Maps and Sections\Geosoft Sections\DCIP\L9900N smDC.map[2]

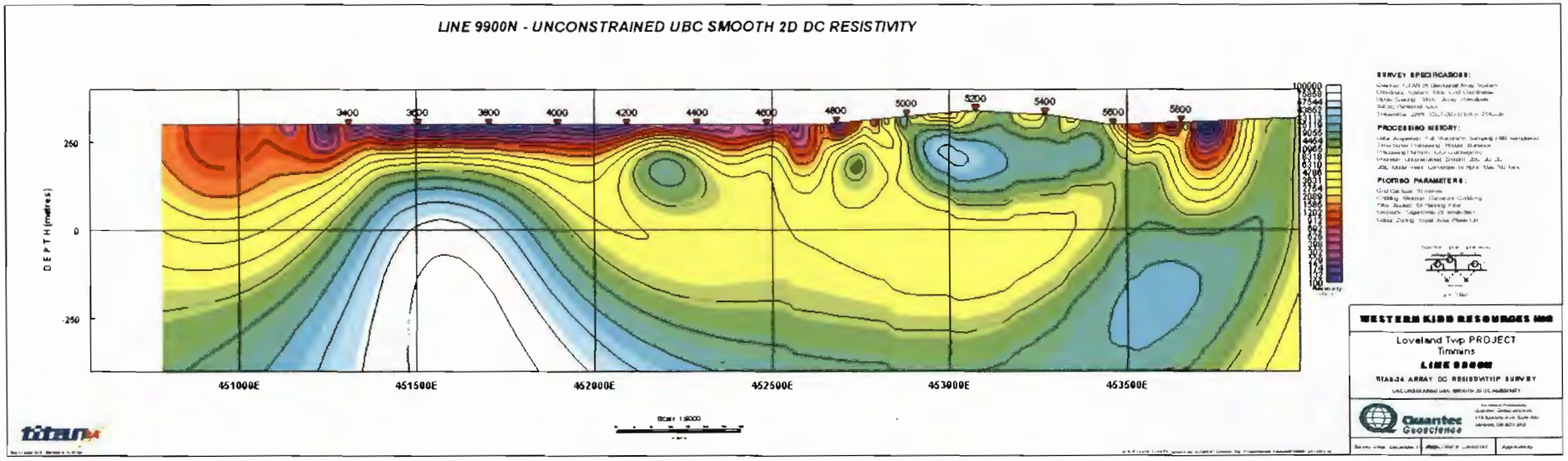

[1] *The Oasis Sections presented in this appendix are the most consistent models according to the degree of association with the DC and MT results and the available geological information. Additional models are available in the Digital Archive attached to this Interpretation Report. OasisMontaj Viewer available @ http://www.geosoft.com/pinfo/oasismontaj/free/montajviewer.asp*

[2] *Digital Archive Folder Path and map name (Line#maptype.map)*

DVD:\CA00516T- Loveland Project\Maps and Sections\Geosoft Sections\DCIP\L9900N smIP nullcon.map

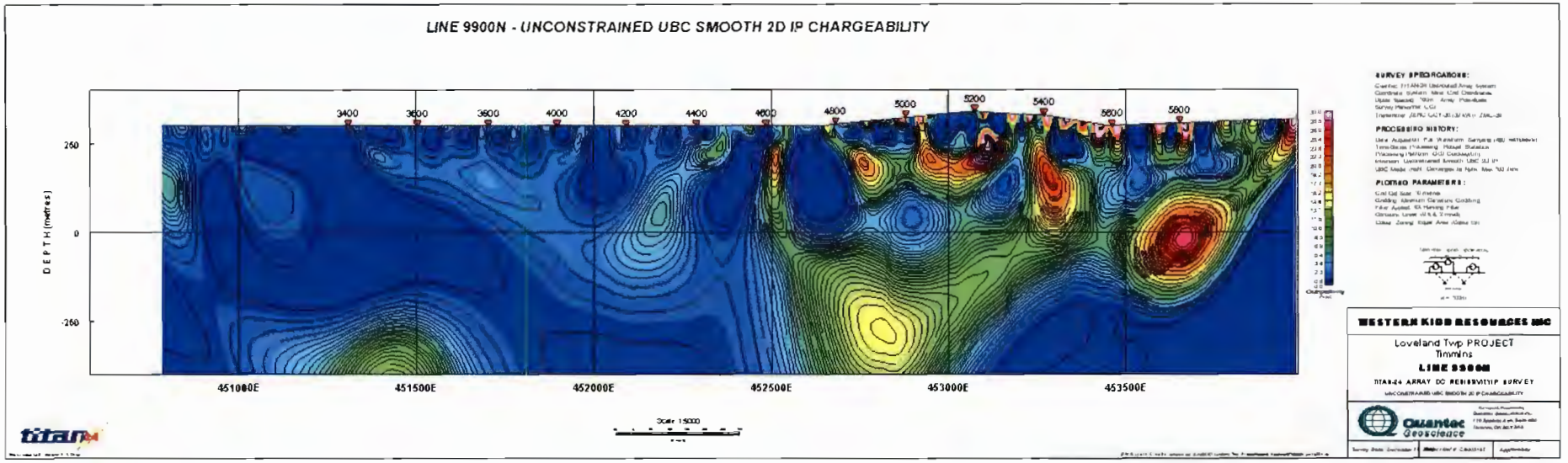

DVD:\CA00516T- Loveland Project\Maps and Sections\Geosoft Sections\DCIP\L9900N smIP.map

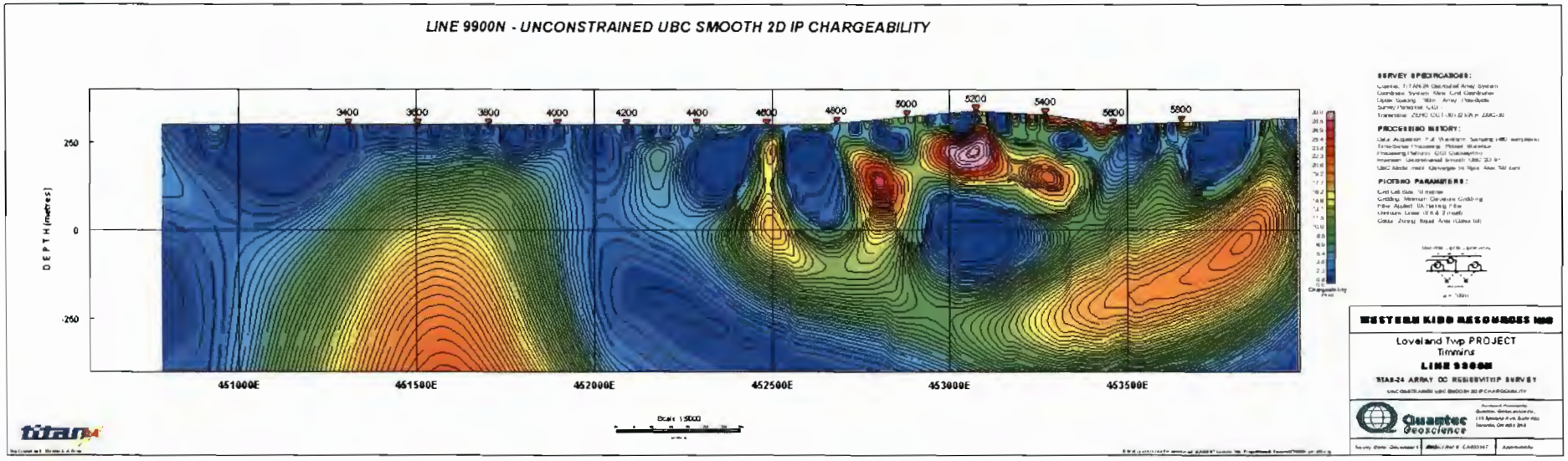

DVD:\CA00516T- Loveland Project\Maps and Sections\Geosoft Sections\MT\L9900N pw4_it30.map

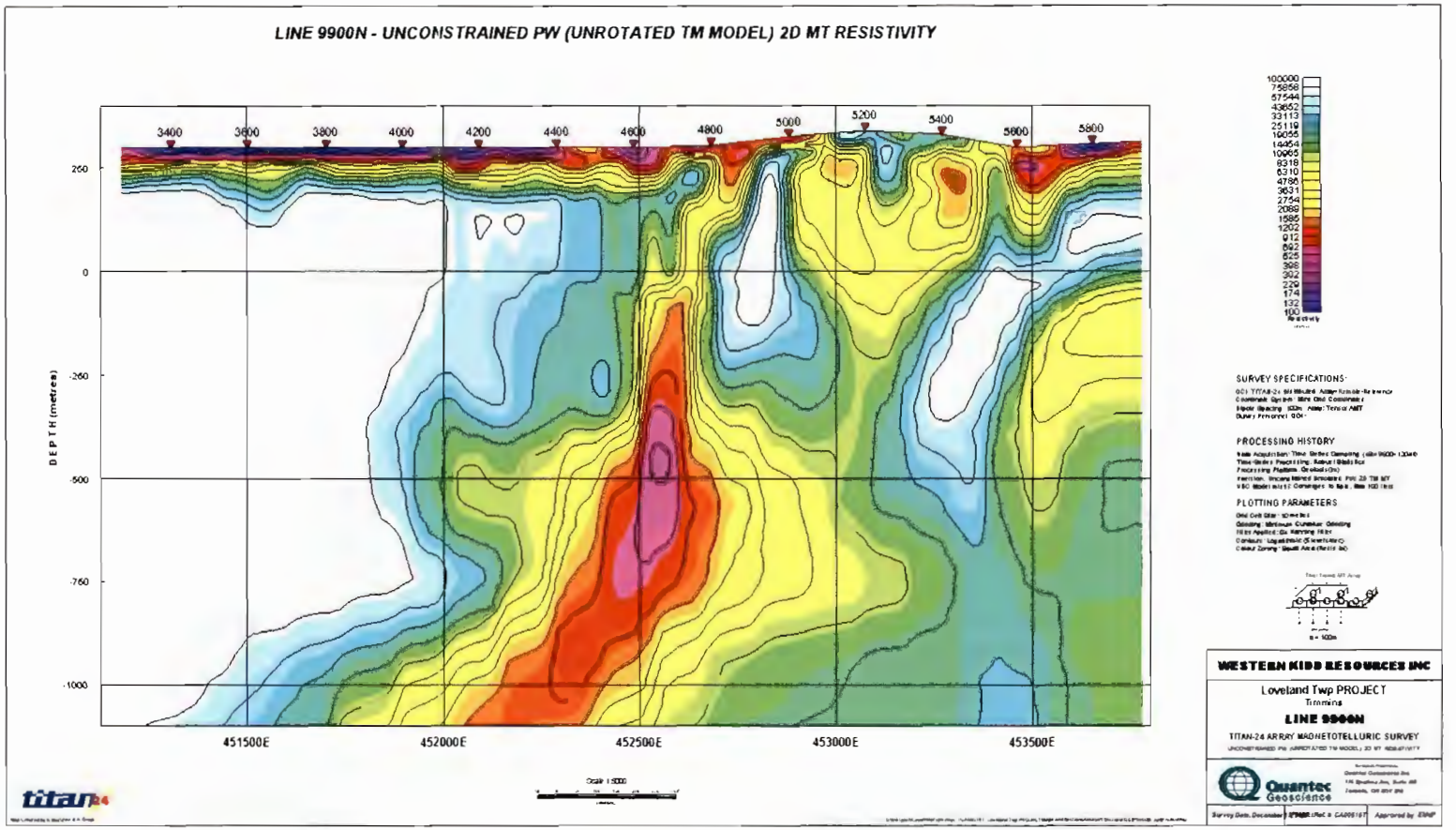

DVD:\CA00516T- Loveland Project\Maps and Sections\Geosoft Sections\DCIP\L10200N smDC.map[3]

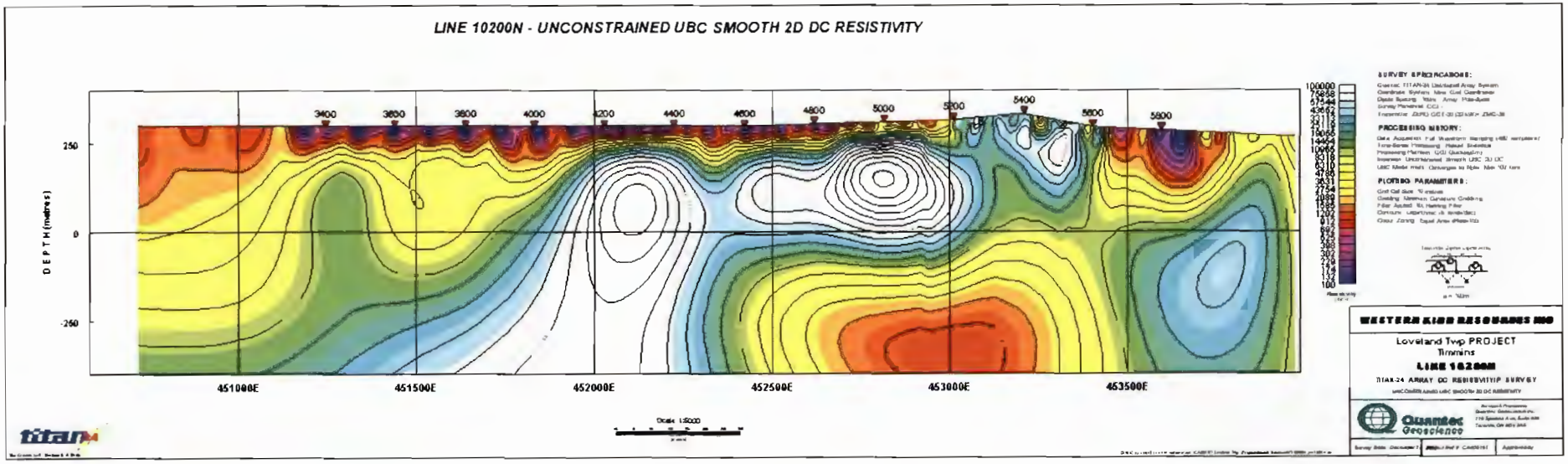

[3] *Digital Archive Folder Path and map name (Line#maptype.map)*

DVD:\CA00516T- Loveland Project\Maps and Sections\Geosoft Sections\DCIP\L10200N smIP nullcon.map

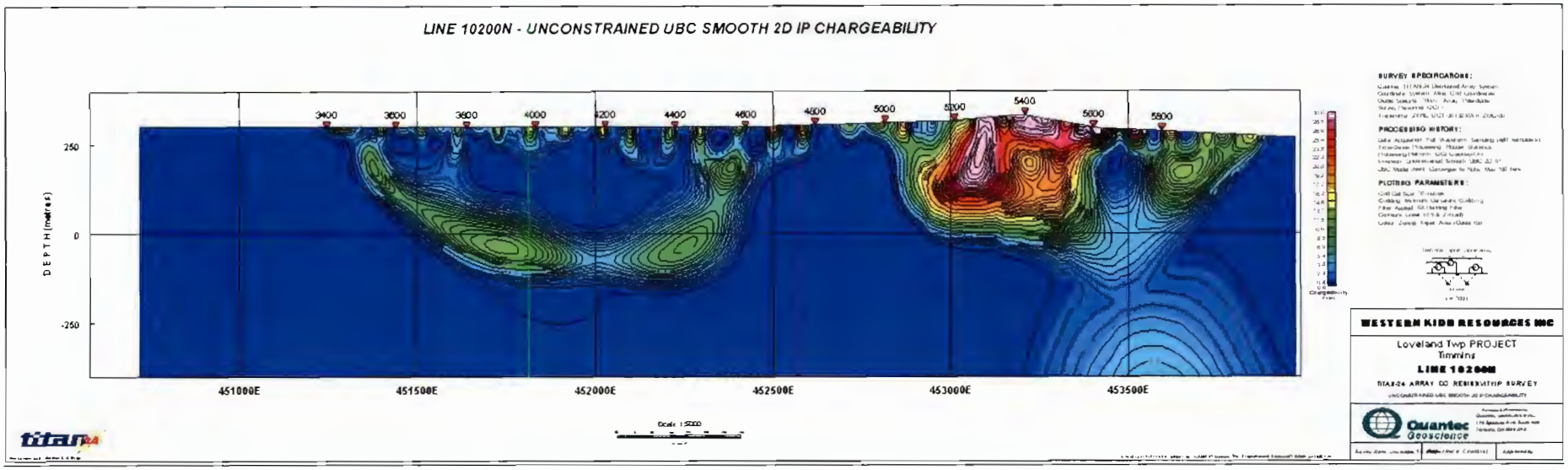

DVD:\CA00516T- Loveland Project\Maps and Sections\Geosoft Sections\DCIP\L10200N smIP.map

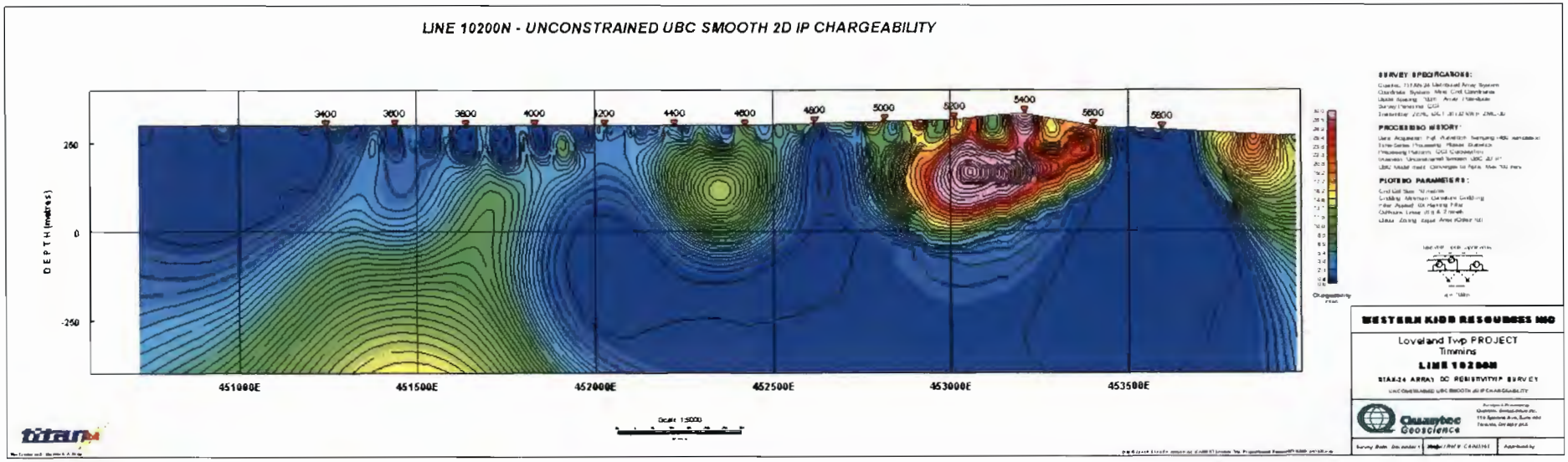

DVD:\CA00516T- Loveland Project\Maps and Sections\Geosoft Sections\MT\L10200N pw4_it30.map

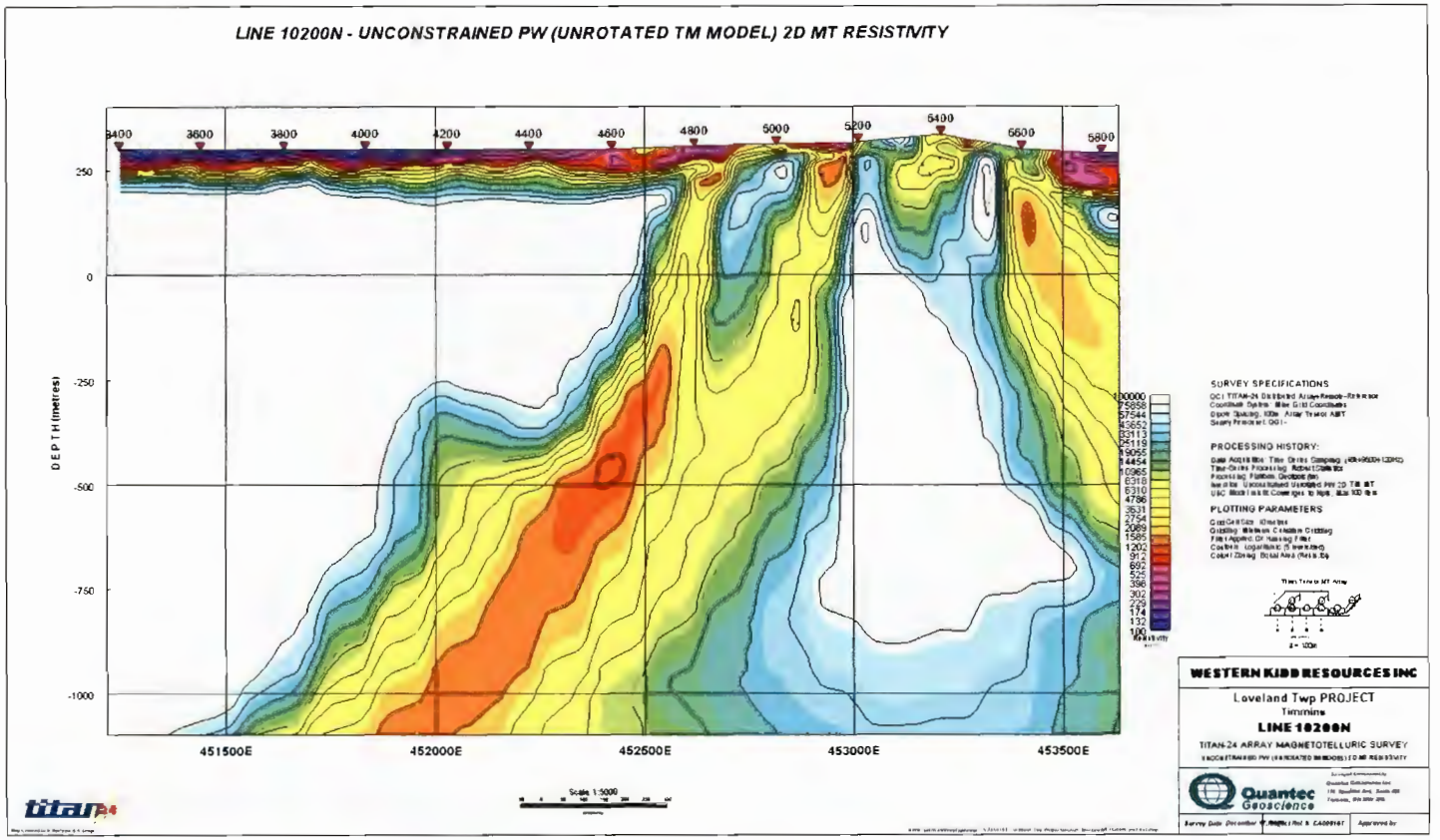

DVD:\CA00516T- Loveland Project\Maps and Sections\Geosoft Sections\DCIP\L10400N smDC.map[4]

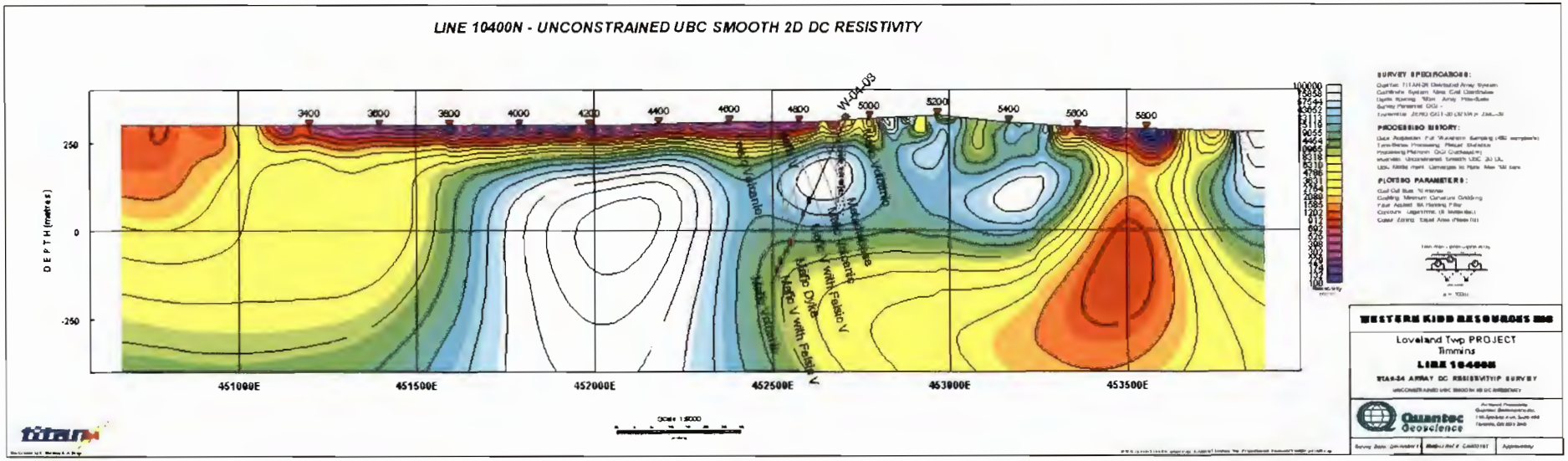

[4] *Digital Archive Folder Path and map name (Line#maptype.map)*

DVD:\CA00516T- Loveland Project\Maps and Sections\Geosoft Sections\DCIP\L10400N smIP nullcon.map

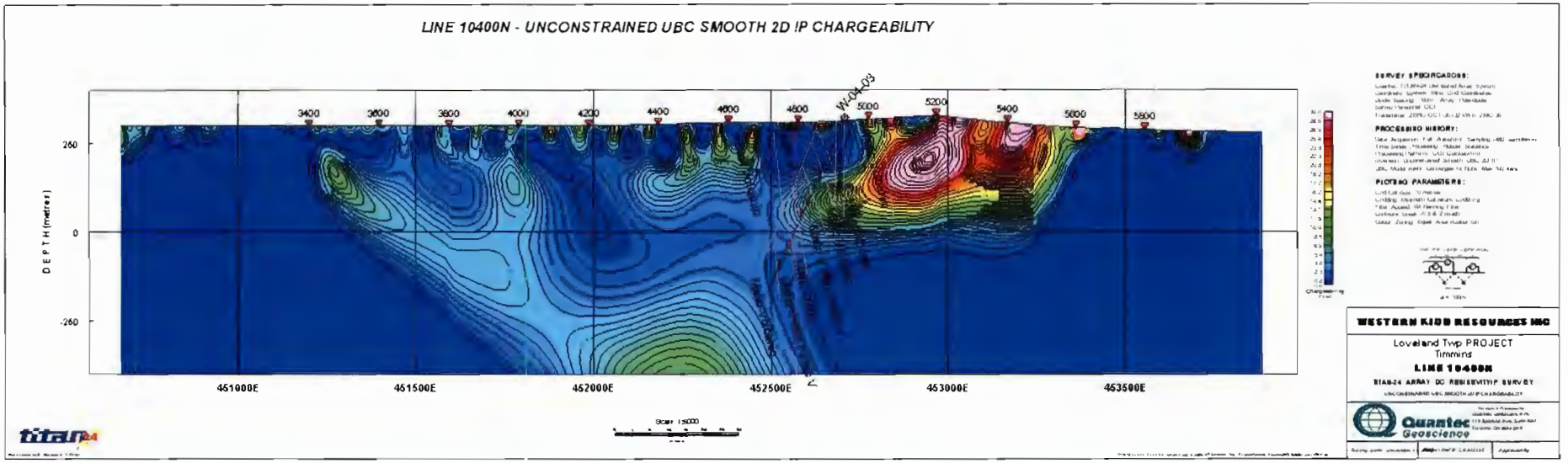

DVD:\CA00516T- Loveland Project\Maps and Sections\Geosoft Sections\DCIP\L10400N smIP.map

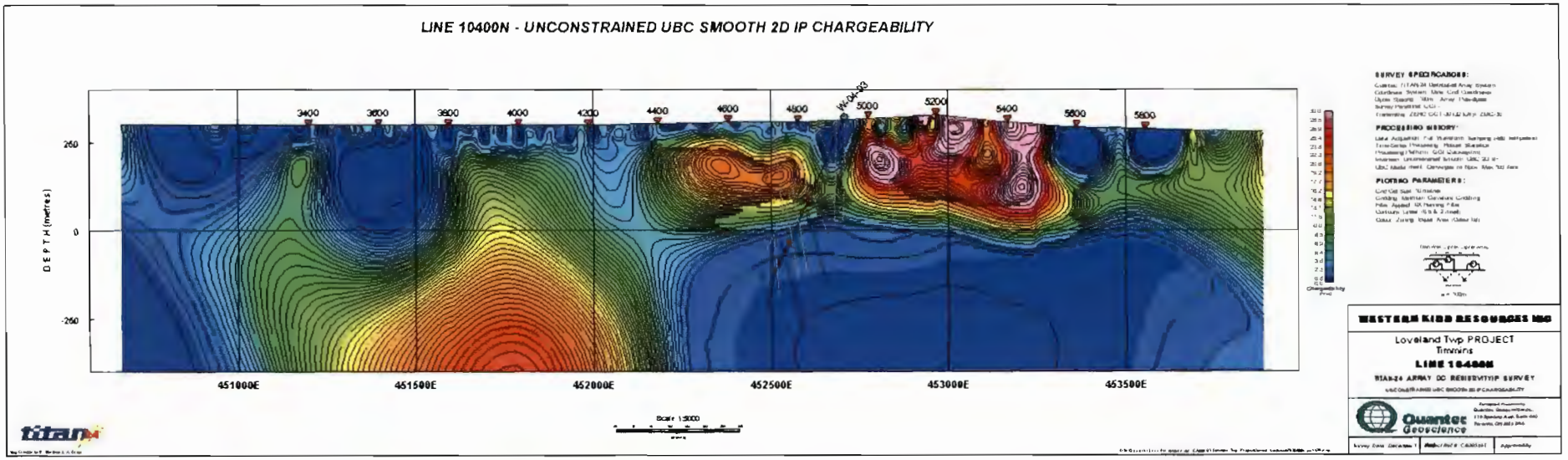

DVD:\CA00516T- Loveland Project\Maps and Sections\Geosoft Sections\MT\L10400N pw4_it30.map

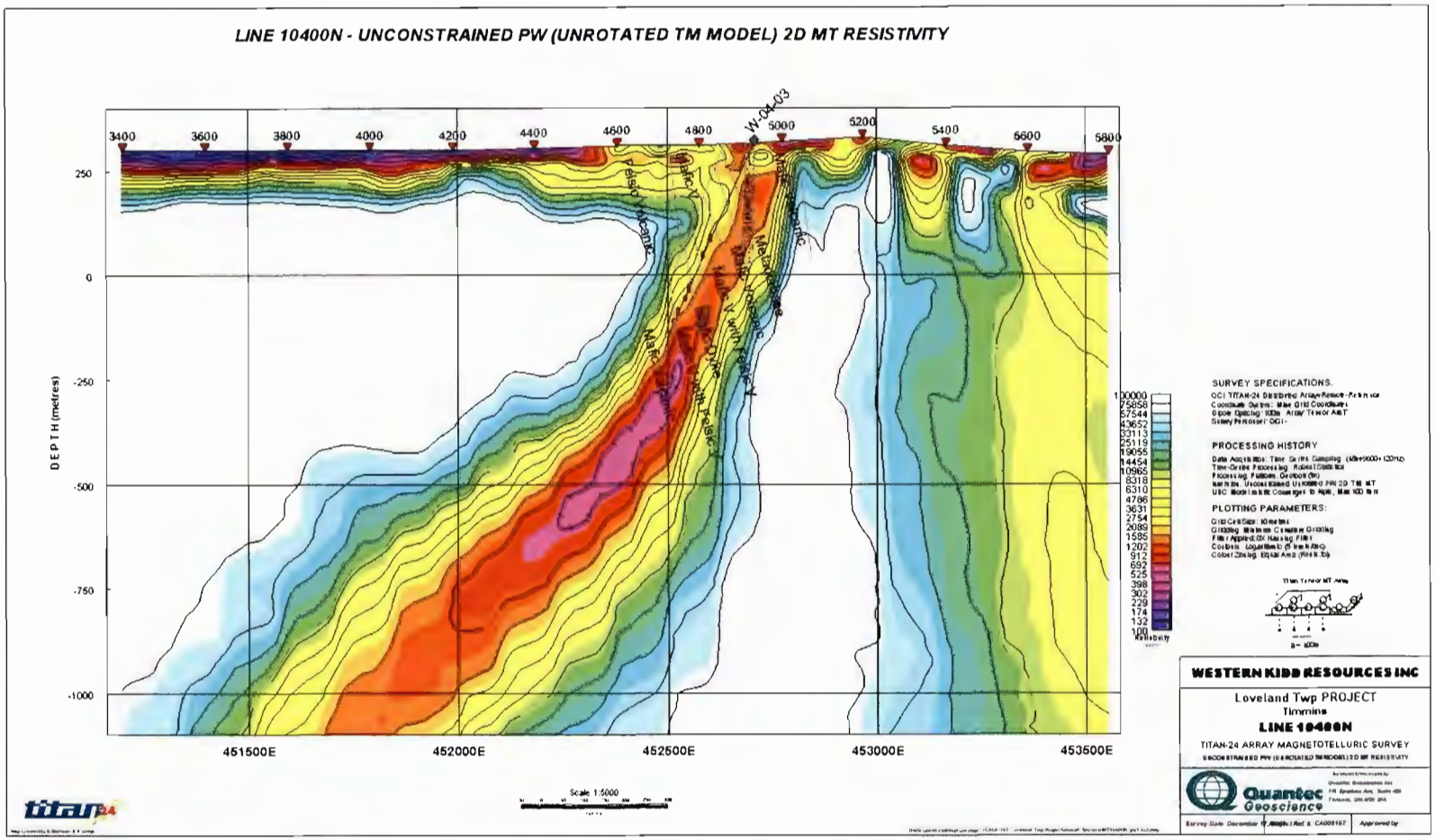

DVD:\CA00516T- Loveland Project\Maps and Sections\Geosoft Sections\DCIP\L10600N smDC.map[5]

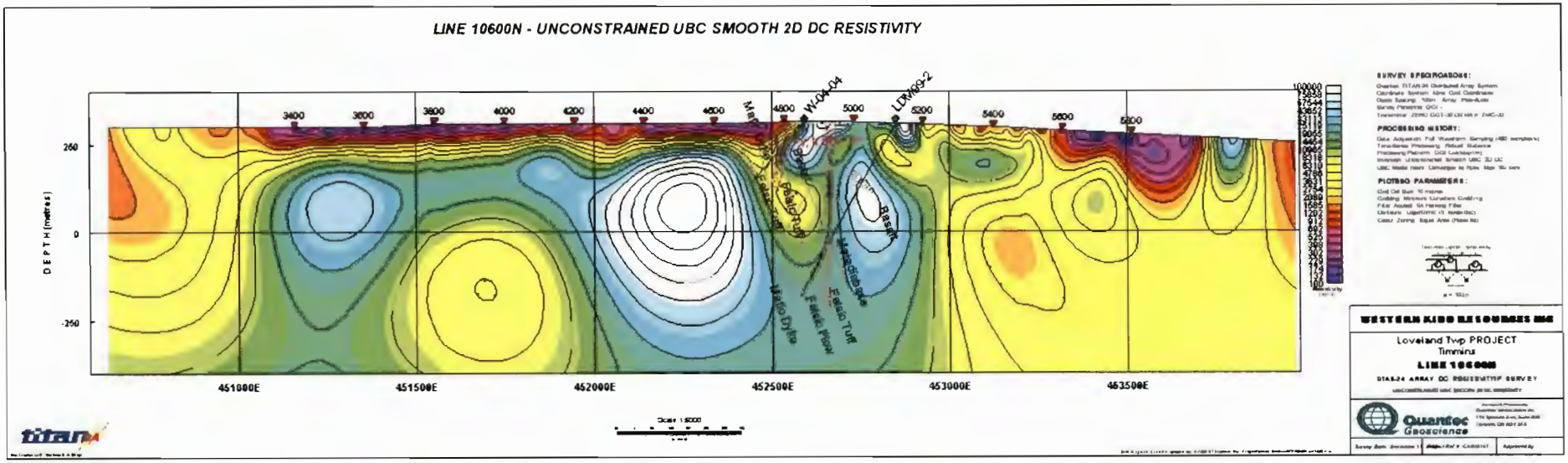

[5] *Digital Archive Folder Path and map name (Line#maptype.map)*

DVD:\CA00516T- Loveland Project\Maps and Sections\Geosoft Sections\DCIP\L10600N smIP nullcon.map

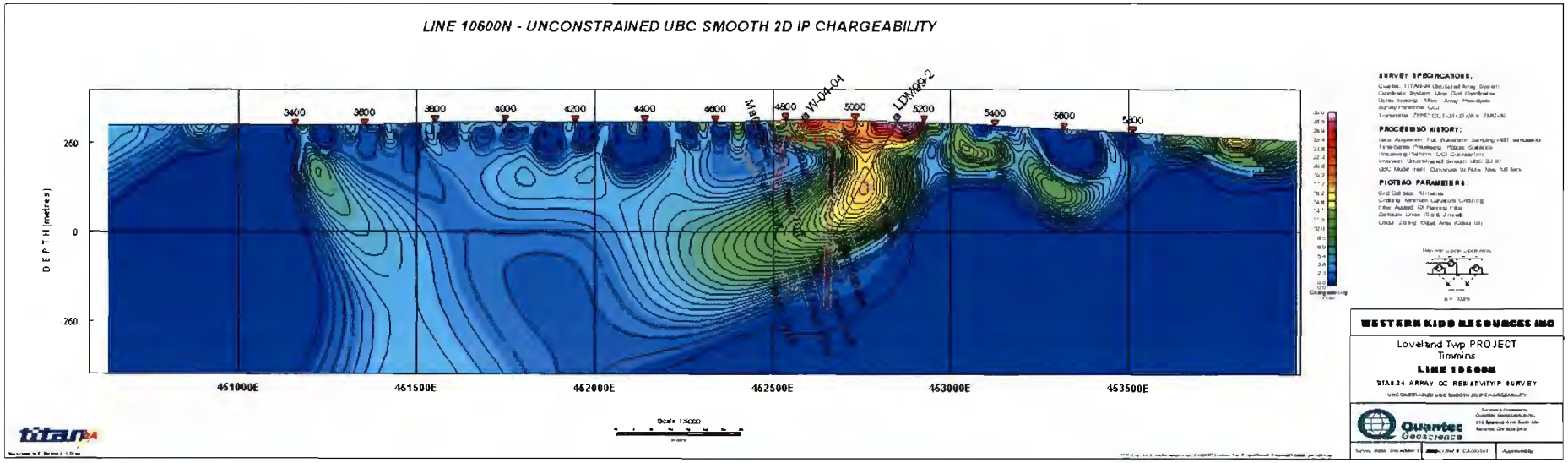

DVD:\CA00516T- Loveland Project\Maps and Sections\Geosoft Plans\DCIP\smDC at 250m depth.map

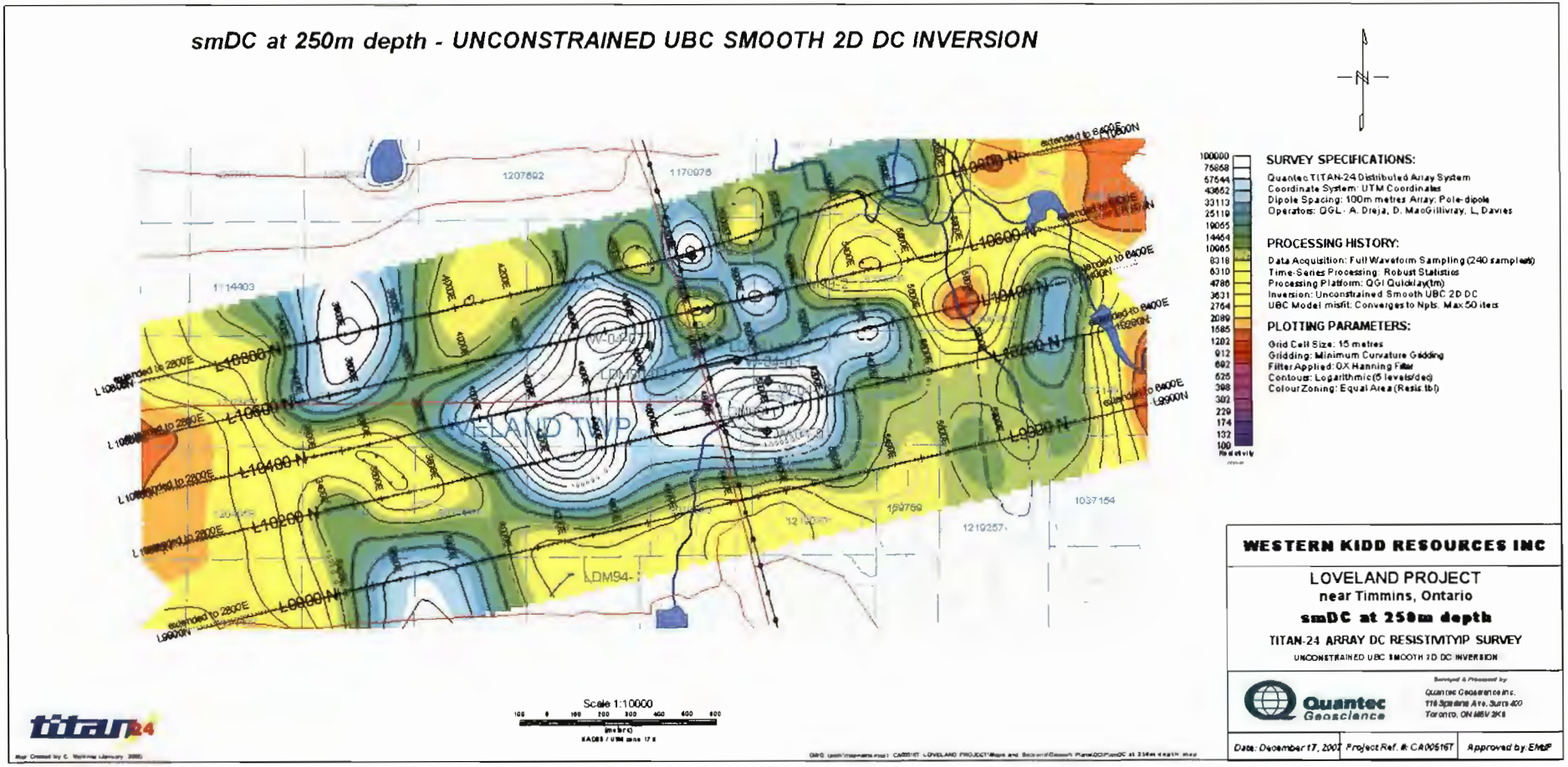

DVD:\CA00516T- Loveland Project\Maps and Sections\Geosoft Plans\DCIP\smDC at 400m depth.map

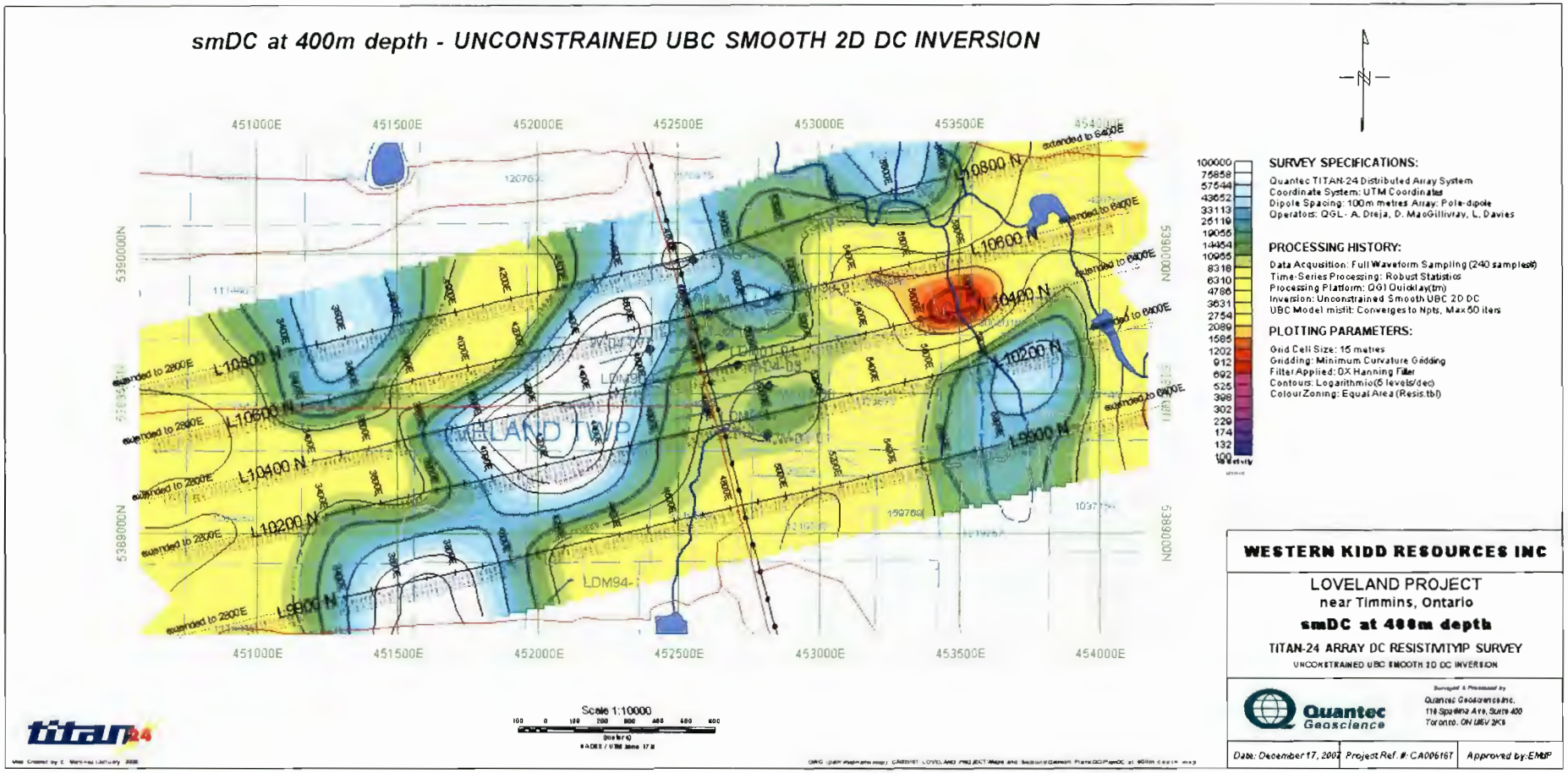

DVD:\CA00516T- Loveland Project\Maps and Sections\Geosoft Plans\DCIP\smDC at 600m depth.map

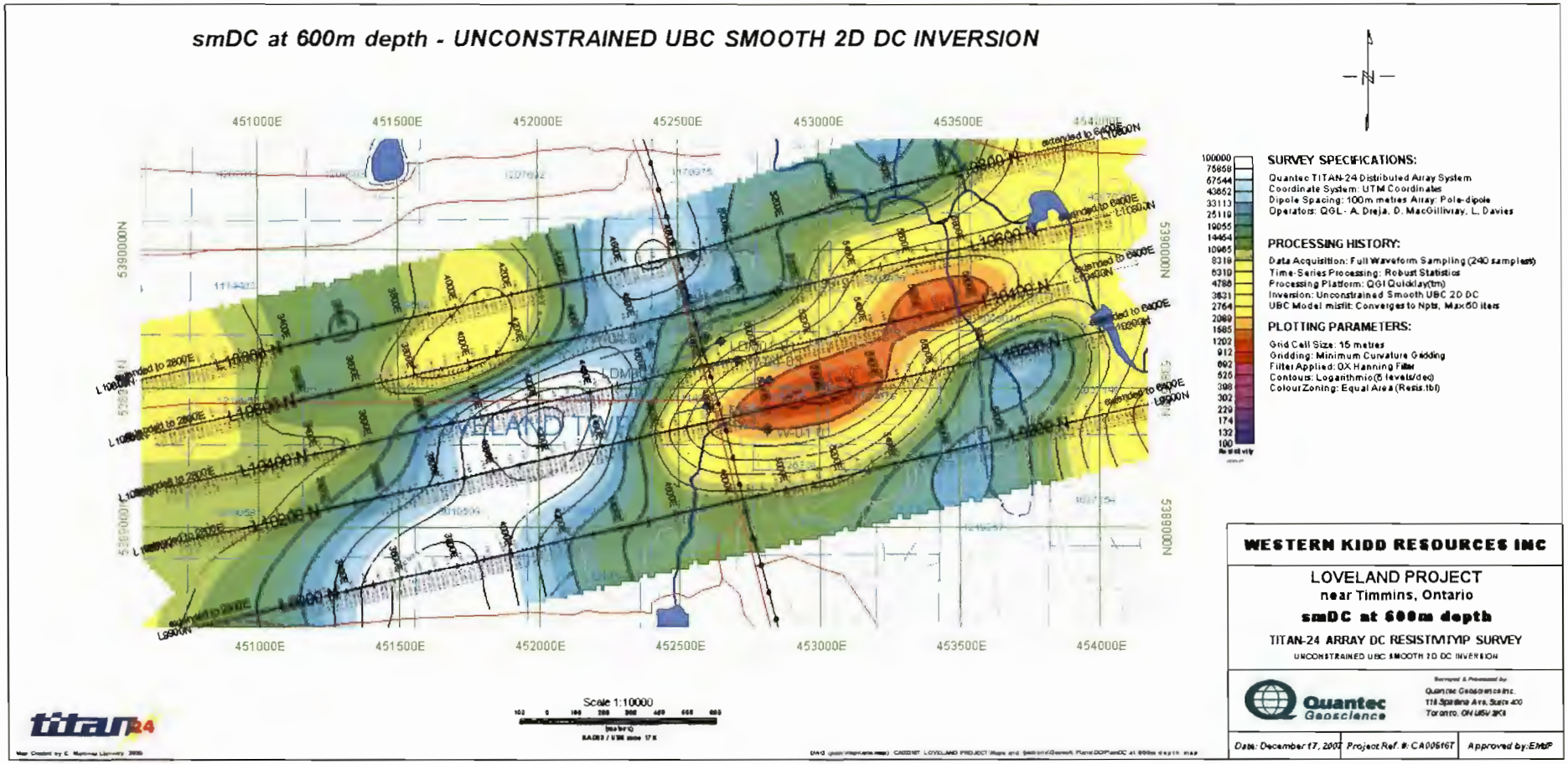

DVD:\CA00516T- Loveland Project\Maps and Sections\Geosoft Plans\DCIP\smIP nullcon at 50m depth.map

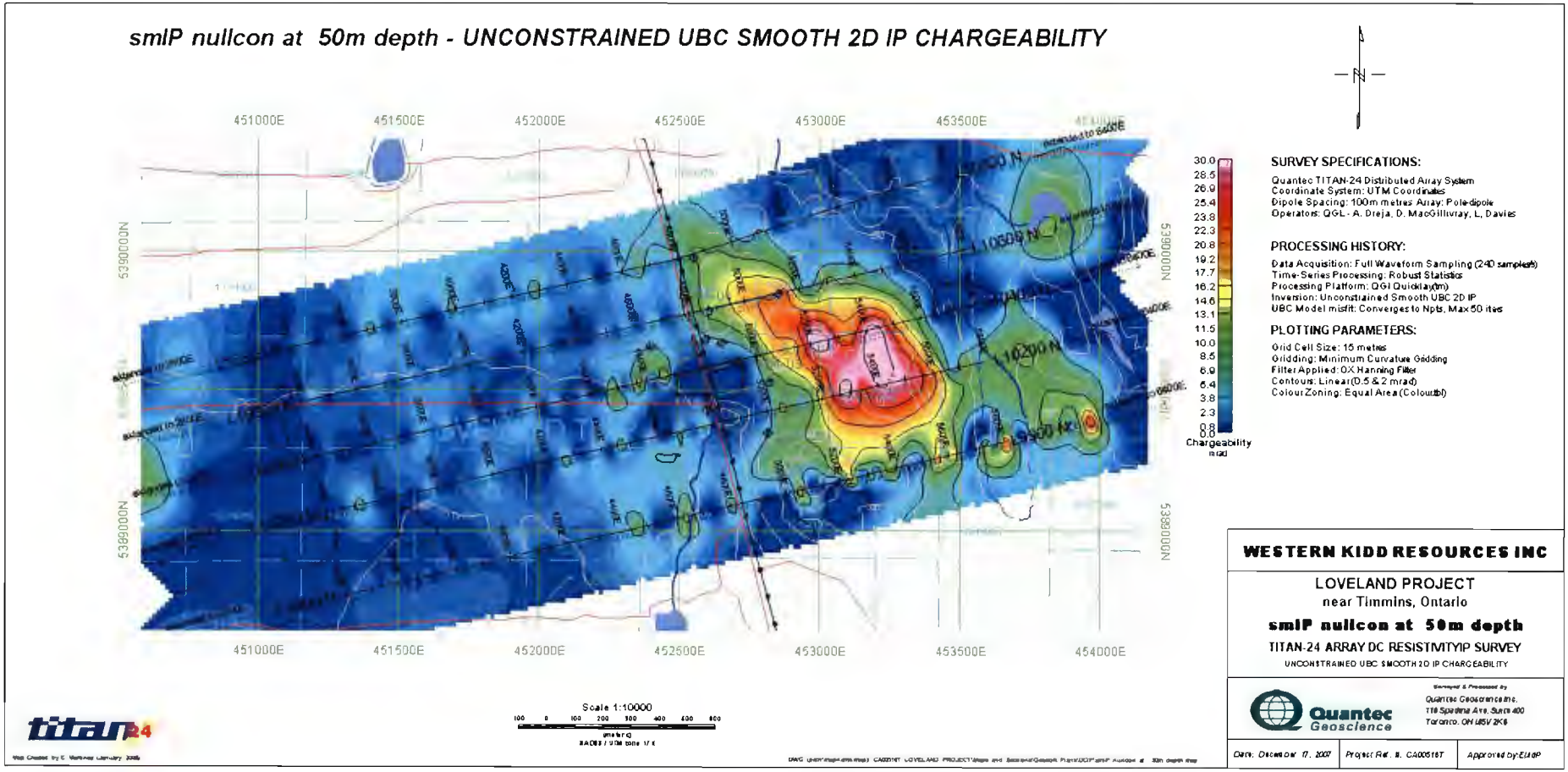

DVD:\CA00516T- Loveland Project\Maps and Sections\Geosoft Plans\DCIP\smIP nullcon at 100m depth.map

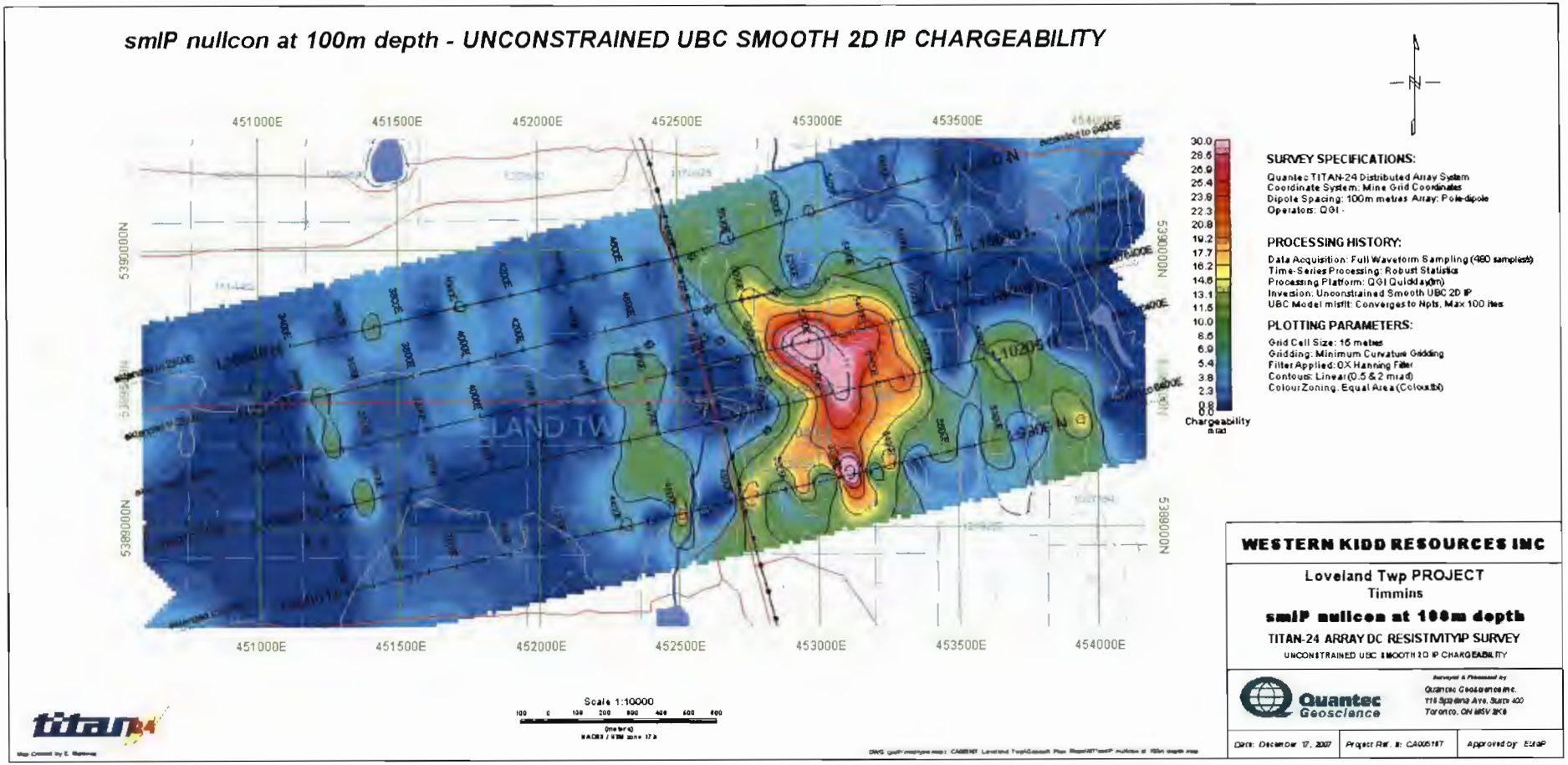

DVD:\CA00516T- Loveland Project\Maps and Sections\Geosoft Plans\DCIP\smIP nullcon at 250m depth.map

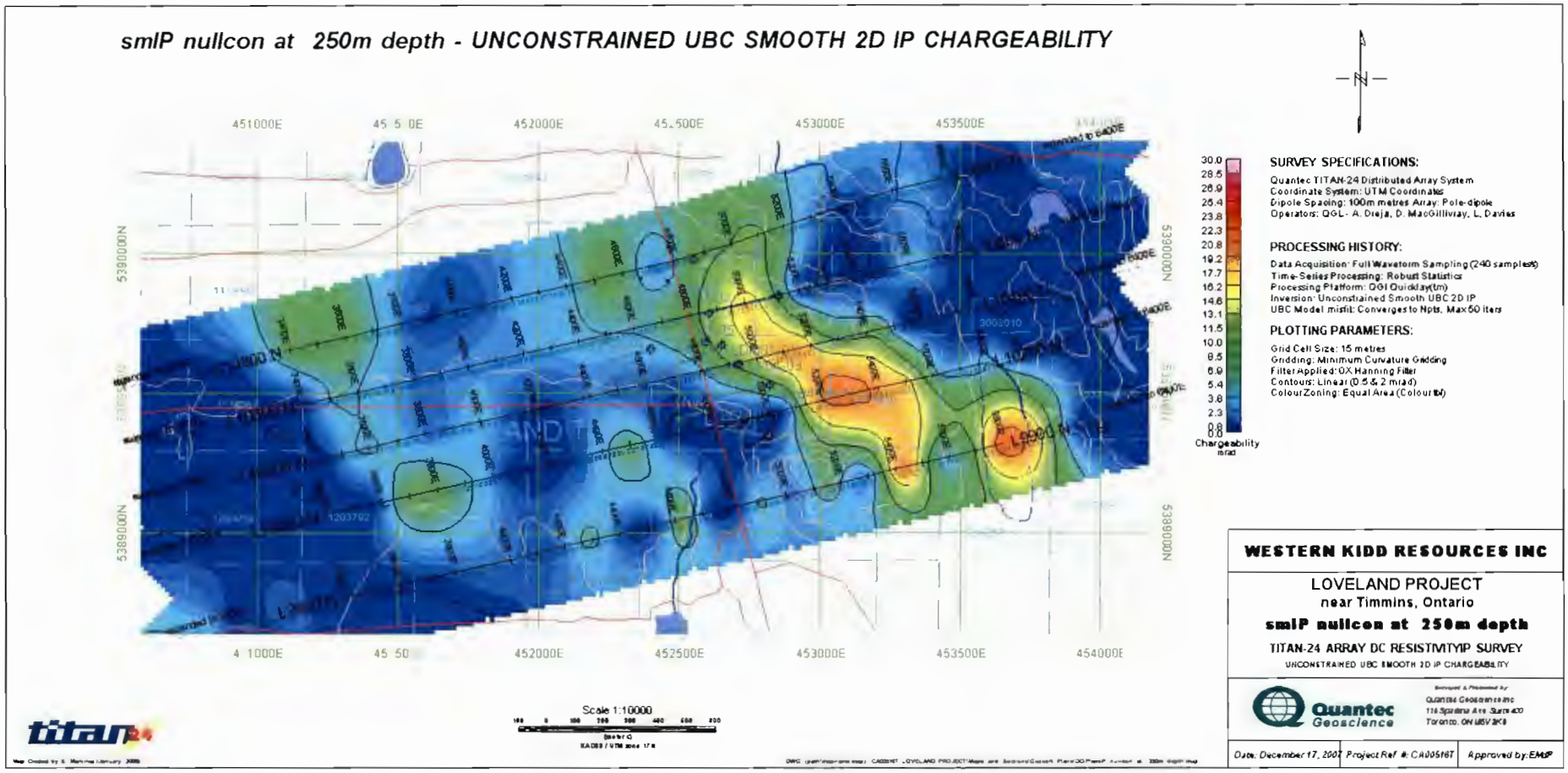

DVD:\CA00516T- Loveland Project\Maps and Sections\Geosoft Plans\DCIP\smIP nullcon at 400m depth.map

smIP nullcon at 400m depth - UNCONSTRAINED UBC SMOOTH 2D IP CHARGEABILITY

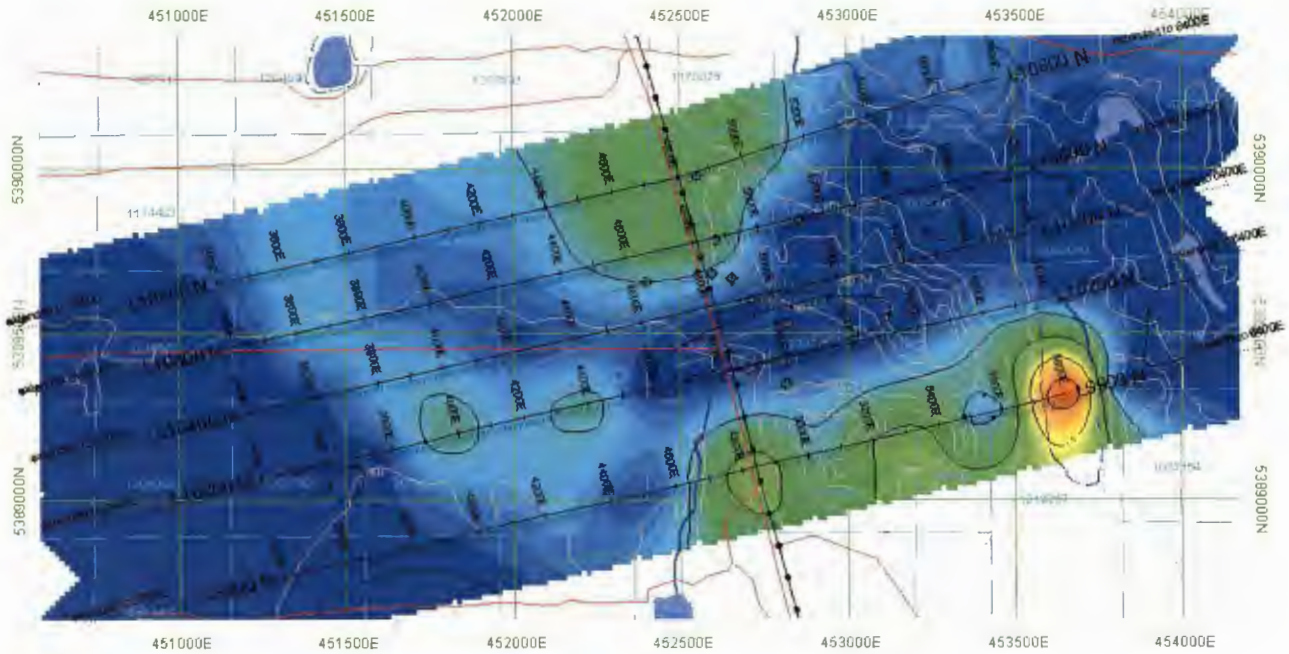

SURVEY SPECIFICATIONS:

Quantec TITAN-24 Distributed Array System
Coordinate System: UTM Coordinates
Dipole Spacing: 100m metres Array: Pole-dipole
Operators: QGL - A. Dreja, D. MacGillivray, L. Davies

PROCESSING HISTORY:

Data Acquisition: Full Waveform Sampling (240 samples/s)
Time-Series Processing: Robust Statistics
Processing Platform: QGI Quicklay(tm)
Inversion: Unconstrained Smooth UBC 2D IP
UBC Model misfit: Converges to Npts, Max 50 iters

PLOTTING PARAMETERS:

Grid Cell Size: 15 metres
Gridding: Minimum Curvature Gridding
Filter Applied: 0X Hanning Filter
Contours: Linear (0.5 & 2 mrad)
Colour Zoning: Equal Area (Colourbl)

Scale 1:10000

WESTERN KIDD RESOURCES INC

LOVELAND PROJECT
near Timmins, Ontario

smIP nullcon at 400m depth

TITAN-24 ARRAY DC RESISTIVITYIP SURVEY
UNCONSTRAINED UBC SMOOTH 2D IP CHARGEABILITY

Surveyed & Processed by
Quantec Geoscience Inc
110 Spadina Ave, Suite 400
Toronto, ON M5V 2K4

Date: December 17, 2007 | Project Ref. #: CA00516T | Approved by: EdP

DVD:\CA00516T- Loveland Project\Maps and Sections\Geosoft Plans\DCIP\smIP nullcon at 600m depth.map

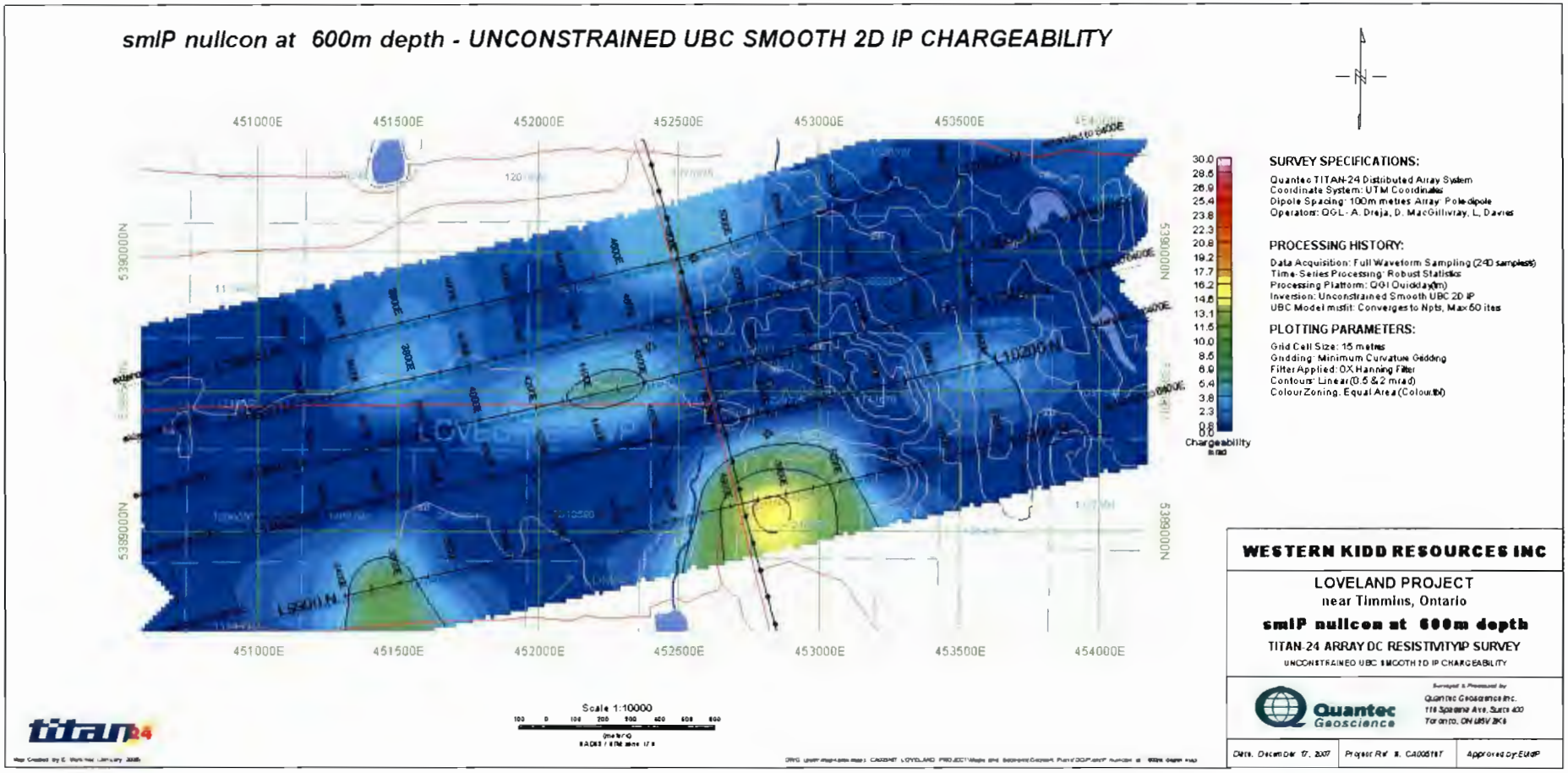

DVD:\CA00516T- Loveland Project\Maps and Sections\Geosoft Plans\MT\mtRes PW4 at 50m depth.map

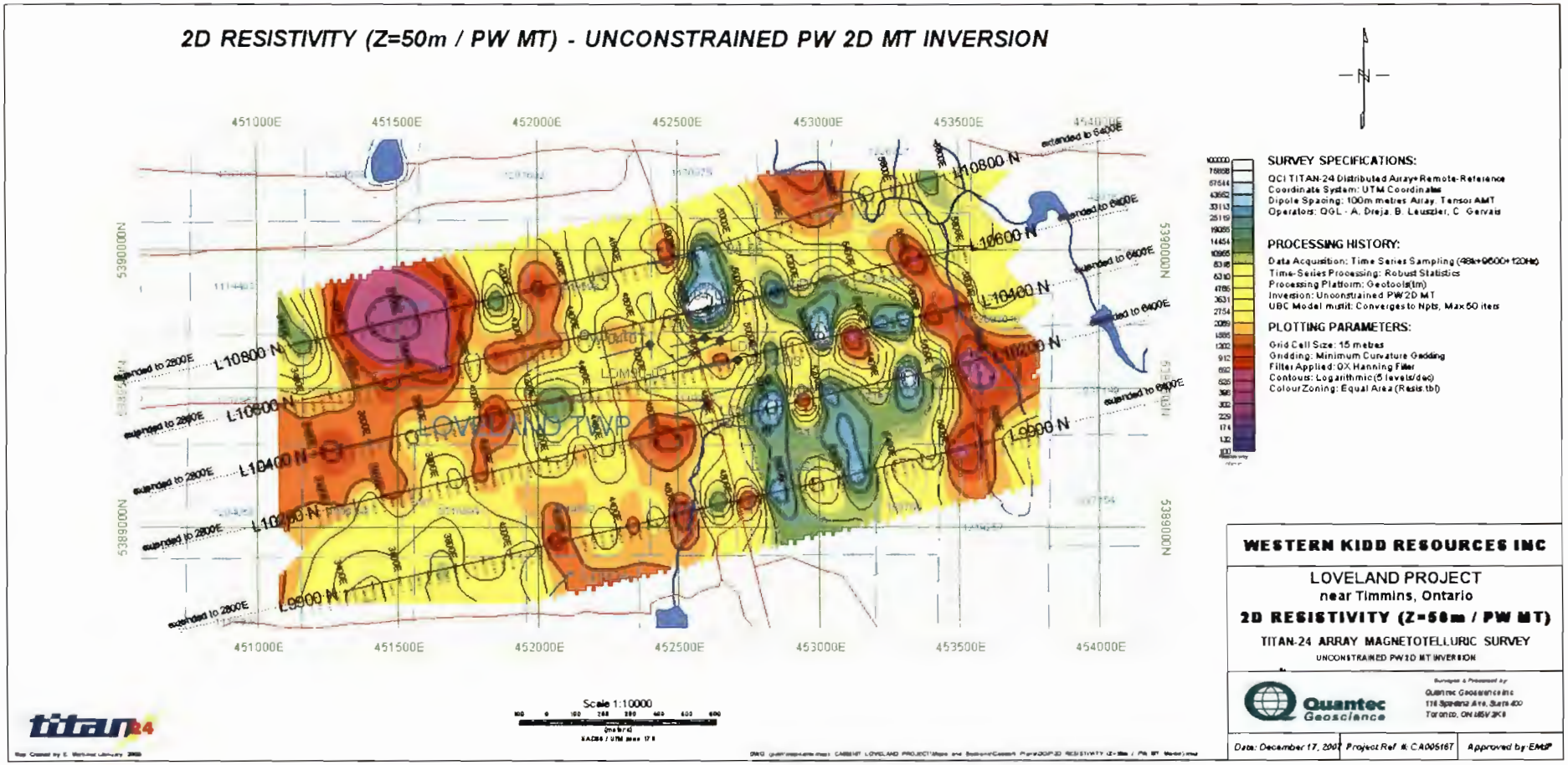

DVD:\CA00516T- Loveland Project\Maps and Sections\Geosoft Plans\MT\mtRes PW4 at 100m depth.map

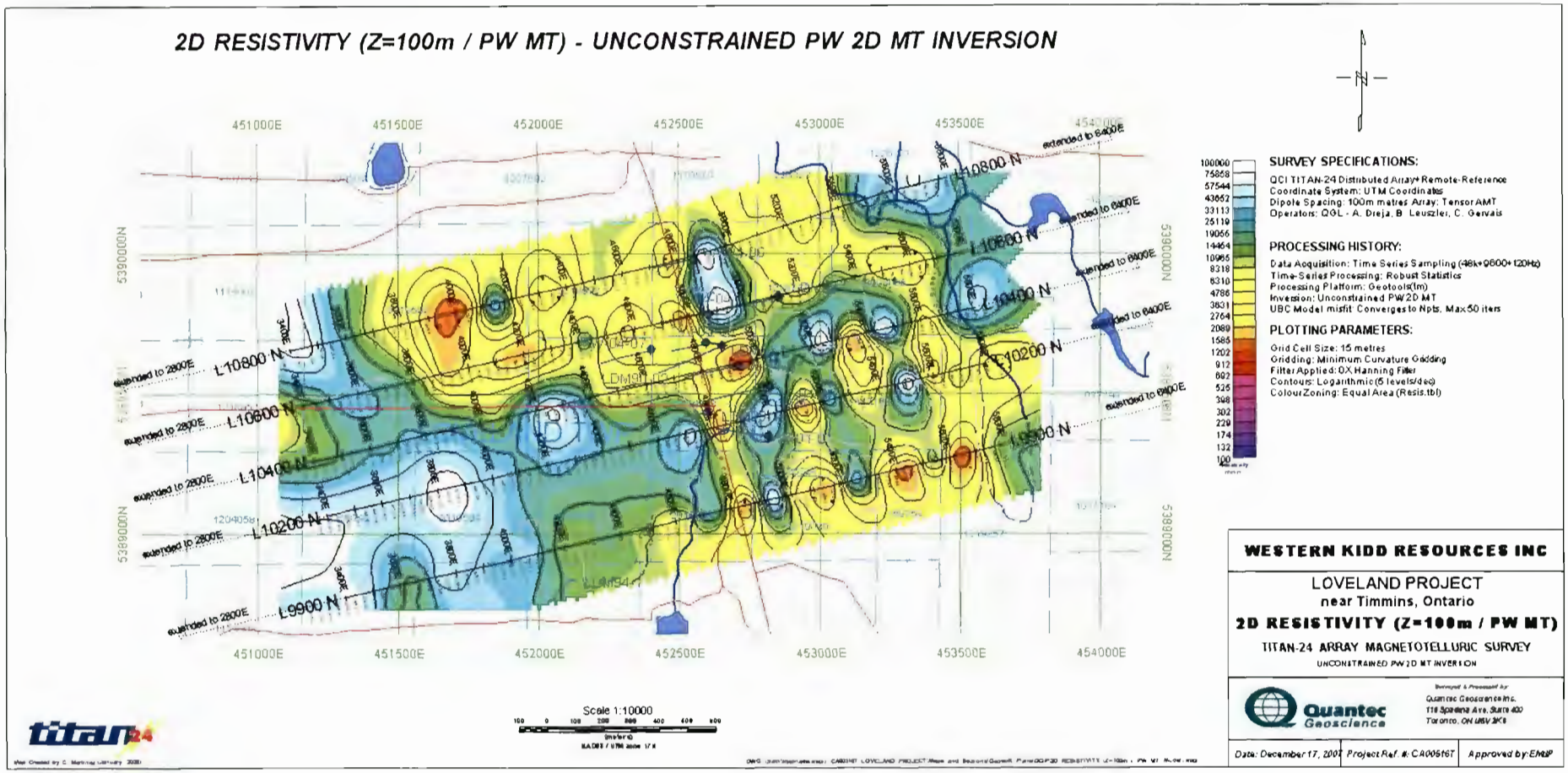

DVD:\CA00516T- Loveland Project\Maps and Sections\Geosoft Plans\MT\mtRes PW4 at 250m depth.map

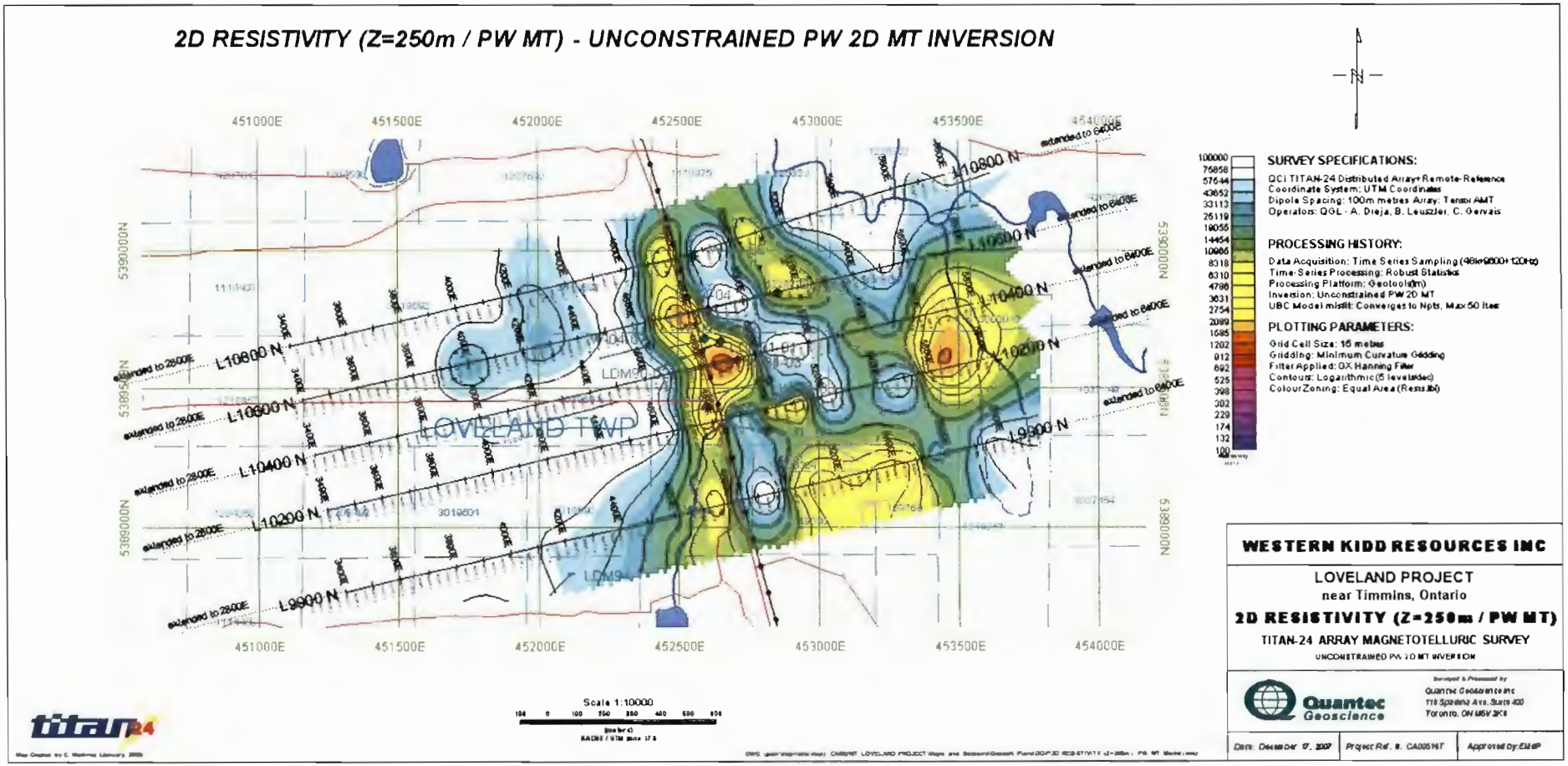

DVD:\CA00516T- Loveland Project\Maps and Sections\Geosoft Plans\MT\mtRes PW4 at 400m depth.map

2D RESISTIVITY (Z=400m / PW MT) - UNCONSTRAINED PW 2D MT INVERSION

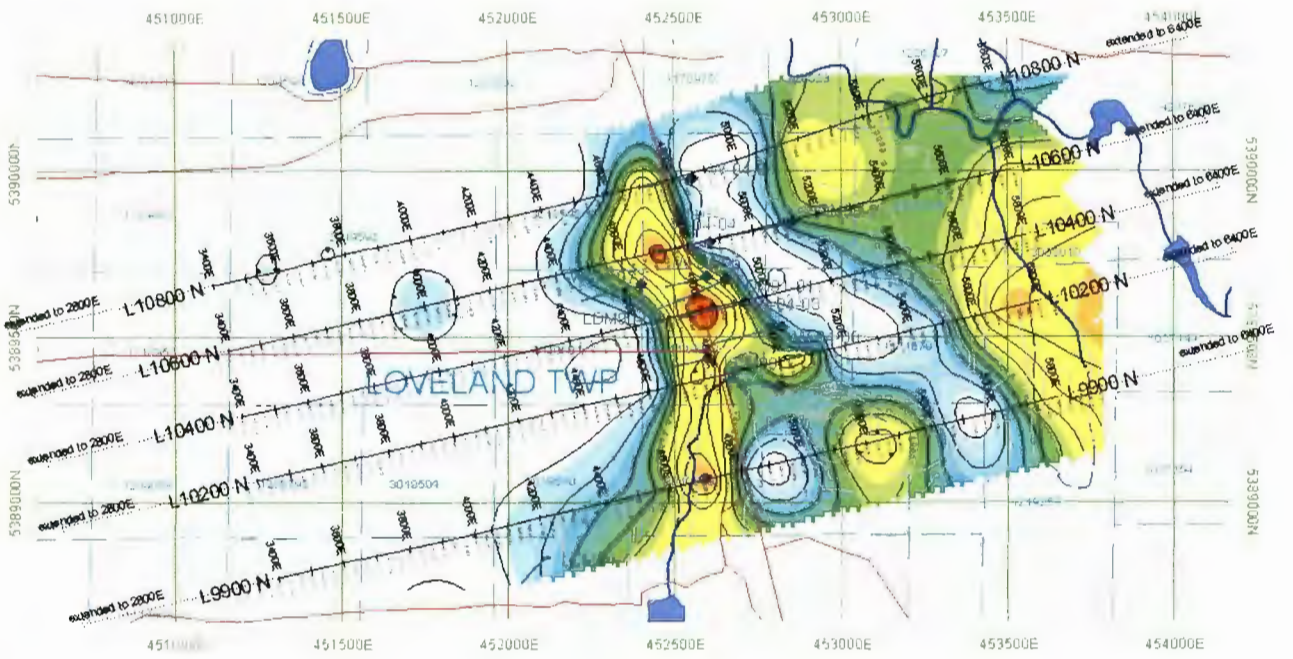

100000
76866
67544
43662
33113
26119
19055
14454
10966
8316
6310
4786
3631
2754
2089
1586
1202
912
692
525
398
302
229
174
132
100

SURVEY SPECIFICATIONS:

QCI TITAN-24 Distributed Array+Remote-Reference
Coordinate System: UTM Coordinates
Dipole Spacing: 100m metres Array: Tensor AMT
Operators: QGL - A. Dreja, B. Leuszler, C. Gervais

PROCESSING HISTORY:

Data Acquisition: Time Series Sampling (48k+9600+120Hz)
Time-Series Processing: Robust Statistics
Processing Platform: Geotools(tm)
Inversion: Unconstrained PW2D MT
UBC Model misfit: Converges to Npts. Max 50 iters

PLOTTING PARAMETERS:

Grid Cell Size: 15 metres
Gridding: Minimum Curvature Gridding
Filter Applied: 0X Hanning Filter
Contours: Logarithmic (5 levels/dec)
Colour Zoning: Equal Area (Resis tbl)

WESTERN KIDD RESOURCES INC

LOVELAND PROJECT
near Timmins, Ontario
2D RESISTIVITY (Z=400m / PW MT)
TITAN-24 ARRAY MAGNETOTELLURIC SURVEY
UNCONSTRAINED PW 2D MT INVERSION

Quantec Geoscience

Surveyed & Processed by:
Quantec Geoscience Inc.
116 Spadina Ave, Suite 400
Toronto, ON M5V 2K6

Date: December 17, 2007 | Project Ref. #: CA00516T | Approved by: EMbP

DVD:\CA00516T- Loveland Project\Maps and Sections\Geosoft Plans\MT\mtRes PW4 at 600m depth.map

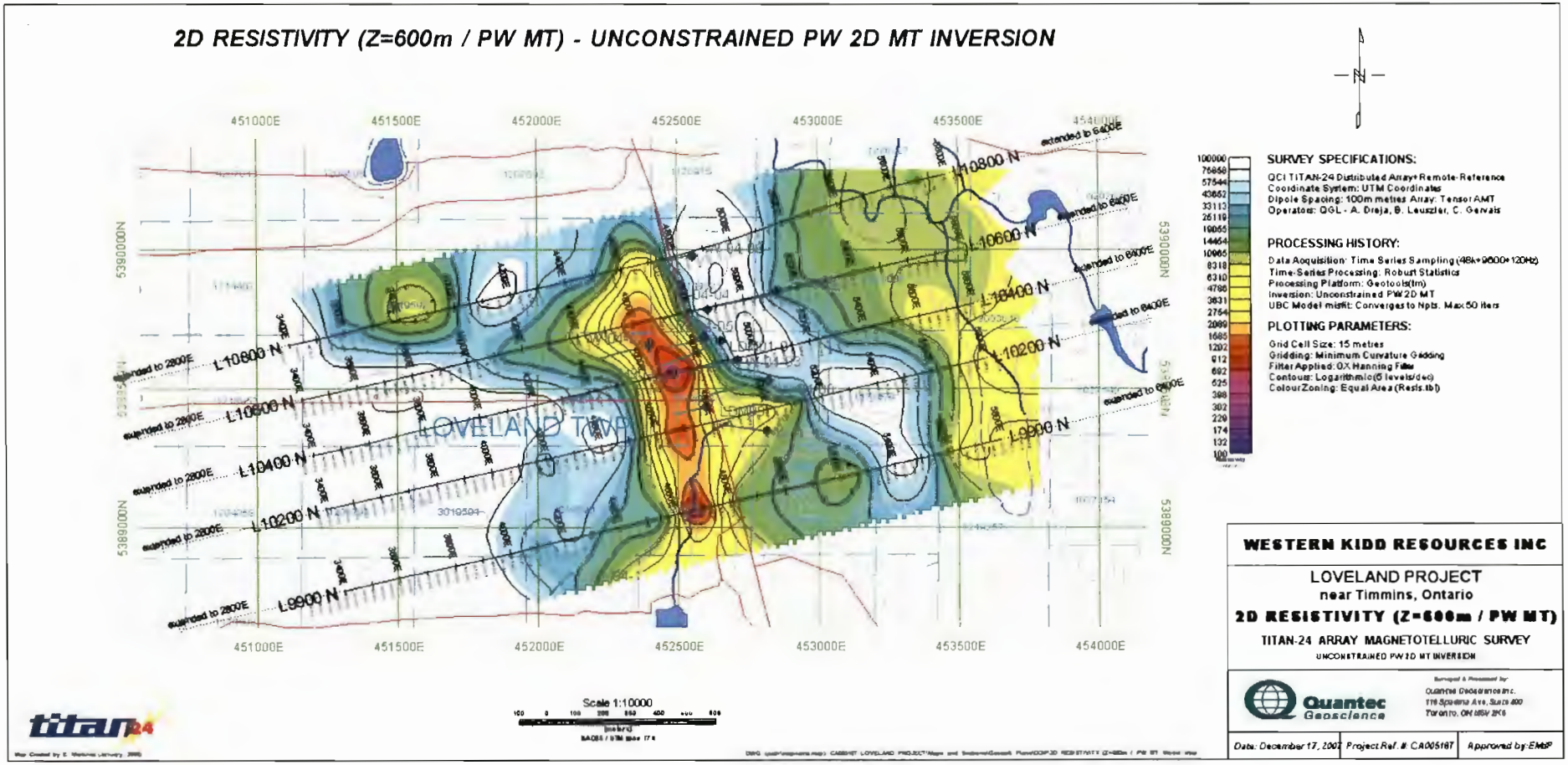

DVD:\CA00516T- Loveland Project\Maps and Sections\Geosoft Plans\MT\mtRes PW4 at 1000m depth.map

2D RESISTIVITY (Z=1000m / PW MT) - UNCONSTRAINED PW 2D MT INVERSION

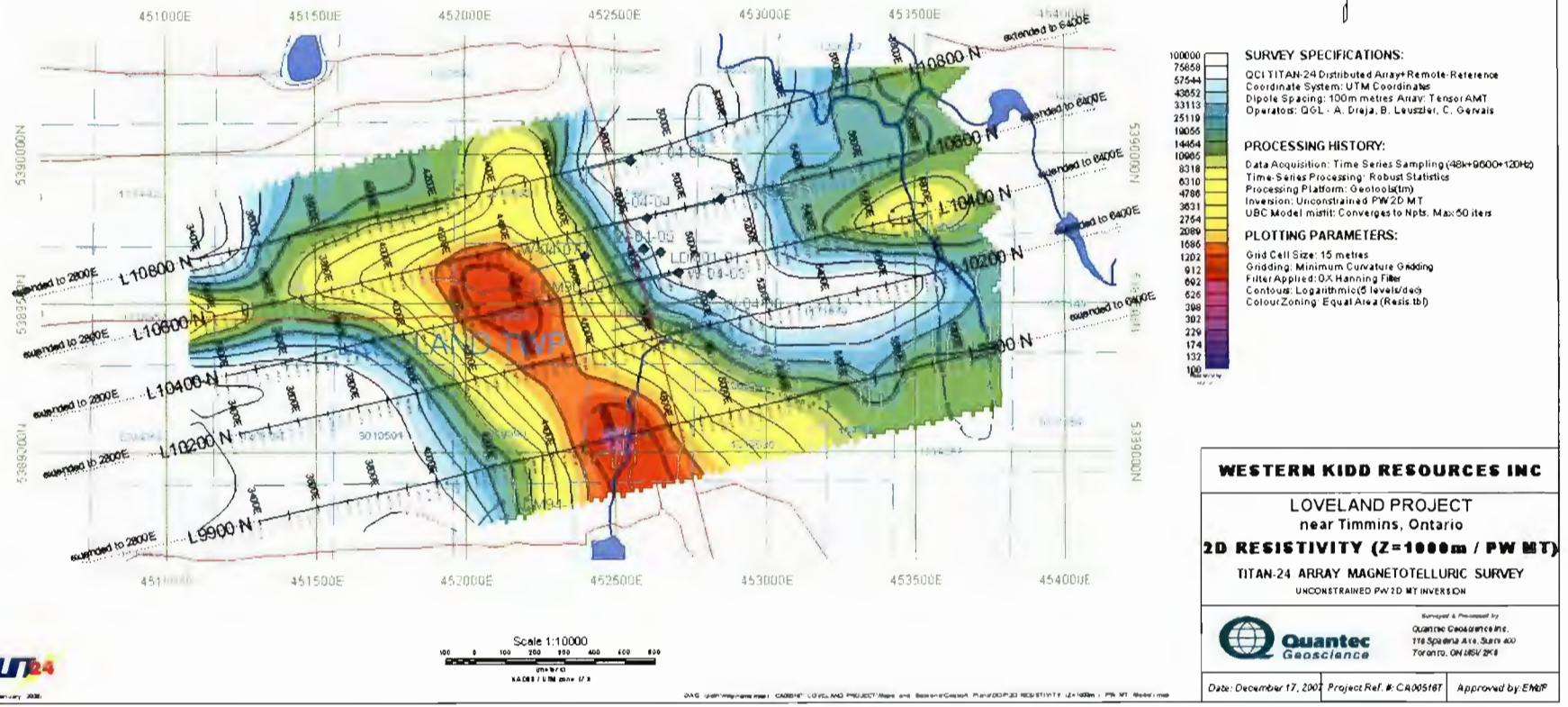

DVD:\CA00516T- Loveland Project\Maps and Sections\Geosoft Plans\MT\mtRes PW4 at 1500m depth.map

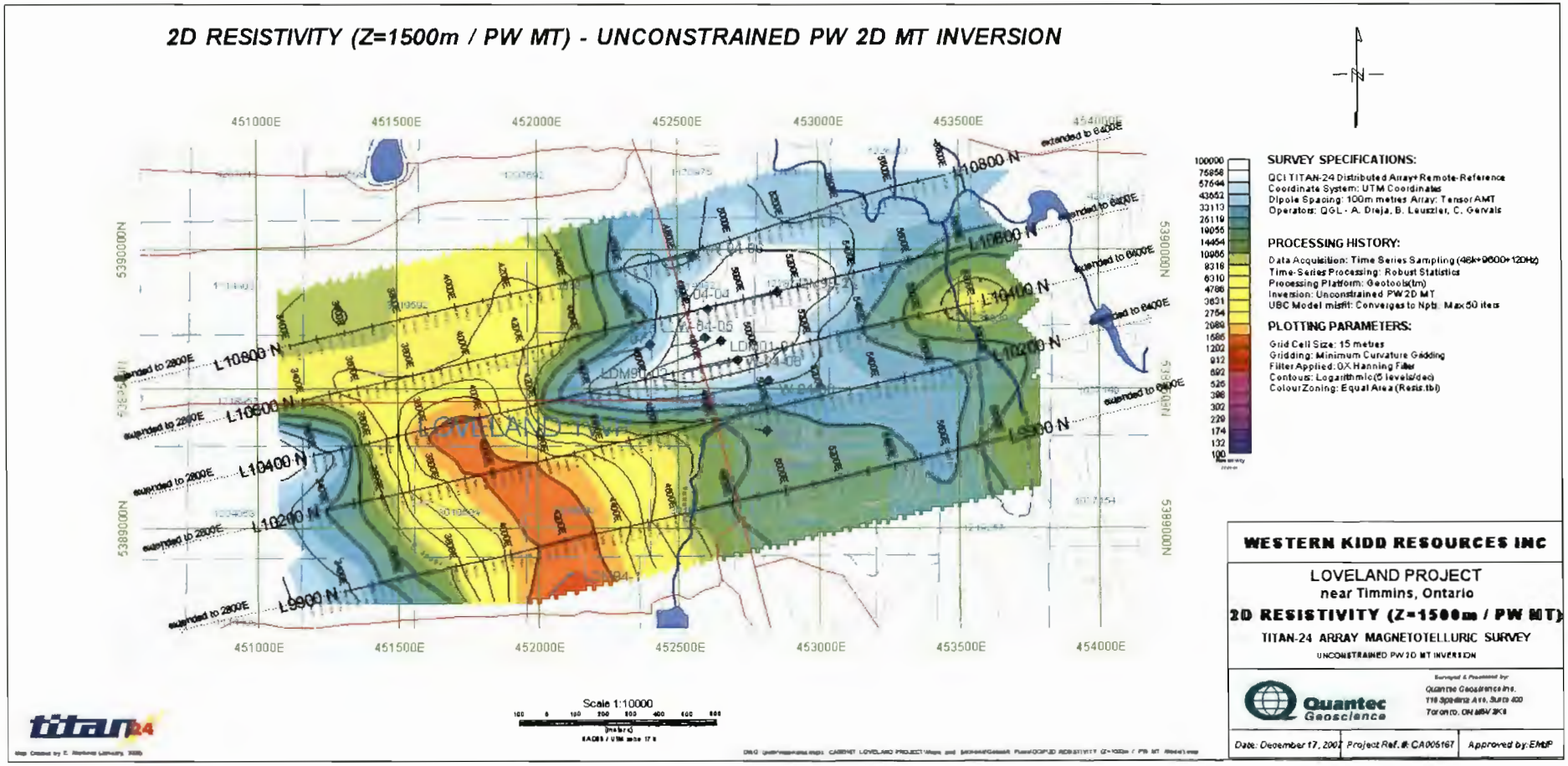

DVD:\CA00510T- Kistabiche Project\Maps and Sections\Geosoft Plans\Interpretation\ Interpretation Plan over 2D Chargeability at 200m depth.map

INTERPRETATION PLAN OVER 2D CHARGEABILITY AT 100M DEPTH

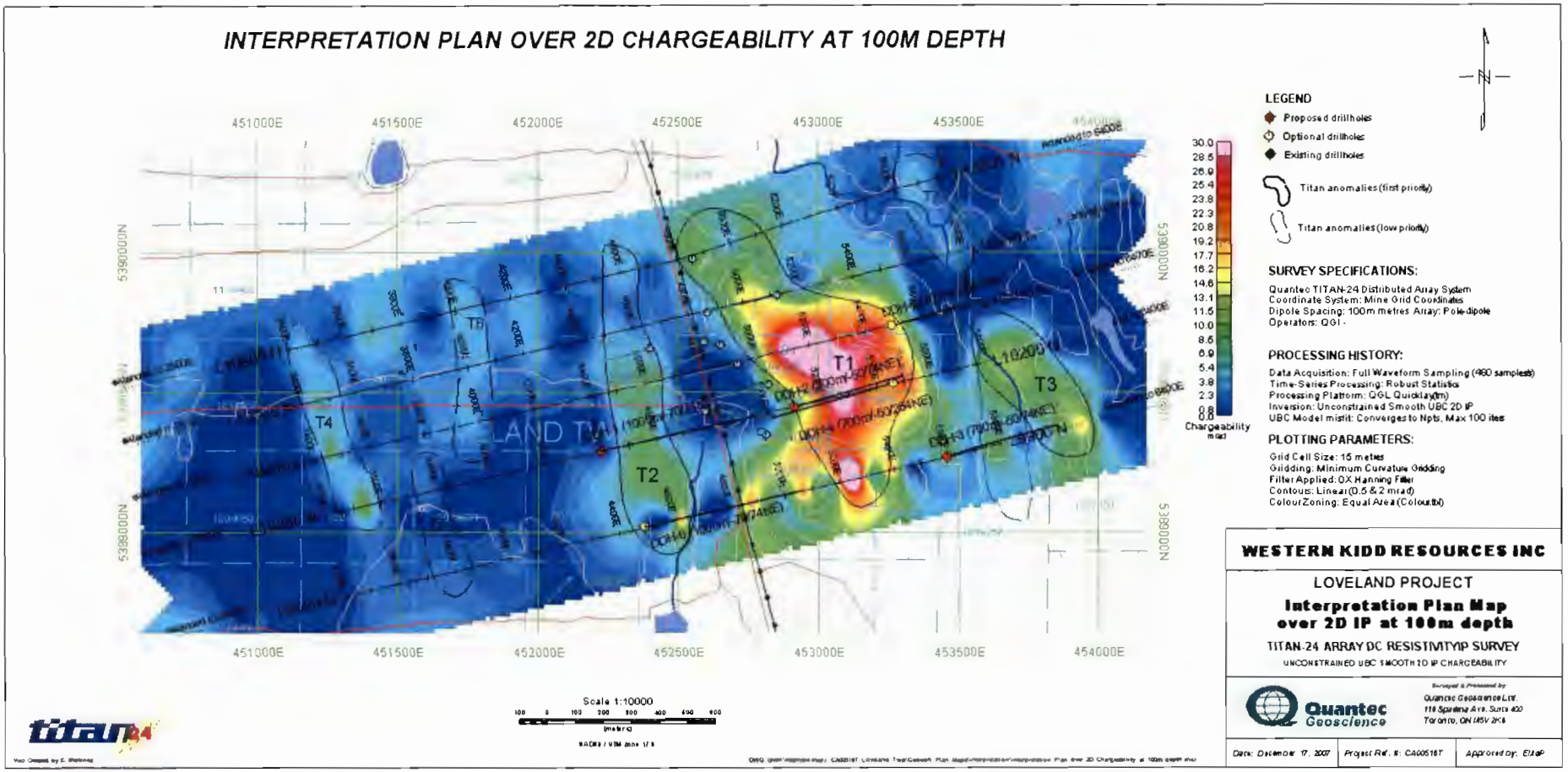

APPENDIX H: BASE MAPS AND 3D VIEWS

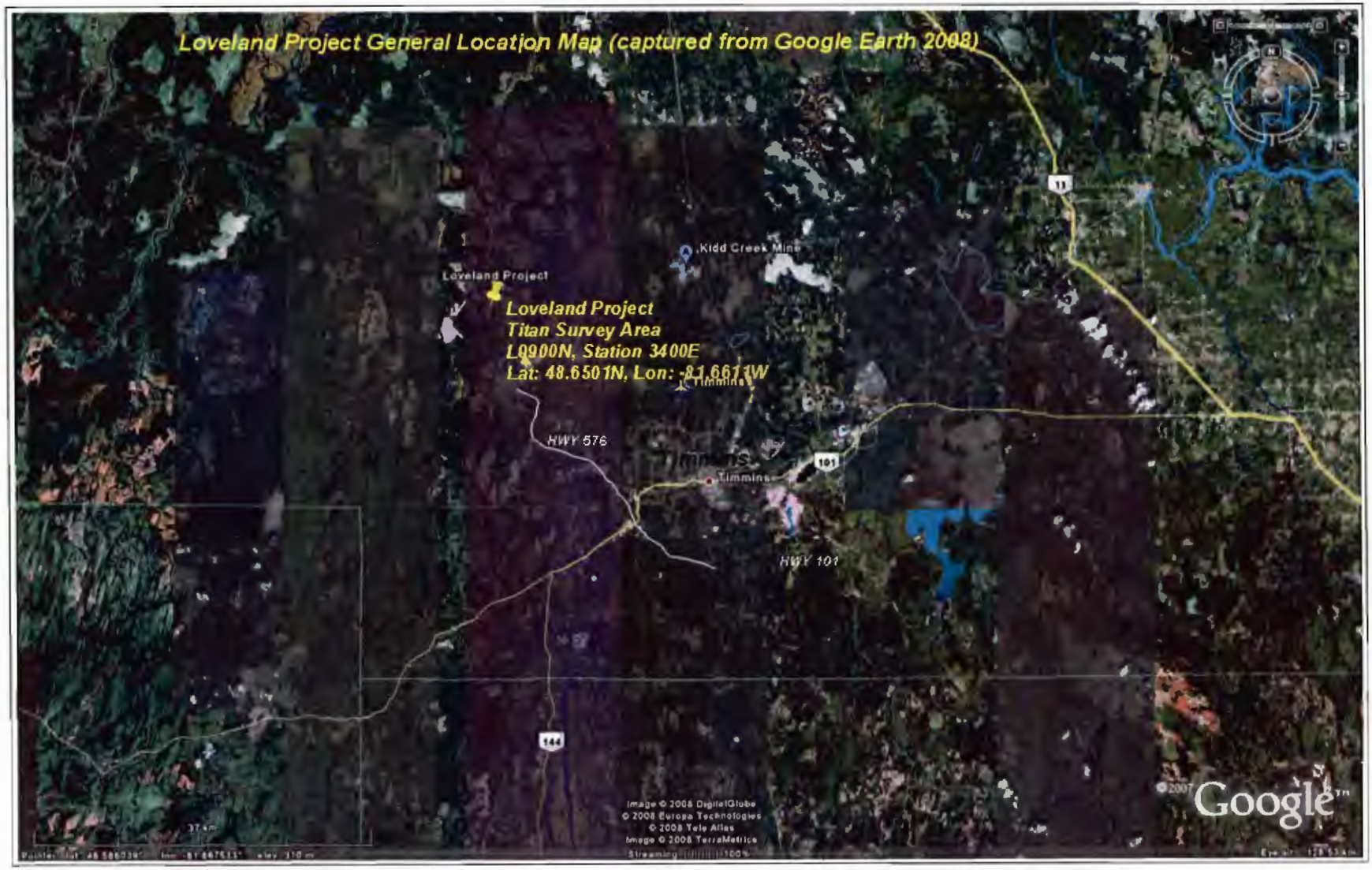

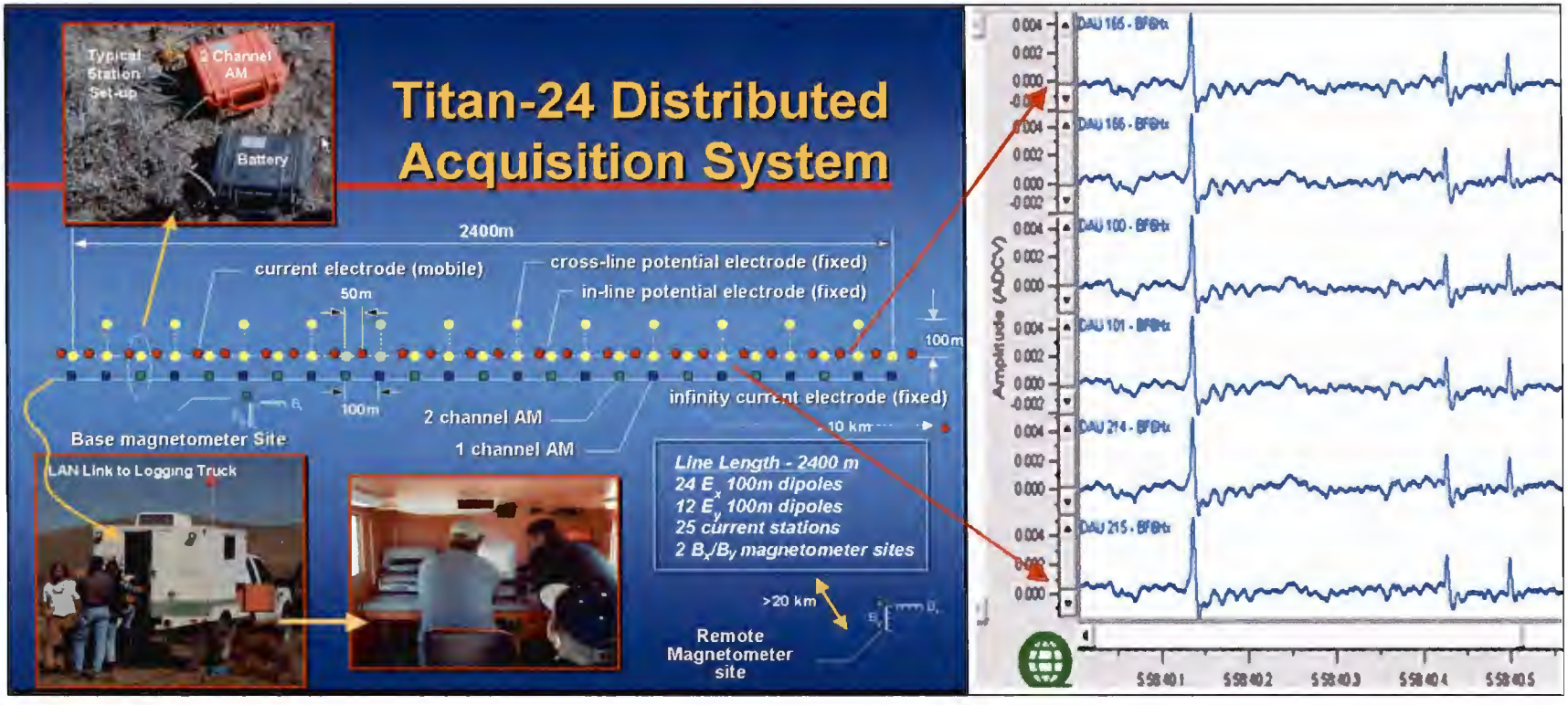
Titan-24 Distributed Acquisition System
Typical Station Set-up
2 Channel AM
Battery
2400m
current electrode (mobile)
50m
cross-line potential electrode (fixed)
in-line potential electrode (fixed)
100m
100m
2 channel AM
1 channel AM
infinity current electrode (fixed)
10 km
Base magnetometer Site
LAN Link to Logging Truck
Line Length - 2400 m
24 Ex 100m dipoles
12 Ey 100m dipoles
25 current stations
2 Bx/By magnetometer sites
>20 km
Remote Magnetometer site
Amplitude (ADCV)

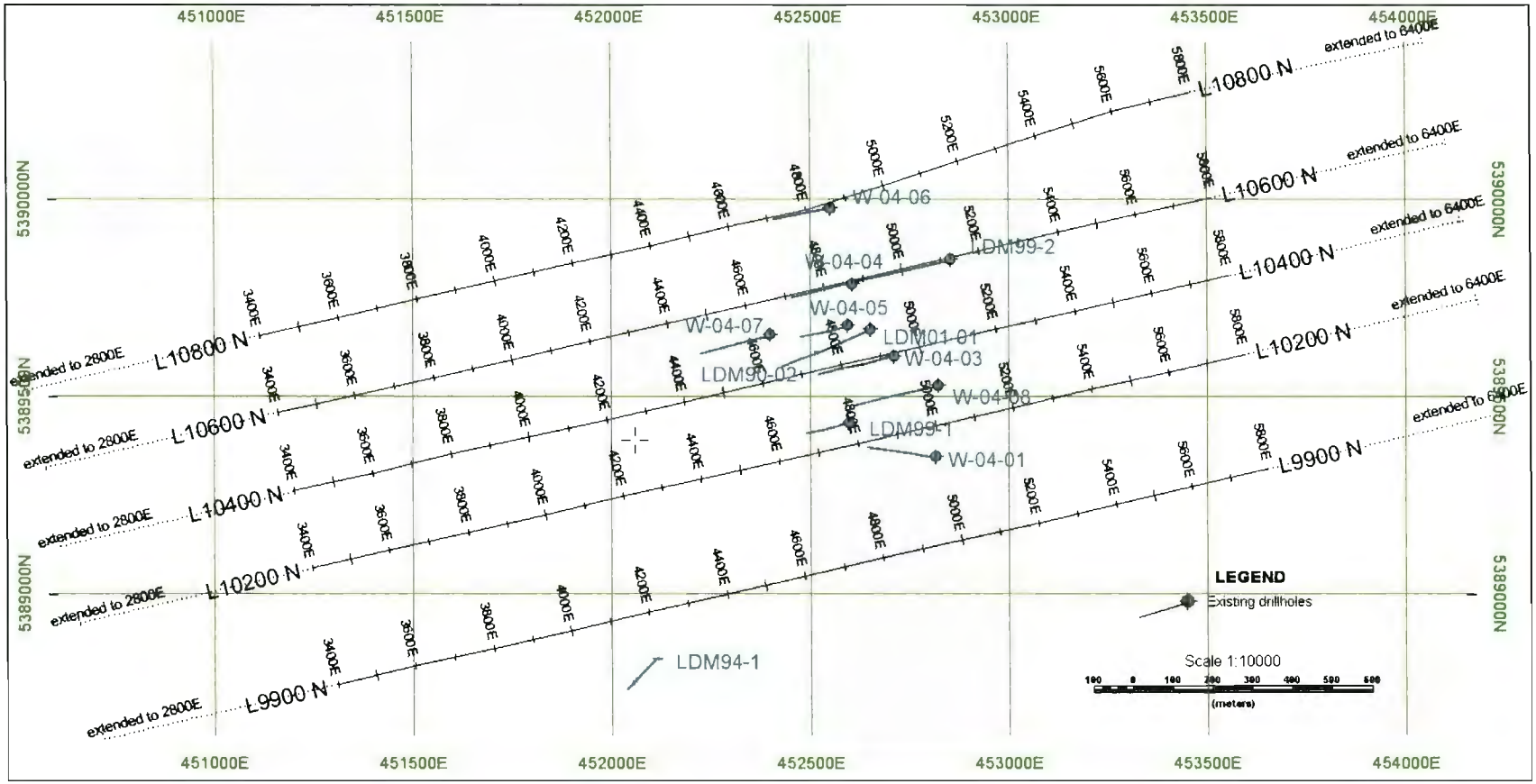
451000E
451500E
452000E
452500E
453000E
453500E
454000E
5390000N
5389500N
5389000N
L10800 N
L10600 N
L10400 N
L10200 N
L9900 N
extended to 6400E
extended to 2800E
W-04-06
W-04-04
W-04-05
W-04-07
W-04-03
W-04-08
W-04-01
LDM99-2
LDM01-01
LDM00-02
LDM99-1
LDM94-1
LEGEND
Existing drillholes
Scale 1:10000
(meters)

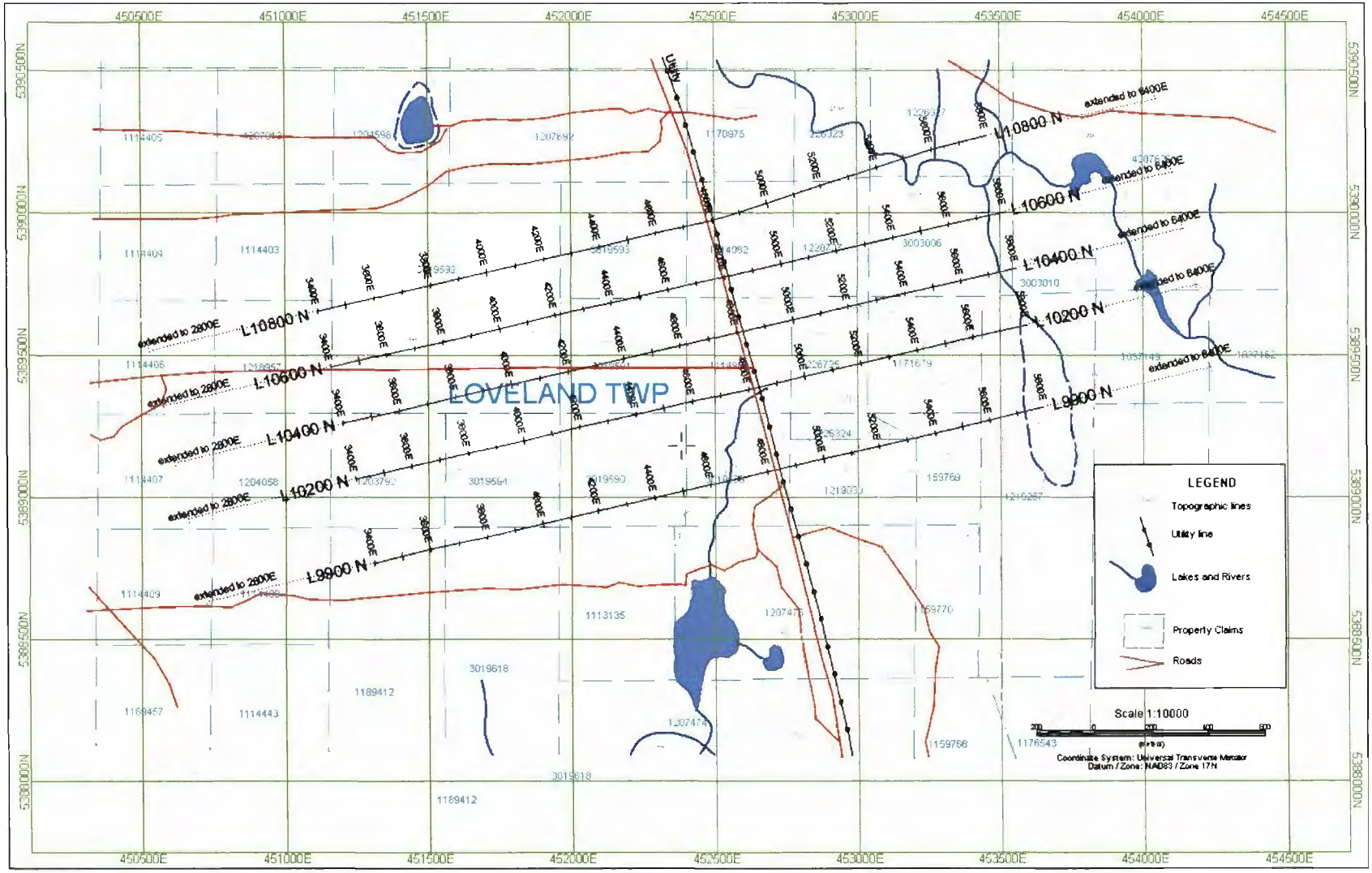
LOVELAND TWP
L10800 N
L10600 N
L10400 N
L10200 N
L9900 N
extended to 2800E
extended to 6400E
LEGEND
Topographic lines
Utility line
Lakes and Rivers
Property Claims
Roads
Scale 1:10000
Coordinate System: Universal Transverse Mercator
Datum / Zone: NAD83 / Zone 17N

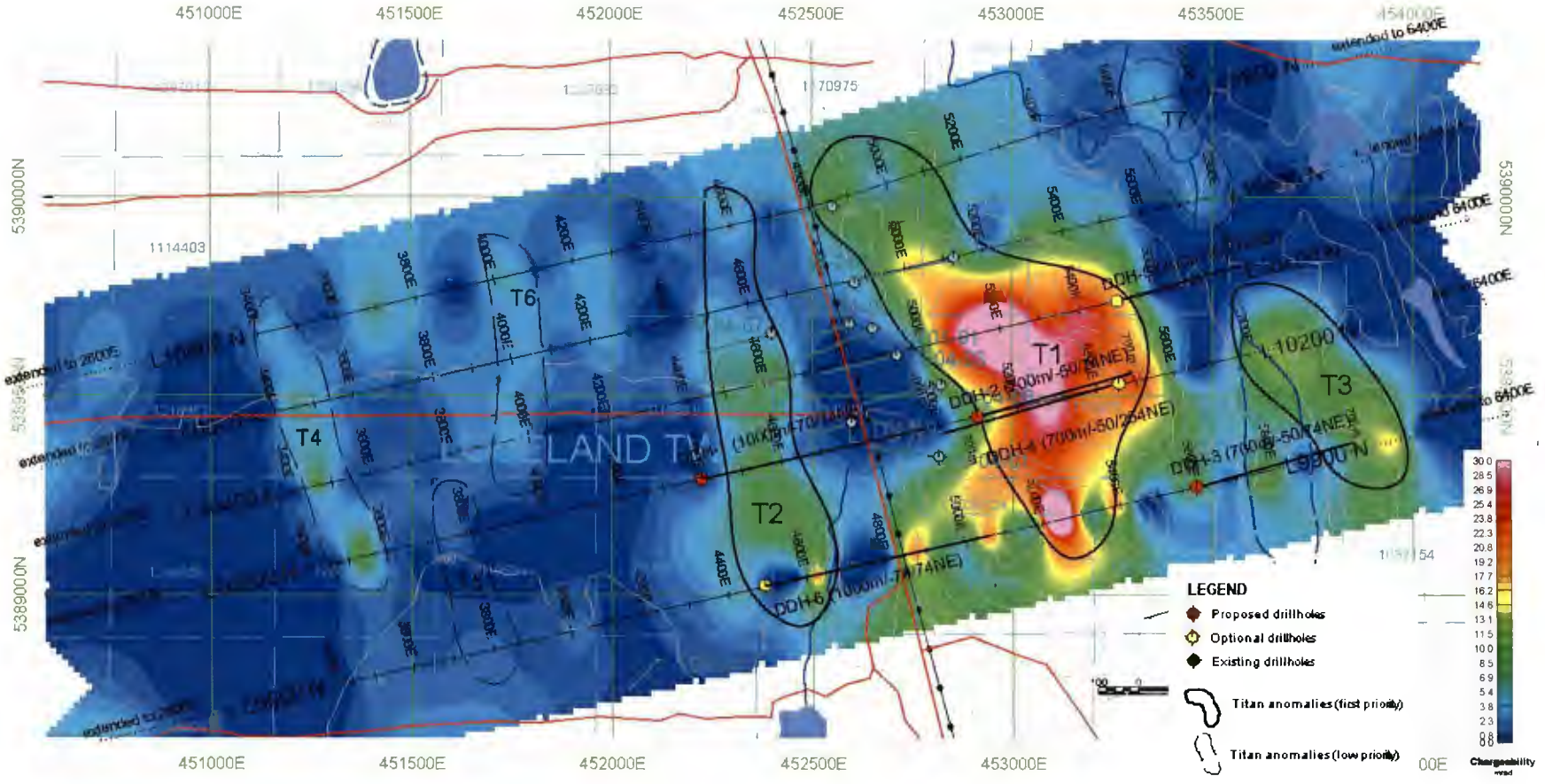
451000E
451500E
452000E
452500E
453000E
453500E
5390000N
T1
T2
T3
T4
T6
T7
DDH-1 (300mV-70/145NE)
DDH-2 (300mV-50/254NE)
DDH-3 (700mV-50/74NE)
DDH-4 (700mV-50/254NE)
DDH-6 (1000mV-74/74NE)
L9900 N
L10200 N
LEGEND
Proposed drillholes
Optional drillholes
Existing drillholes
Titan anomalies (first priority)
Titan anomalies (low priority)
Chargeability
mrad

Loveland Project - line L10800N Interpretation Results

2D MT PW4 Resistivity Model (TM)

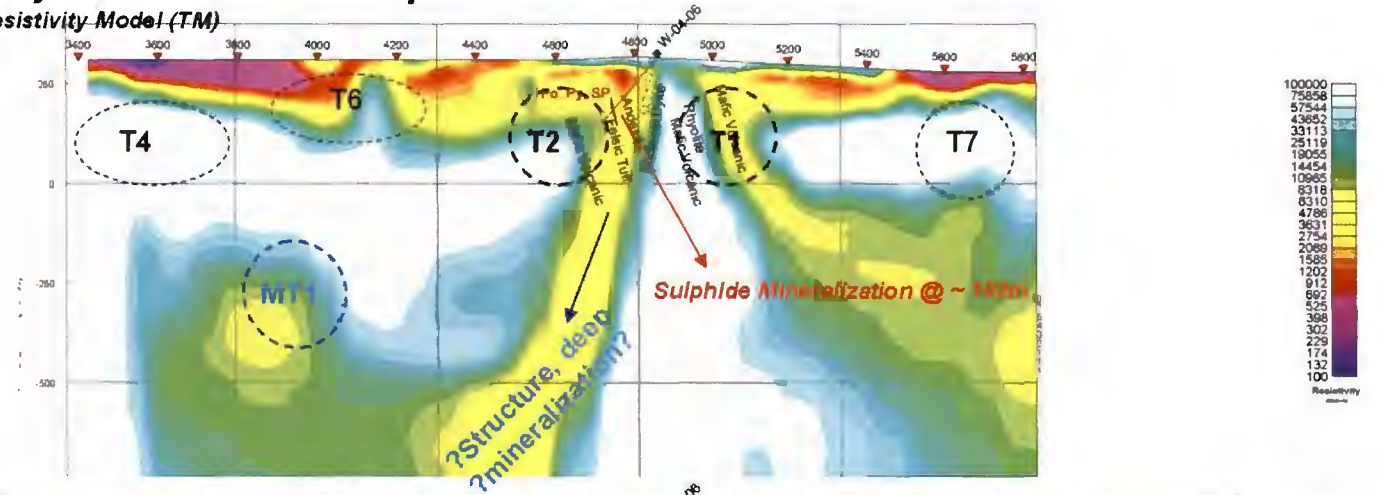

2D DC Resistivity Smooth Model

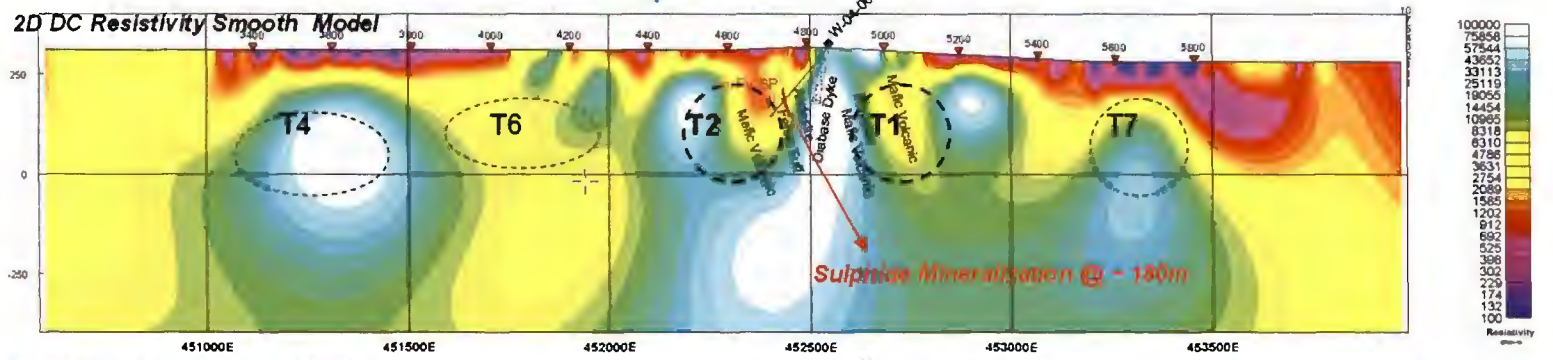

2D Chargeability Smooth Model

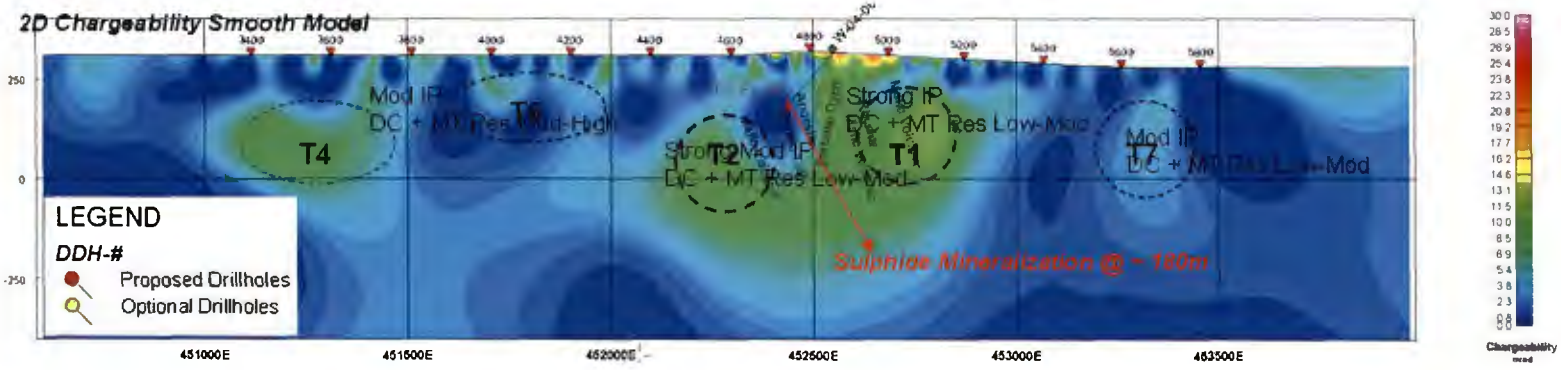

Loveland Project - line L10600N Interpretation Results

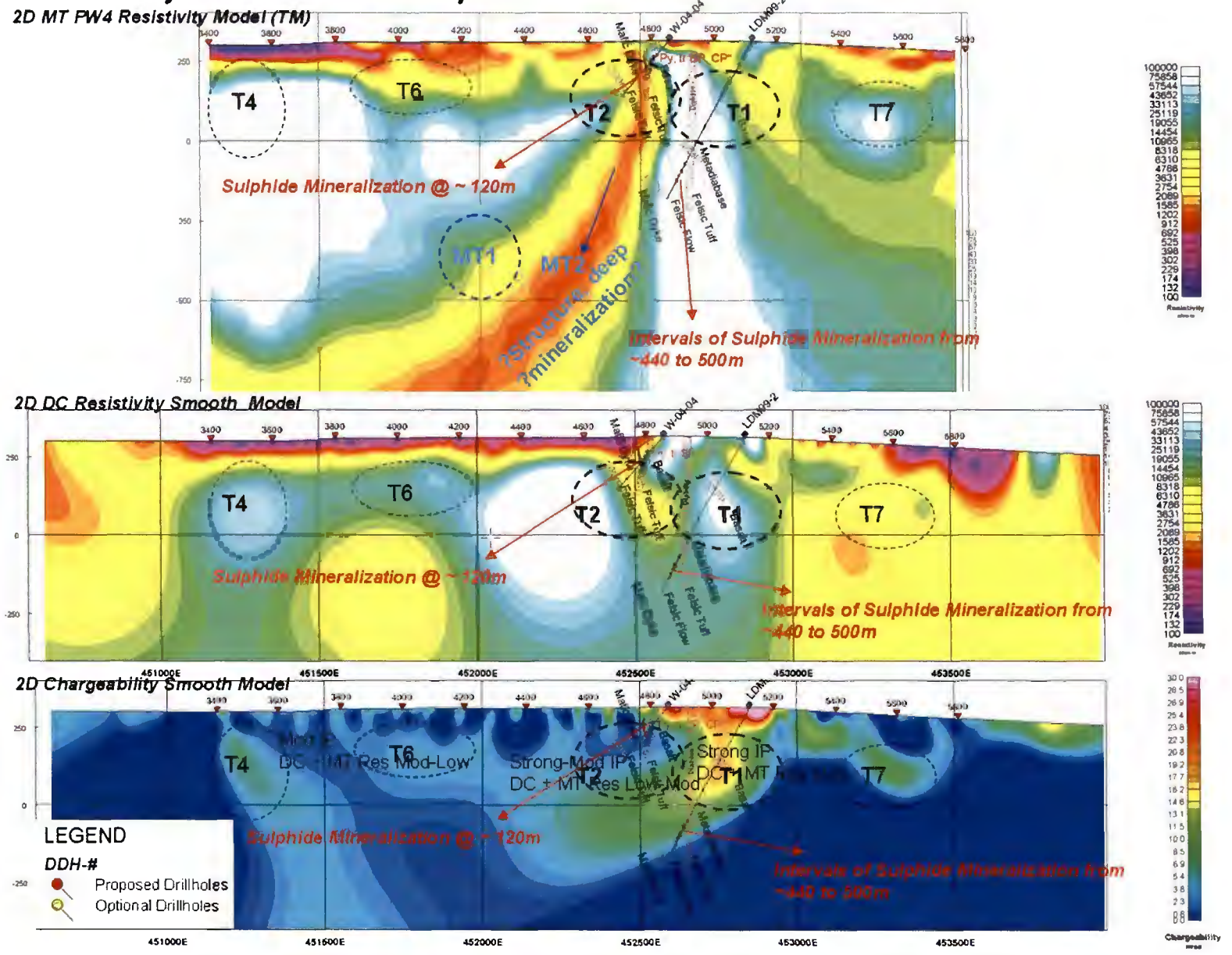

Loveland Project - line L10400N Interpretation Results

2D MT PW4 Resistivity Model (TM)

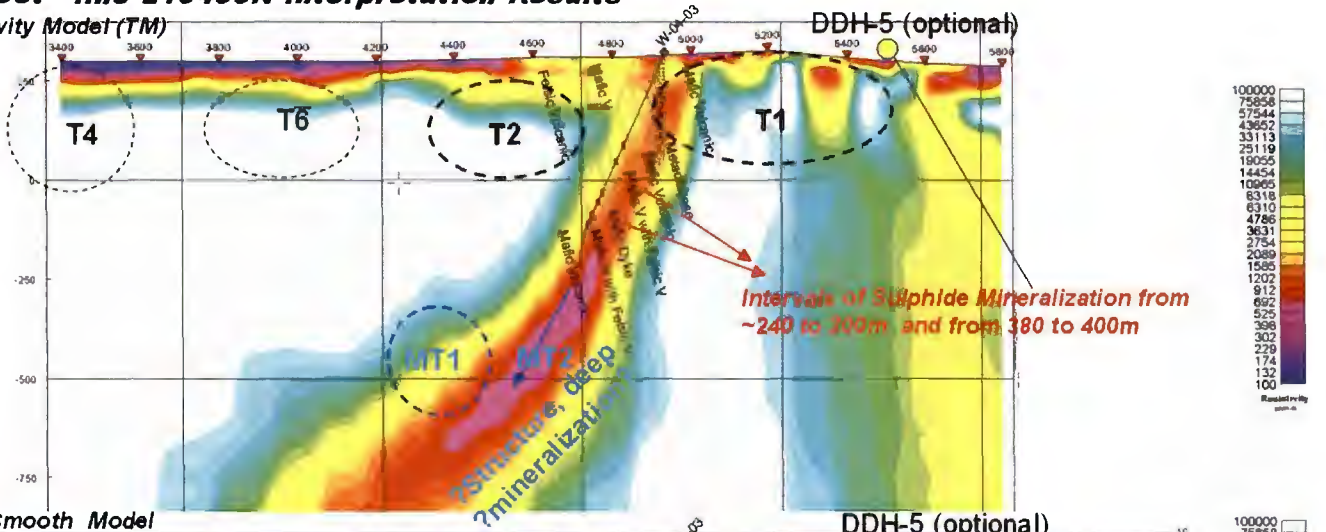

2D DC Resistivity Smooth Model

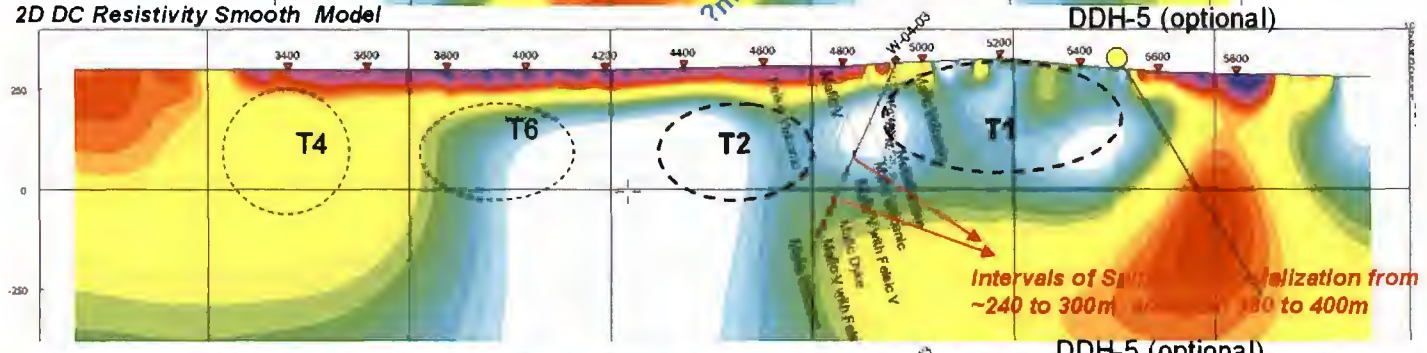

2D Chargeability Smooth Model

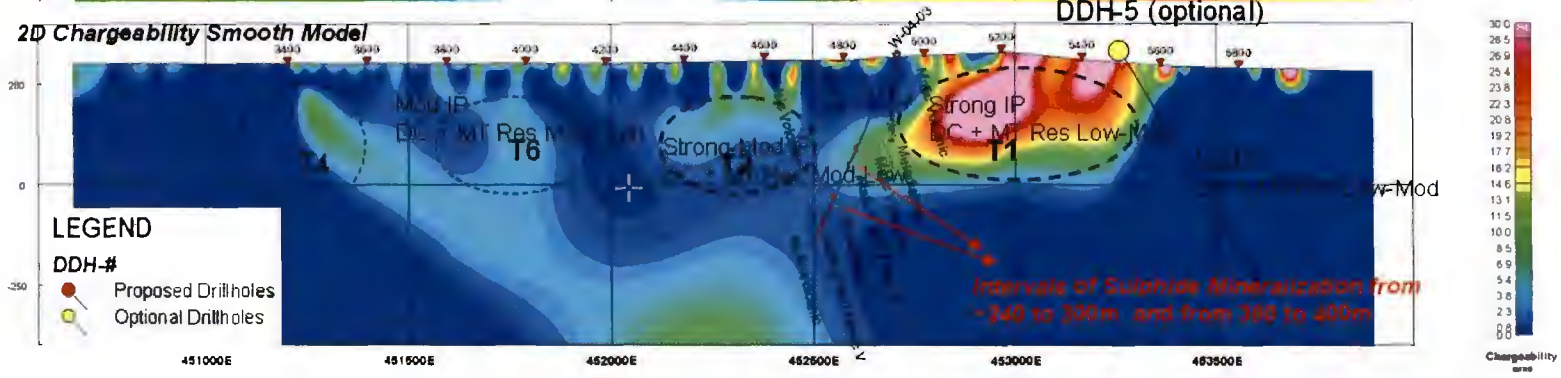

Loveland Project - line L10200N Interpretation Results

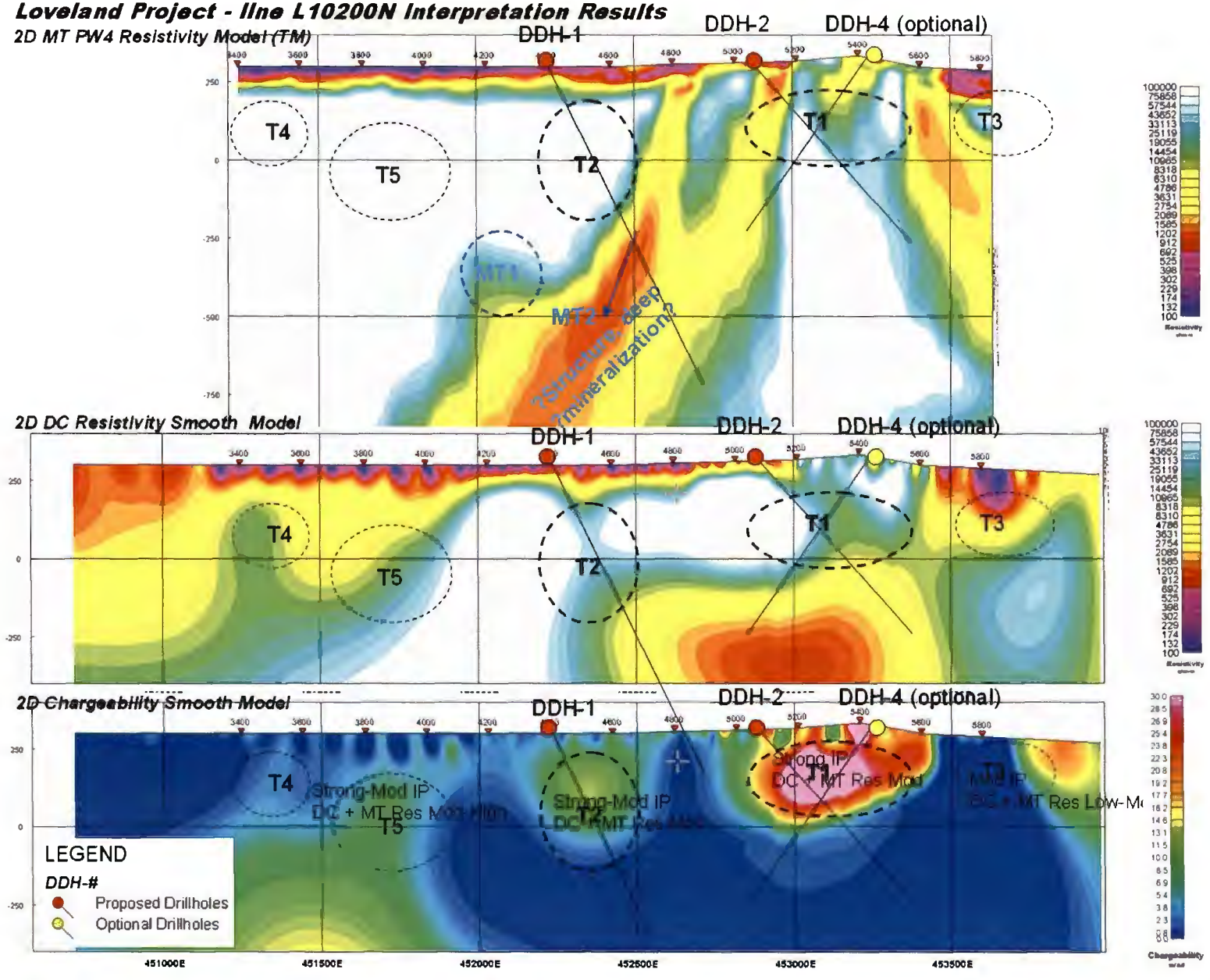

Loveland Project - line L9900N Interpretation Results

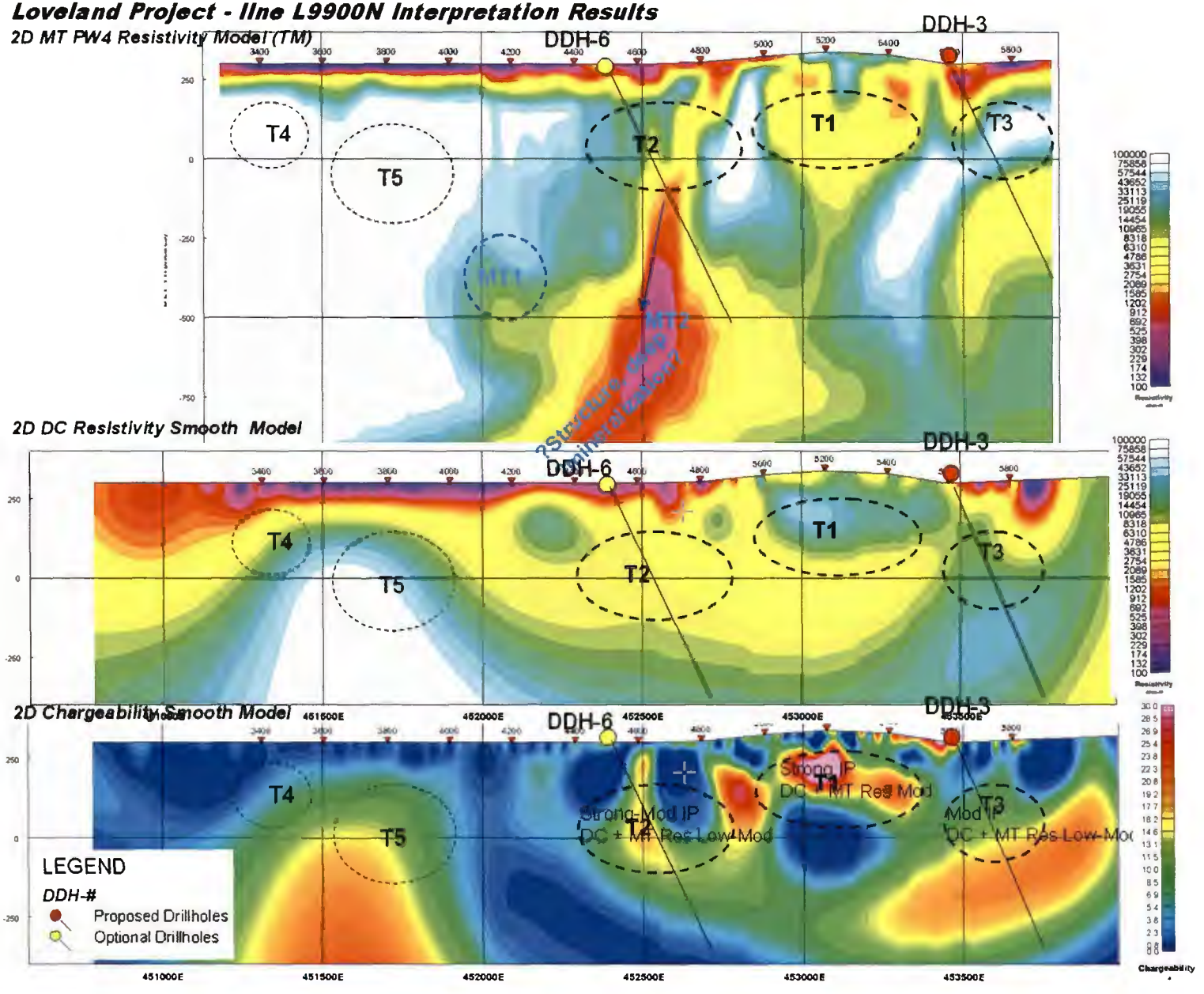

3D Chargeability Isosurfaces for
10 milliradians (violet) and 20 milliradians (red)

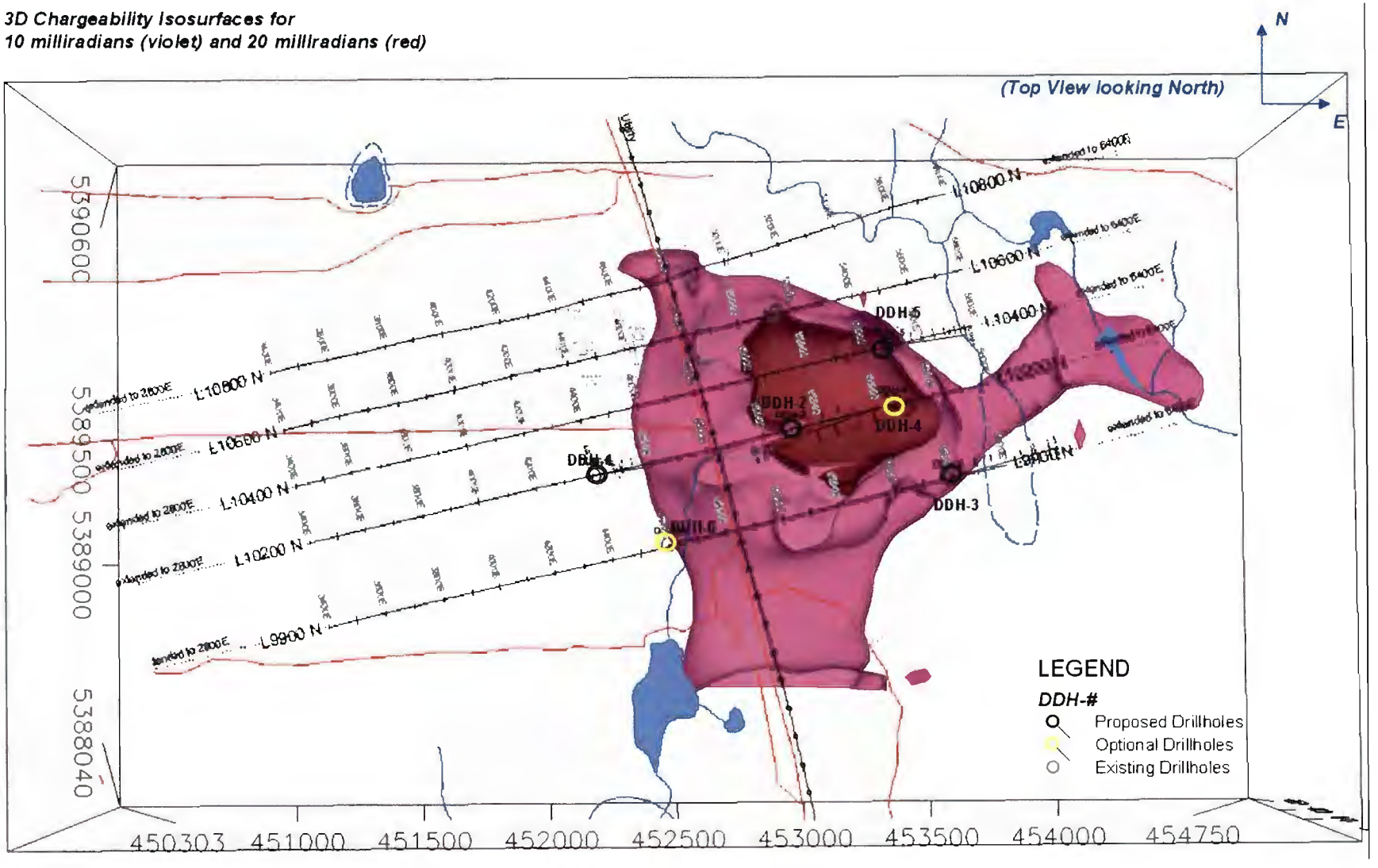

3D Chargeability Isosurfaces for
10 milliradians (violet) and 20 milliradians (red)

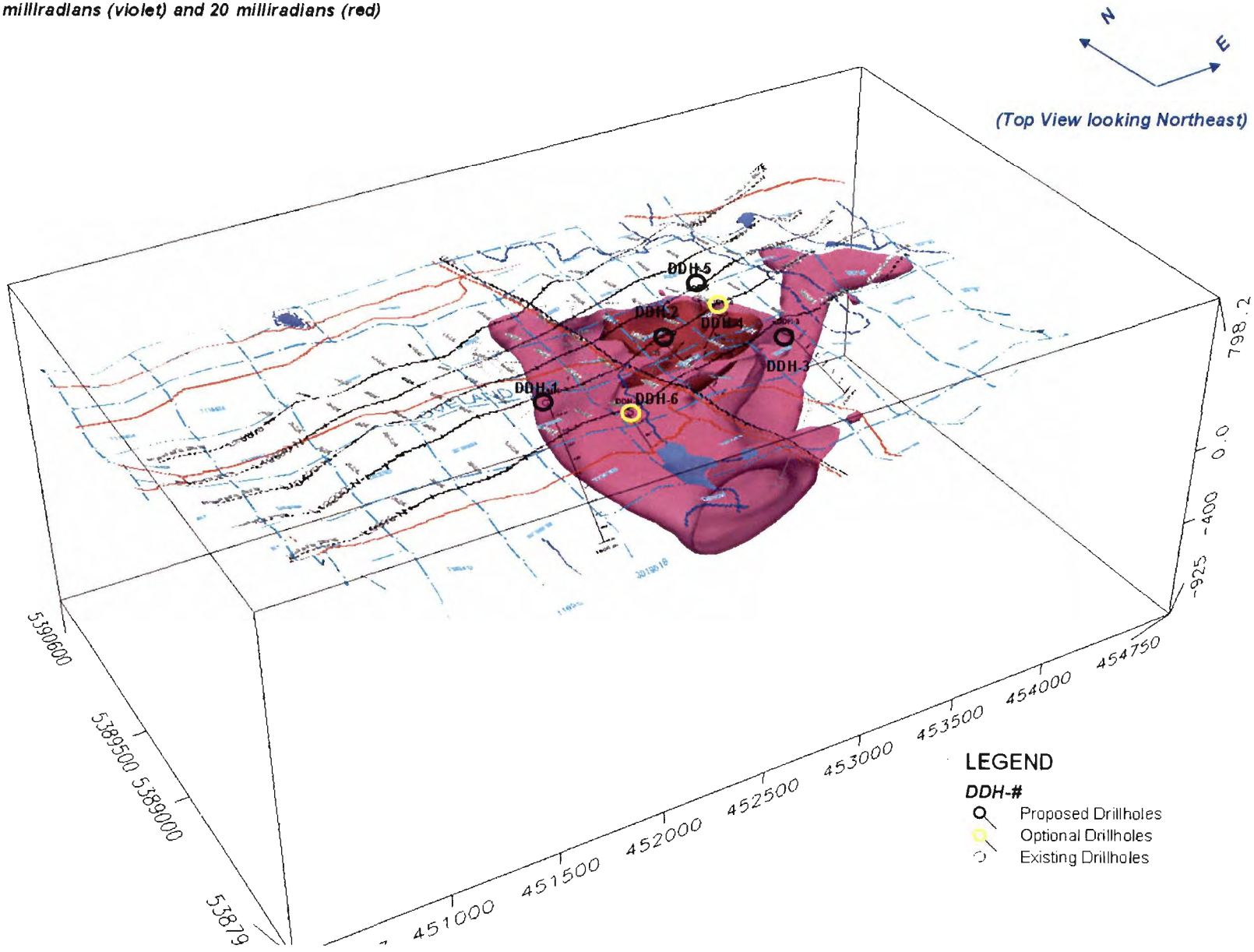

2D Chargeability Isosurfaces for 10 milliradians (violet) and 20 milliradians (red) with 2D PW MT Resistivity Section overlay, L9900E

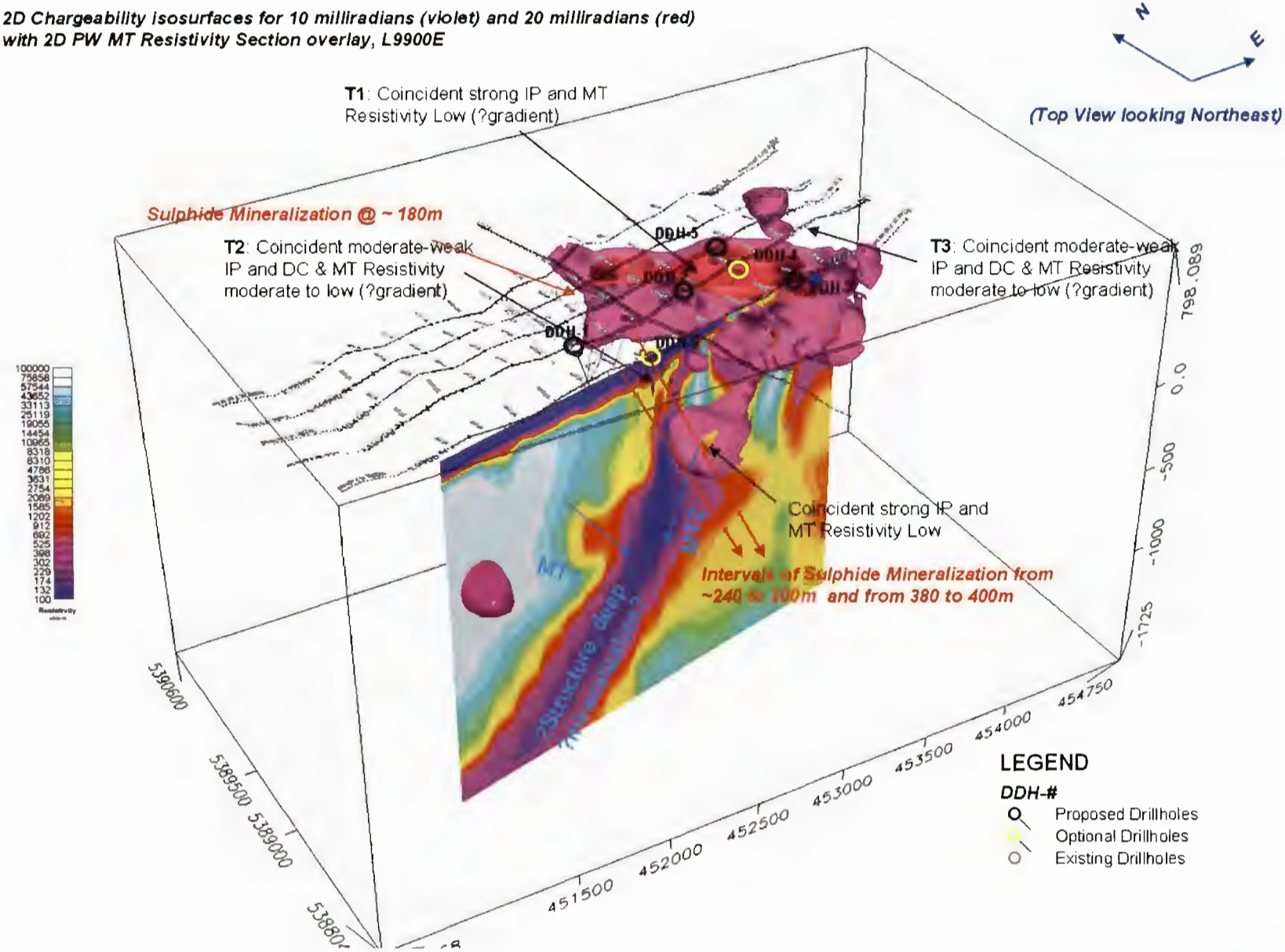

2D Chargeability Isosurfaces for 10 milliradians (violet) and 20 milliradians (red) with 2D PW MT Resistivity Section overlay, L10200E

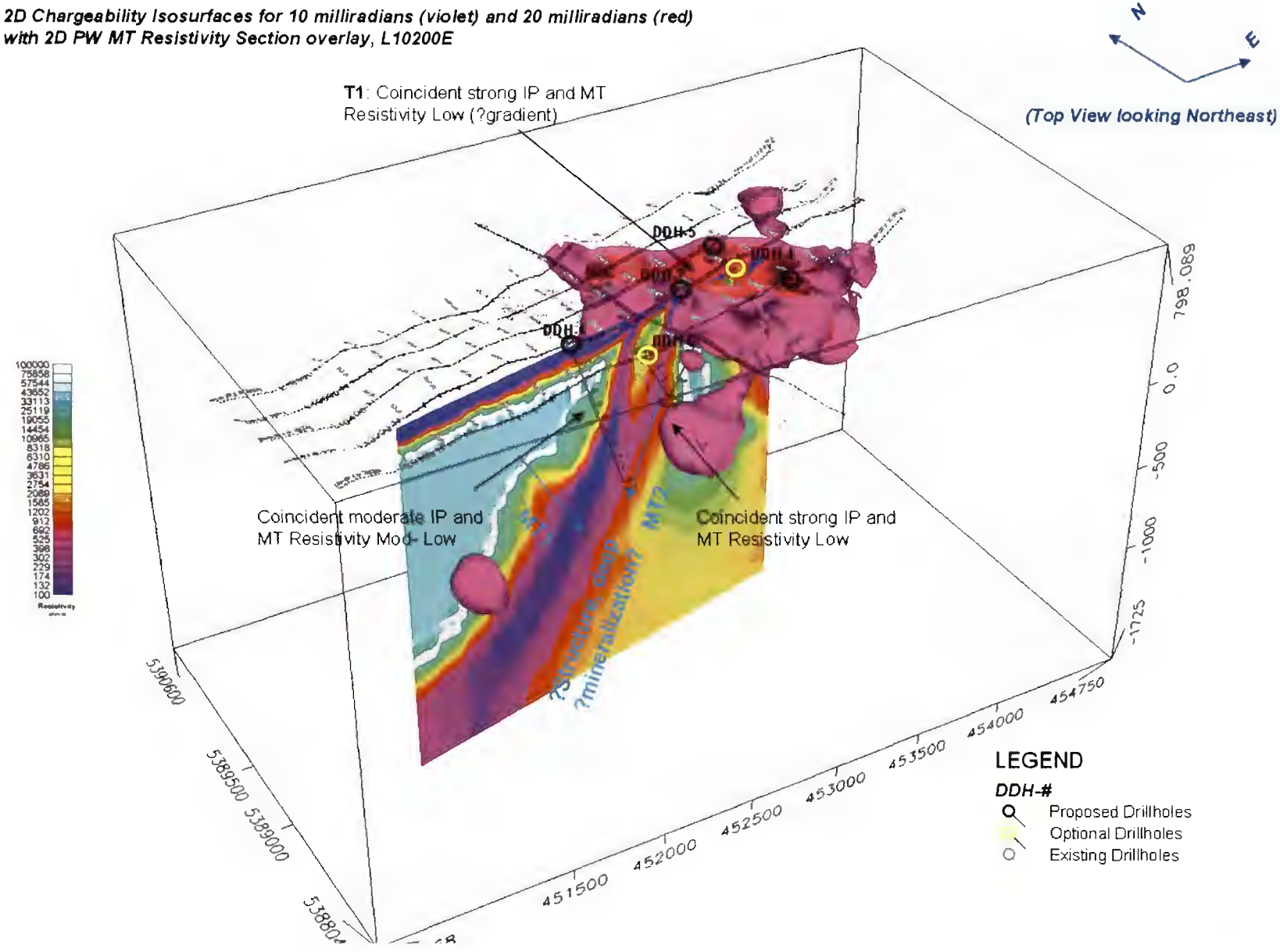

2D Chargeability Isosurfaces for 10 milliradians (violet) and 20 milliradians (red) with 2D PW MT Resistivity Section overlay, L10400E

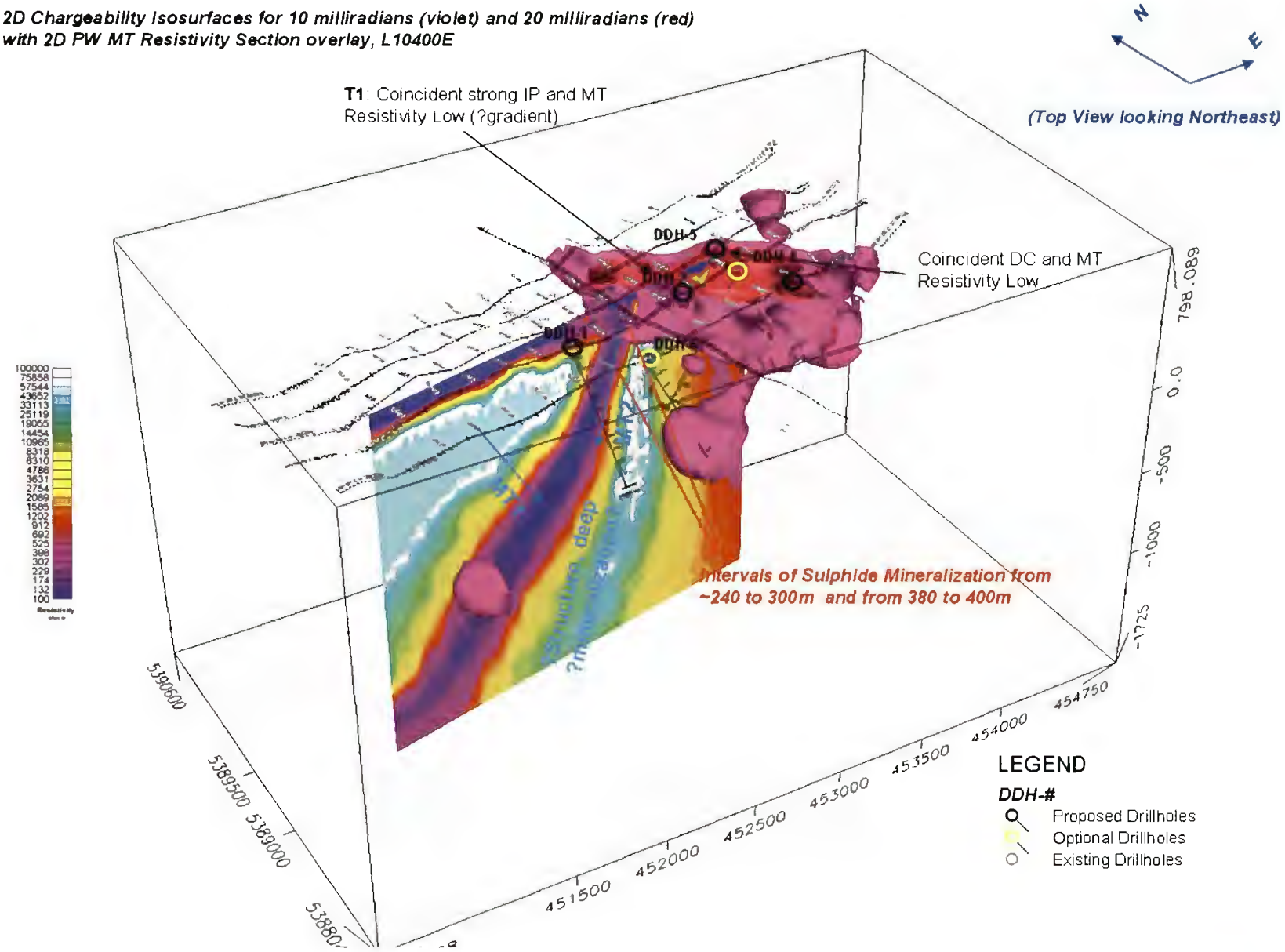

2D Chargeability Isosurfaces for 10 millIradians (violet) and 20 milliradians (red) with 2D PW MT Resistivity Section overlay, L10600E

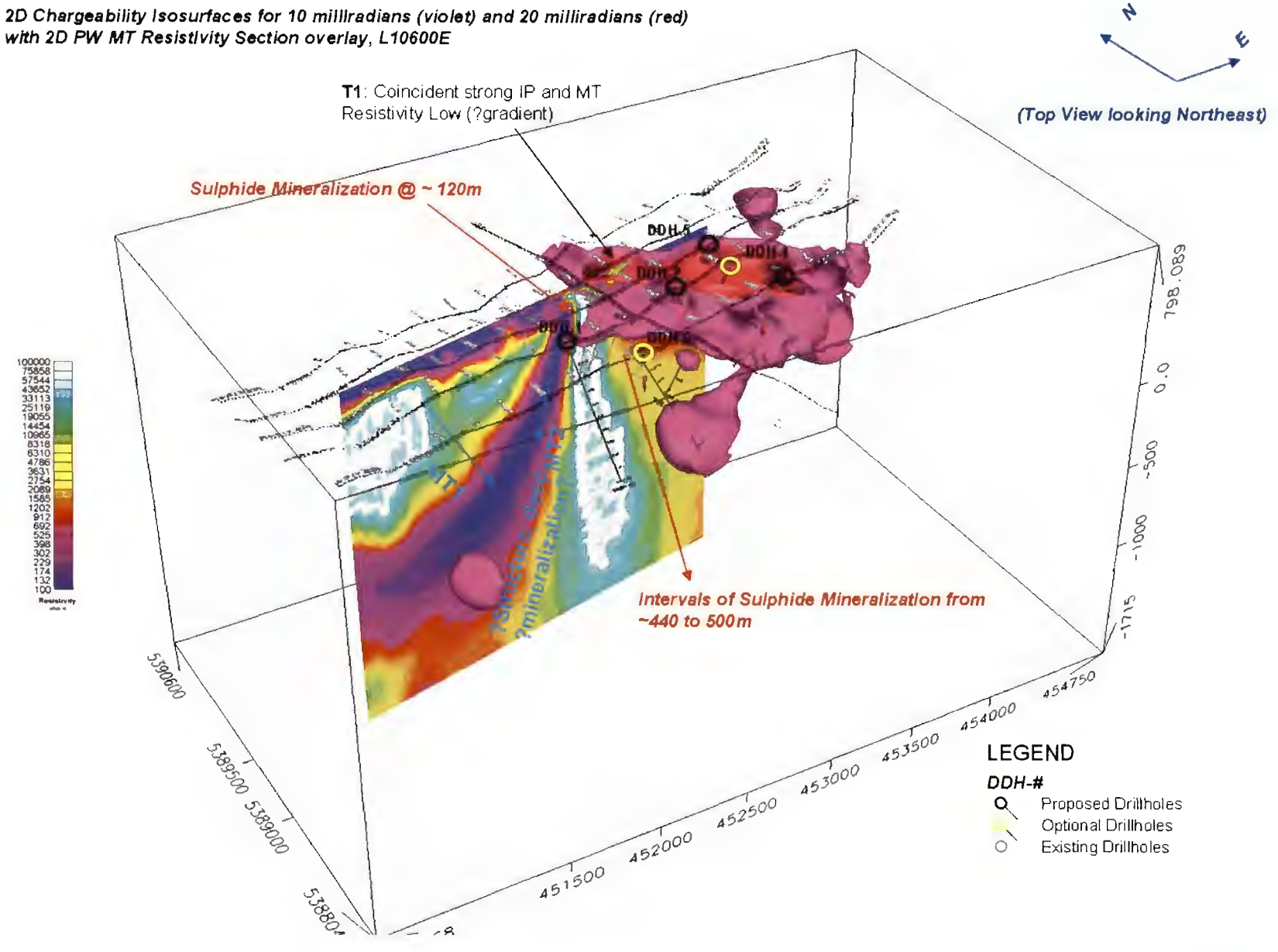

2D Chargeability Isosurfaces for 10 milliradians (violet) and 20 milliradians (red) with 2D PW MT Resistivity Section overlay, L10800E

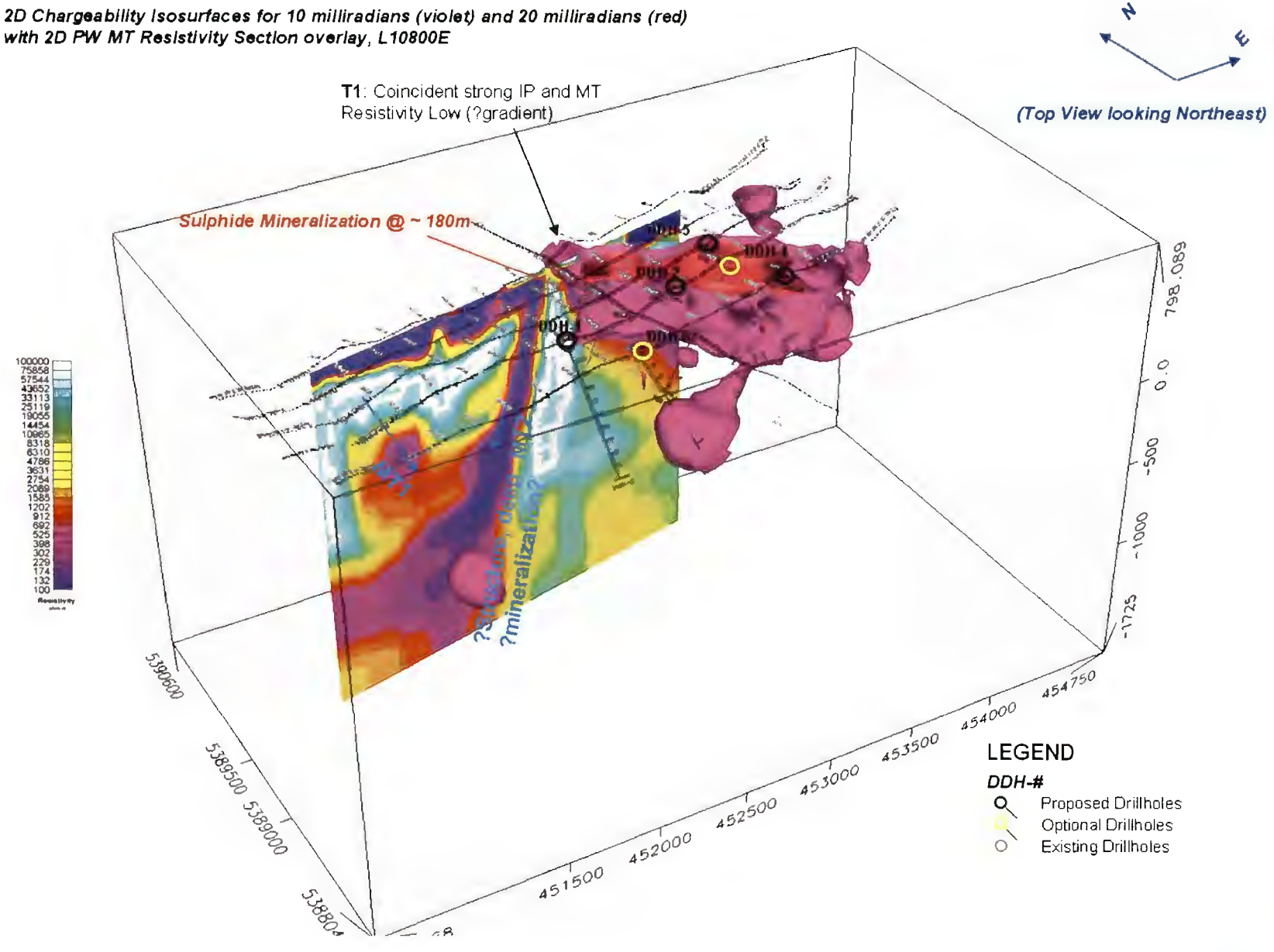

APPENDIX I - DIGITAL ARCHIVE

DVD'S ATTACHED ONTO INTERPRETATION REPORT INCLUDES:

- **DVD 1 OF 1:\CA00516T-LOVELAND PROJECT FOR WESTERN KIDD RESOURCES**